Communication in Membrane Repair

A Thesis
SUBMITTED TO THE FACULTY OF
UNIVERSITY OF MINNESOTA

Ryan W. Mahling

IN PARTIAL FULFILLMENT OF THE REQUIREMENTS
FOR THE DEGREE OF MASTER OF SCIENCE

Dr. Anne Hinderliter

June, 2015

Acknowledgements

I would like to thank Dr. Anne Hinderliter, for training and pushing me over the past three years, without which this work would not have been possible. I also owe a large thank you to former graduate students Michael E. Fealey (for always having the perfect words of inspiration), Samantha R. Jaworski (for the great deal of help when I first started in the lab), as well as Troy Hendrickson, Justine and Stephanie Schramel, Ben Horn and all members of the Hinderliter lab who have been a great during my time in lab. I also own a special thanks to my fiancé Phuong Tran for always being willing to check my work and keep me in check.

This material is based upon work supported by the National Science Foundation under Grant Number (MCB-0845676). Any opinions, findings, and conclusions or recommendations expressed in this material are those of the authors and do not necessarily reflect the views of the National Science Foundation. Circular dichroism spectroscopy was performed at the Biophysical Spectroscopy Center at the University of Minnesota in Minneapolis, MN.

Abstract

The force generated by muscle cells places a high amount of stress on their plasma membranes creating lesions which must be effectively repaired in order for the cell to survive. Multiple proteins have been implicated in the membrane repair process, one of which is dysferlin, a seven C2 domain containing protein. Of the seven C2 domains within dysferlin, only the C2A domain exists in two isoforms and has been suggested to be the Ca^{2+} sensor within dysferlin. Mutations within dysferlin have been found to cause several types of muscular dystrophies including Limb-Girdle muscular dystrophy, Myoshi Myopathy and Distal Anterior Compartment Myopathy. *In vivo* studies have revealed that after membrane rupture, dysferlin interacts with multiple proteins including annexin A2. In order to gain a better understanding of how this system functions, this author used methods including differential scanning calorimetry (DSC) and spectroscopy (fluorescence and circular dichroism) to examine both isoforms of the C2A domain and annexin A2. All three proteins were found to be marginally stable suggestive of a system that is highly capable of information propagation. From this, a picture emerges where mutations within dysferlin could result in a dramatic shift in the conformational ensemble available to the protein, which would interfere with its ability to properly interact and communicate with the other members of the membrane repair machinery. This would result in the loss of the ability to properly repair the membrane.

Table of Contents

List of Tables

List of Supplementary Tables

List of Figures

List of Supplementary Figures

List of Abbreviations

Syt I - synaptotagmin I
Ca2+ - calcium ion
POPS/PS- phosphatidylserine
PE- phosphoethanolamine
PI - phosphatidylinositol bisphosphate
POPC/PC - phosphatidylcholine
DSC - differential scanning calorimetry
ITC- isothermal titration calorimetry
CD- circular dichroism
TF - tryptophan fluorescence
KCl - potassium chloride
MOPS - 3-(N-morpholino)propanesulfonic acid
EGTA - ethylene glycol tetraacetic acid
LUVs - large unilamellar vesicles
SUVs- small unilamellar vesicles
BAPTA - (1,2-bis(o-aminophenoxy)ethane-N,N,N',N'-tetraacetic acid)
MBP - maltose binding protein
A2 – Annexin A2
a5- Annexin a5

Chapter 1: Dysferlin and Muscle Membrane Repair

1.1 Ca^{2+} and the Muscle Cell

Calcium ion (Ca^{2+}) influx into the cell provides a means of initiating a plethora of signaling events that simultaneously stimulate the activity of many proteins. This ion plays a particularly important role within the muscle tissue. Every movement we make is dependent upon the coordinated effort of multiple cells within this tissue. The process of muscle contraction actually begins in the nervous system where the signal is generated, and propagated ending at the muscle cell. This then results in an influx of Ca^{2+} from the sarcoplasmic reticulum (SR) into the cytosol. The increase in the cytosolic Ca^{2+} concentration leads to the dissociation of tropomyosin from actin, allowing myosin to bind to and pull the actin filaments leading to the generation of force that is responsible for muscle cell contraction. Immediately after its release from the SR, the Ca^{2+} is pumped from the cytosol back to within the SR where it will await another impulse from the nervous system. Given the intricate role played by Ca^{2+} in this process it comes as no surprise that the ions levels are tightly regulated within these cells, with the cytosolic concentration being kept extremely low (roughly 50nM) [1].

While generating this force is the main function of the muscle cell, it can also have unintended and deleterious consequences. Notably among these is that the force generated through muscle contraction places a high amount of stress on the plasma membranes of these cells. This stress regularly leads to the formation of micro lesions within the membrane. Which if the cell is to survive must be rapidly and effectively

repaired, as if not extracellular Ca^{2+} will flow unchecked into the cell overwhelming the machinery that is generally responsible for maintaining these levels. In order to prevent this a finely tuned system has evolved involving the concerted action of multiple proteins including dysferlin, TRIM 72, caveolin 3, and the annexins A1 and A2 to facilitate this process.

1.2 Dysferlinopathies

Dysferlinopathies are defined as autosomal recessive disorders that result from mutations within the dysferlin gene, which lead to the lack of a functional dysferlin protein. The symptoms of these mutations are not apparent during the early years of life but rather appear over a broad time range anywhere from the individuals twenties to fifties and the severity of the disease varies greatly [2,3]. Interestingly these mutations do not cause a specific disease state in afflicted individuals, but rather can lead to several types of muscular dystrophy, including limb-girdle type 2B, Miyoshi myopathy, and distal myopathy with tibialis onset [4]. However, all of these conditions result in progressive weakening of the muscle tissue and eventual loss of function as the muscle cells themselves are not able to properly heal.

To date there have been 508 unique mutations identified within dysferlin that have been linked to disease (http://www.dmd.nl). The type of mutation varies greatly as well, while the large impact of some these mutations can be clearly seen, such as the incorporation of an early stop codon within the sequence or frame shift mutations, these result in errors in how the RNA product will be read to produce the protein. However,

even point mutations which change only a single amino acid within the sequence can also cause these myopathies. Unlike many conditions that result from mutations there are regions within the dysferlin gene in which mutations consistently results in disease, but rather the mutations are spread throughout the gene occurring with seemingly no rhyme or reason. There is another complicating factor in these myopathies, namely that there does not appear to be any connection between the type and severity of myopathy experienced by the patient and the mutation type or location.

This data begins to paint a very interesting picture of dysferlin; it appears that each amino acid in the sequence is important for the function of the protein. Despite its identification as a mediator of membrane repair within myocytes over 15 years ago, how this protein functions in this process is poorly understood [5]. In the chapters that follow a combination of techniques will be used to investigate the physical properties of the first C2 domain within dysferlin (chapter 2). This data will then be expanded upon by considering both C2 domain of dysferlin as well as the C2 domains of a related protein, Synaptotagmin I, and the possible role of this motif in information flow at the membrane (chapter 3). Finally the physical properties of annexin A2 are examined in order to investigate whether or not information flow may extend beyond dysferlin itself (chapter 4).

Chapter 2: Alternate splicing of dysferlin C2A confers Ca^{2+}-dependent and Ca^{2+}-independent binding for membrane repair*

*Note: The following chapter was reproduced in its entirety in accordance with rights given to authors by Elsevier publications from the following article: Fuson, K., Rice, A., Mahling, R., Snow, A., Nayak, K., Shanbhogue, P., Meyer, A. G., Redpath, G. M., Hinderliter, A., Cooper, S. T., and Sutton, R. B. (2014). Alternate splicing of dysferlin C2A confers Ca2+-dependent and Ca2+-independent binding for membrane repair. *Structure*, *22*(1), 104–115.
With contribution of this author being the differential scanning calorimetry studies. All structural studies were carried out by Fuson, K., Snow, A., Nayak, K., Shanbhogue, P., Meyer, A. G., and Sutton, R. B.. All *in vivo* work was completed by Redpath, G. M., and Cooper, S. T..

2.1 Introduction

Muscle tissue generates mechanical force. The associated stress placed on the sarcolemmal membrane as a result of this force introduces micro-lesions in muscle cell membrane, which without *in vivo* repair mechanisms, would result in cell death[6]. Repair of membrane lesions depends on the activity of dysferlin, a multiple C2 domain-containing protein proposed to play a role in the vesicle fusion associated with membrane repair[7]. Mutations within the 8.5 kb *dysferlin (DYSF)* gene can result in recessive forms of muscular dystrophy, such as Limb-Girdle Muscular Dystrophy (LGMD), Mioshi Myopathy (MM) or Distal Anterior compartment myopathy (DMAT)[8], depending on the affected muscle groups. Currently, 457 unique human mutations have been cataloged in the *DYSF* gene (Dunnen, 2012). These include point mutations within folded domains and linker regions, and premature truncations of the primary sequence (Dunnen, 2012).

The physiological mechanism of action of dysferlin is not yet understood; however, several hypotheses have been proposed. Dysferlin deficient mice accumulate sub-

sarcolemmal vacuoles at the surface of muscle cell membranes; consequently, dysferlin has been implicated in vesicle fusion at the site of injury [7,9]. Dysferlin could also play a synaptotagmin-like role to interact with SNARE proteins that mediate the fusion of patching vesicles[10,11], or dysferlin may act as a scaffold for other fusion-related proteins such as MG53[12–15]. Dysferlin localizes to the t-tubule network[16,17] and may therefore be involved in vesicle trafficking to the sarcolemma through its interactions with tubulin[18]. In addition, it may be instrumental in signal transduction pathways related to membrane repair[19]. The most prevalent view is that dysferlin mediates the Ca^{2+}-dependent fusion of intracellular vesicles with micro-tears in the sarcolemma through the concerted interaction of its seven C2 domains with Ca^{2+} and phospholipid[20].

To date, there is evidence for 14 distinct splice isoforms of human dysferlin[21]. These are derived from differential splicing of Exons 1, 5a, 17 and 40a. Most of these exons encode inter-domain linker sequences, connecting C2 domains; however, C2A is the only folded domain in dysferlin with two alternative primary sequences[22]. Exon 1 in the dysferlin gene (*DYSF*) encodes the first 29 amino acids of the canonical dysferlin C2A domain, which is currently the most thoroughly characterized (Fig. 1a). An alternative exon 1a encodes the first 30 amino acids of the dysferlin C2A variant 1 domain (C2Av1). This alternative exon is embedded within the intronic sequences located between exons 1 and 2, but no physiological function has been demonstrated for this isoform. To determine the differences between the canonical C2A and the C2Av1 isoforms, we merged biophysical studies with *in vitro* approaches to gain structure-function insight into the role of these two domains in membrane repair. We solved the

X-ray structure of each C2A domain to high resolution, characterized the Ca^{2+} and phospholipid binding activities of each, and established their sub-cellular localization in cultured muscle cells. We show that the canonical C2A domain of dysferlin possesses two Ca^{2+} binding sites with discrete biophysical roles. The first is a high-affinity Ca^{2+} binding site that stabilizes the domain, but does not contribute to membrane binding. The second is a low-affinity Ca^{2+} binding site that mediates the interaction between the C2 domain and a negatively charged phospholipid membrane, consistent with its role as a Ca^{2+}-dependent phospholipid binding domain. Interestingly, the C2Av1 is Ca^{2+} insensitive, but acquires the ability to bind Ca^{2+} only when bound to phospholipids. Further, both C2A domains exhibit some of the lowest free energies of stability yet measured in a folded protein, suggesting remarkable conformational plasticity. This flexibility allows the C2A domains of dysferlin to explore different sub-sets of conformations for maximal ligand and effector binding potential[23]. In addition, since both isoforms of dysferlin are co-expressed in the same tissues, and both occur at the plasma membrane, it is likely that the Ca^{2+}-independent C2Av1 could act in concert with the Ca^{2+}-dependent C2A-dysferlin at the plasma membrane to regulate and fine-tune the membrane repair response.

2.2 Experimental Procedures

2.2.1 Expression constructs

The gene encoding the human dysferlin C2A domain was obtained from Dr. Elizabeth McNally [24]. The DNA sequence corresponding to Human dysferlin C2A (residues 1-125) was cloned into pGEX-4T. The gene encoding human dysferlin C2Av1 (residues 1-126) was subcloned into a pET28a expression vector with an N-terminal His_6-MBP tag and a Tobacco Etch Virus (TEV) protease cleavage site. A Cys2Ala was introduced into the gene, as we predicted that it should be exposed to solvent, and therefore, could interfere with purification and crystallization.

Both the canonical and the C2Av1 constructs were expressed in BL21 (DE3) cells. Ten liters of cells were grown in a BioFlo 3000 fermentor at 30 °C in Terrific Broth to an optical density (OD600) of 1.3. The temperature of the cell cultures was then lowered to 18 °C and heterologous protein expression was induced by adding 400 μM IPTG. The cells were grown for an additional 12 hours and harvested by centrifugation. The cell pellets were frozen in liquid Nitrogen and stored at -80 °C until needed.

2.2.2 Protein expression and purification

For the canonical C2A, 30 g of the bacterial cell pellet was resuspended in Lysis buffer (50 mM HEPES, pH 8, 250 mM NaCl, 1% TX-100, 1 mM PMSF, 1 mM EDTA). The cells were processed through a Microfluizer (Model M-110EHI, Microfluidics) at 4 °C until lysis was complete. The resulting slurry was centrifuged at 42,000 rpm in a Ti-45 rotor to separate the insoluble material. The cell lysate was then applied to a GST-

Sepharose column and allowed to bind for 4 hours at 4 °C. The GST-sepharose was packed into a column and the unbound protein was washed out with 1L of Lysis buffer. The dysferlin C2A protein was eluted from the column in Lysis buffer plus 15 mM reduced glutathione. 500 μg of human α-thrombin was added to the elution and dialyzed against thrombin cleavage buffer (50 mM HEPES, pH 7.5, 250 mM NaCl, 2 mM $CaCl_2$) overnight at 20 °C. After cleavage, the C2A was buffer exchanged into S-Sepharose buffer (50 mM HEPES, pH 7.5, 50 mM NaCl) and immediately purified over a 125 ml S-Sepharose column (GE Healthcare) and eluted with a NaCl gradient from 50 mM to 1 M over 20 column volumes. This protein was then size selected over a 70 ml Superdex 75 gel filtration column (GE Healthcare). The eluted protein was then tested for purity by SDS PAGE electrophoresis. The protein was then concentrated to 10 mg/ml for crystallization.

For C2Av1, 30 g of cells were resuspended in Lysis buffer (40 mM HEPES pH 7.4, 250 mM NaCl, 1% TX-100, 1 mM PMSF and 10 mM imidazole). Cells were lysed by passage through a microfluidizer processor (Model M-110EHI, Microfluidics), and the lysate was cleared by centrifugation at 42,000 rpm at 4 °C for 45 min using Ti-45 rotor. Cleared lysate was applied to a Ni-NTA (Qiagen) column prewashed with Lysis buffer, the bound protein was washed with 1L wash buffer (40 mM HEPES pH 7.4, 250 mM NaCl and 30 mM imidazole) and was eluted with 250 mM imidazole. TEV protease was added to the protein at a ratio of 1:10 (w/w), and the fusion protein was digested for 8 hr at 20 °C. The resulting C2Av1 domain was purified over 125 ml S-Sepharose resin (GE Healthcare) with an increasing NaCl gradient from 250 mM to 1 M over 20 column

volumes. The C2Av1 eluted from S-Sepharose at 400 mM NaCl. This protein was then size selected over a 70 ml Superdex 75 gel filtration column (GE Healthcare). Protein concentration was determined by absorbance at 280 nm using the calculated extinction coefficients for each domain (15470 $M^{-1}cm^{-1}$ and 12490 $M^{-1}cm^{-1}$ for canonical C2A and C2Av1 domains, respectively). The eluted protein was tested for purity by SDS PAGE electrophoresis, and the mass of the both constructs were confirmed by matrix-assisted laser desorption/ionization time-of flight mass spectroscopy (MALDI-TOF). The protein was then concentrated to 10 mg/ml for crystallization.

2.2.3 Crystallization

The canonical C2A domain was crystallized in 2.8 M Sodium Formate, 0.1 M sodium acetate, pH 5.5 using the hanging droplet method with purified protein at a stock concentration of 10 mg/ml. Crystals were grown at 7 °C. Typically, the crystals reached full size overnight. C2Av1 was crystallized in 16% PEG 20000, 0.1 M sodium citrate, pH 6.2. Crystals were grown using the hanging drop methods with purified protein at 10 mg/ml. Crystals were also grown at 7 °C. Typically, the crystals reached full size within 3 days.

2.2.4 Data collection

The crystals of both C2 domains were captured into nylon loops and frozen in liquid N_2. Initial data sets were collected on a Rigaku ScreenMachine. Subsequent data sets were collected at SLAC beamline 7-1. The wavelength of the final data sets was

0.9796 Å, and the data were collected at 90 K. X-ray data was processed with imosflm [25] and the data were scaled using SCALA as a part of the CCP4 package [26]. A summary of the crystal statistics are presented in Table 1.

2.2.5 Isothermal Titration Calorimetry

Isothermal titration calorimetry experiments to determine the binding of Ca^{2+} and POPC:POPS containing lipid LUVs to dysferlin were performed on a TA Instruments Nano ITC at 15 °C. Both the Ca^{2+} and lipid titrant solutions were prepared in buffer consisting of 20 mM HEPES and 100 mM KCl at pH 7.5 that was passed through Bio-Rad 100 Chelex resin to remove cation impurities and filtered using a 0.2 µm Nalgene PES disposable filter unit. The protein was buffer exchanged into the same 20 mM HEPES and 100 mM KCl buffer using Bio-Rad 10DG disposable chromatography columns. The Ca^{2+} concentrations used in the experiments were verified using BAPTA fluorescence (Invitrogen/Molecular Probes) and Ca^{2+} electrode (Fisher). The titrant lipid concentration was verified by phosphate assay according to standard protocols [27]. Heats of dilution were conducted with replicate titrations in the absence of protein and subtracted from the corresponding data sets in order to determine the binding parameters.

2.2.6 Differential Scanning Calorimetry Methods

DSC experiments were performed on a NanoDSC (TA Instruments, New Castle, DE) at a scan rate of 1 °C/min. To see if measured enthalpies varied with concentration or scan rate, both constructs were denatured over a range of concentrations and scan

rates. All scans were conducted in Chelex-ed 20 mM MOPS, 100 mM KCl, pH 7.5. Scans performed in the absence of Ca^{2+} contained 5 mM EGTA. All scans in the presence of Ca^{2+} were done at a concentration of 5 mM to ensure near saturated conditions. The concentration of the Ca^{2+} stock solution used for all scans was verified using both a calcium ion selective electrode (ThermoScientific) and a BAPTA chelating assay (Invitrogen/Molecular Probes, Eugene, OR). Scans carried out in the presence of lipid contained LUVs composed of a 60:40 mixture of POPC:POPS and were done at a concentration of 2 mM.

2.2.7 Cellular Localization of C2A versus C2Av1

Flow Cytometry

C2C12 transfected with EGFP-$FL_{C2A}Dysferlin_{MycHis}$ or EGFP-$FL_{C2Av1}Dysferlin_{MycHis}$ were trypsinized on the morning of the experiment, replated into the same dish, and incubated for 3 hours at 37 ^{o}C to recover and re-express surface dysferlin. Cells were then dissociated from the plate by incubation for 5 min at 37 °C with Versene (0.48mM $EDTA_{4Na}$ in PBS). Cells were gently triturated from the plate in HBSS + 10% FCS, transferred to a falcon tube and pelleted by centrifugation at 300 *g* for 2 min. The 3 hour replating step assisted with cell dissociation, yielding >90% live cells as assessed by propidium iodide (PI) exclusion. Cells were resuspended in cold PBS containing 1% BSA with mouse anti-His (1:200) and incubated for 90 mins at 4 °C, washed with PBS, pelleted as before, then resuspended in buffer containing donkey anti-$mouse^{Alexa647}$ for 1 h at 4 °C. Cells were then washed twice and resuspended in PBS

containing propidium iodide (PI, 5 μg/ml). Flow cytometry was performed using a Becton Dickenson LSRII cytometer equipped with FACSDivaTM software (BDBiosciences). Postacquisition analysis was performed using FlowJo software (Tree Star Inc). Gating for live cells was performed based on PI exclusion (not shown), gating for transfected and untransfected cells is shown in Fig. 7B.

2.3 Supporting Materials

Derivation of ITC fitting model

Isothermal titration calorimetry (ITC) was used in order to determine the dysferiln construct's affinity for calcium ions in both the absence and presence of membrane. Because the shapes of the binding profiles indicate two distinct binding events as evidenced from the multiple inflection points in the curve, the model used to fit the data assumed that there were two distinct classes of binding sites within the molecule. This means that each set of calcium ion binds independently and with different affinities from the other.

The ITC measures the rate at which heat is evolved (dQ/dt) over the course of the titration in uW. In order to determine the enthalpy of binding associated with the reaction, the absolute change in heat at each injection point must be determined. In order to determine this, it is necessary to integrate the graph with respect to time. Thus the discrete integration of each peak yields the total heat associated with each injection point.

$$\int_{ta}^{tb} \frac{dQ}{dt} dt = \Delta Q_{\mathrm{i}} \qquad (1a)$$

Equation 1 shows the calculation of ΔQ_i which is the heat evolved at each i^{th} injection point where ta and tb are the bounds of each titration injection. This integration was done using TA instrument's Nano Analyze program.

The heat evolved during the titration is due to several different factors. There is an evolution of heat associated with the binding of ligand to macromolecule and an evolution of heat due to the dilution of the sample from each injection. In order to determine the heat of the binding events only, the heat of dilution for each titration was

subtracted from the experimental data. This is done using a second titration as a control in which all experimental parameters are kept constant but no macromolecule was added. It is this corrected heat that was fit using the model.

When assuming a model with two sets of independent binding sites, the total heat associated with the binding can be calculated using thermodynamic accounting that takes into account the fraction of each set of sites that generate heat by binding, the enthalpy of that binding, and the number of binding sites involved. This can represented as:

$$Q_T = [Dys]_t(V_0)*(n_1\theta_1\Delta H_1 + n_2\theta_2\Delta H_2) \qquad (2a)$$

Where:

Q_T = Total heat of the titration point up to the i^{th} injection point

$[Dys]_T$ = Total dysferlin concentration at the i^{th} injection point

V_0 = effective sample cell volume

$\Theta_{(1 \text{ or } 2)}$ = fraction of binding sites (of type 1 or 2) occupied by ligand

$[Ca^{2+}]$ = free calcium concentration at the i^{th} injection point

$n_{(1 \text{ or } 2)}$ = number of binding sites (of type 1 or 2)

The fraction of occupied binding sites is directly relatable to the binding affinities of each site through the general equations:

$$\theta_1 = \frac{K_1*[Ca2+]}{1+K_1*[Ca2+]} \qquad (3a)$$

$$\theta_2 = \frac{K_2*[Ca2+]}{1+K_2*[Ca2+]} \qquad (4a)$$

At this point Q_T can be solved for in terms of the fit parameters of n_1, ΔH_1, K_1, n_2, ΔH_2, K_2 and the additional parameter $[Ca^{2+}]$. However, the free calcium ion concentration at

each injection point is not a quantity that can be directly measured during the experiment, thus it is necessary to be able to calculate $[Ca^{2+}]$ in terms of both fit parameters and experimentally observed values. This can be done using equations 3a, 4a and the following mass balance equation which relates it to the total calcium concentration in the cell at each injection point $[Ca^{2+}]$, which can be calculated from experimental conditions.

$$[Ca^{2+}]_T = [Ca^{2+}] + [Dys]_T * (n_1\theta_1 + n_2\theta_2) \qquad (5a)$$

Thus substitution of equations 3a and 4a into 5a creates a cubic equation when like-terms are gathered with respect to $[Ca^{2+}]$. The roots of this equation when solved for using either Newton's Method or a depressed cubic assumption yield $[Ca^{2+}]$ at each injection point. Thus after back substitution into eq. 3a and 4a, the fractional saturation of each set of binding sites can be calculated. These fractional occupations of each set of sites can be further back-substituted to estimate the total heat of the titration as in equation 2a.
The values from eq. 2a can then be used in conjunction with non-linear least squares regression analysis to obtain the best values for the six fitting parameters n_1, ΔH_1, K_1, n_2, ΔH_2, and K_2. Most of this analysis was performed using TA instrument's Nano Analyze software.

Fitting of Denaturation Data

All stability data reported was obtained through the use differential scanning calorimetry (DSC). DSC works through heating two cells, one of which is a reference cell containing only the buffer, and the other, the sample cell, contains both the buffer and protein sample, at the same rate. As the denaturation process is endothermic excess

energy is required to heat the sample cell during this process. Once normalized one will obtain the excess heat capacity as a function of temperature, from this the enthalpy of denaturation ($\Delta H°$) is found by integrating the peak in the profile, the change in heat capacity (ΔCp) is determined from the difference in the pre and post transition baselines, and the melting temperature (T_M), which is the X value at the midpoint of the peak. With these parameters the free energy can calculated as a function of temperature through the Gibbs-Hemholtz equation, $\Delta G=\Delta H°(1-T/T_M)+\Delta Cp(T-T_M-Tln(T/T_M)$. The enthalpy obtained from DSC is the global denaturation enthalpy. As such there are minor contributions to the measured enthalpy from events such as ligand dissociation upon denaturation. These minor enthalpic contributions are important in understanding how the binding of a ligand impacts the stability of a protein as they also play a role in the stabilization.

Derivation of The Gibbs-Hemholtz Equation

The free energy of a reaction or a system can be determined through the use of the Gibbs free energy equation which given as:

$$\Delta G=\Delta H-T\Delta S \quad (1)$$

Equation 1 can be further expanded by incorporating the relationships that define enthalpy and entropy under constant pressure:

$$\Delta H=\Delta H°+\Delta Cp(T-T_{Ref}) \quad (2)$$

$$\Delta S=\Delta S°+\Delta Cpln(T/T_{Ref}) \quad (3)$$

Through the incorporation of equations 2 and 3 into equation 1 the Gibbs-Hemholtz equation can be obtained and written as:

$$\Delta G=\Delta H°-T\Delta S°+\Delta Cp(T-T_{Ref}-Tln(T/T_{Ref}) \quad (4)$$

By defining the reference temperature as the temperature at which the free energy is equal to zero equation 4 can be further simplified to give:

$$\Delta G=\Delta H°(1-T/T_{Ref})+\Delta Cp(T-T_{Ref}-Tln(T/T_{Ref}) \quad (5)$$

The proportion of protein present in the denatured (D) and native (N) states can be represented through the equilibrium constant:

$$K=[D]/[N] \quad (6)$$

Equation 6 is related to the free energy through:

$$\Delta G=-RTln(K) \quad (7)$$

Since the melting temperature of the domain is defined as the temperature at which 50% of the domain is found in the denatured state and 50% is present in the native, therefore at this temperature the free energy of stability for the domain is equal to 0Kcal/mol. Substituting this into equation 5 as the reference temperature the Gibbs-Hemholtz equation can be rewritten as:

$$\Delta G=\Delta H°(1-T/T_M)+\Delta Cp(T-T_M-Tln(T/T_M) \quad (8)$$

Through differential scanning calorimetry one can obtain all of the parameters needed to calculate the free energy of stability as a function of temperature as the enthalpy of denaturation ($\Delta H°$), change in heat capacity (ΔCp), and the melting temperature (T_M) are constants. Due to this the only parameter that is varied in the calculation of the free energy of stability is the temperature.

Two State Assumption

As stated above it is often assumed that a protein can exist in one of two states, either the native set of states or the denatured state. As the protein is heated it transitions from the native state to the denatured state, it is this transition that is monitored through the use of DSC and gives the resultant peak in the heat capacity curve. The two state assumption can be checked through the use of the Van't Hoff ratio, which compares the theoretical enthalpy and the enthalpy from the calorimeter, the closer this ratio is to one the more ideally two state the protein behaves. The Van't Hoff enthalpy was calculated according to:

$$\Delta H_{vH}=4RT_m^2(\Delta Cp/\Delta H^\circ) \quad (9)$$

Predicted Change in Heat Capacity

These values were calculated with the use of the following empirical equation (Spolar,Livingstone, and Record, 1992).

$$\Delta Cp_{Fold}=a\Delta A_{np}+b\Delta A_p \quad (10)$$

Where ΔA_{np} and ΔAp are the change in the water accessible nonpolar and polar suffice area respectively and a and b are constants which were determine through fitting experimental data to be -0.33 and 0.16. By substituting these values in equation 10 can be rewritten as:

$$\Delta Cp_{Fold}=-0.33\Delta A_{np}+0.16\Delta A_p \quad (11)$$

Reversibility

While we were not able to characterize any reversibility for either isoform of the C2A domain it has been shown that this, while helpful, reversibility is not required for a valid thermodynamic analysis of protein stability. Rather if it can be shown that the enthalpy of denaturation and melting temperature do not show a significant scan rate dependence the parameters collected can still be considered valid (REF Sanchez). As such, in order to ensure that the stability parameters presented here are valid DSC experiments were completed at different scan rates (Table S-5), neither the enthalpy or melting temperature increased significantly at the higher scan rate supporting the stability parameters reported.

Supplemental Methods

Protein expression and purification

For the canonical C2A, 30 g of the bacterial cell pellet was resuspended in Lysis buffer (50 mM HEPES, pH 8, 250 mM NaCl, 1% TX-100, 1 mM PMSF, 1 mM EDTA). The cells were processed through a Microfluizer (Model M-110EHI, Microfluidics) at 4 °C until lysis was complete. The resulting slurry was centrifuged at 42,000 rpm in a Ti-45 rotor to separate the insoluble material. The cell lysate was then applied to a GST-Sepharose column and allowed to bind for 4 hours at 4 °C. The GST-sepharose was packed into a column and the unbound protein was washed out with 1L of Lysis buffer. The dysferlin C2A protein was eluted from the column in Lysis buffer plus 15 mM reduced glutathione. 500 μg of human α-thrombin was added to the elution and

dialyzed against thrombin cleavage buffer (50 mM HEPES, pH 7.5, 250 mM NaCl, 2 mM $CaCl_2$) overnight at 20 °C. After cleavage, the C2A was buffer exchanged into S-Sepharose buffer (50 mM HEPES, pH 7.5, 50 mM NaCl) and immediately purified over a 125 ml S-Sepharose column (GE Healthcare) and eluted with a NaCl gradient from 50 mM to 1 M over 20 column volumes. This protein was then size selected over a 70 ml Superdex 75 gel filtration column (GE Healthcare). The eluted protein was then tested for purity by SDS PAGE electrophoresis. The protein was then concentrated to 10 mg/ml for crystallization.

For C2Av1, 30 g of cells were resuspended in Lysis buffer (40 mM HEPES pH 7.4, 250 mM NaCl, 1% TX-100, 1 mM PMSF and 10 mM imidazole). Cells were lysed by passage through a microfluidizer processor (Model M-110EHI, Microfluidics), and the lysate was cleared by centrifugation at 42,000 rpm at 4 °C for 45 min using Ti-45 rotor. Cleared lysate was applied to a Ni-NTA (Qiagen) column prewashed with Lysis buffer, the bound protein was washed with 1L wash buffer (40 mM HEPES pH 7.4, 250 mM NaCl and 30 mM imidazole) and was eluted with 250 mM imidazole. TEV protease was added to the protein at a ratio of 1:10 (w/w), and the fusion protein was digested for 8 hr at 20 °C. The resulting C2Av1 domain was purified over 125 ml S-Sepharose resin (GE Healthcare) with an increasing NaCl gradient from 250 mM to 1 M over 20 column volumes. The C2Av1 eluted from S-Sepharose at 400 mM NaCl. This protein was then size selected over a 70 ml Superdex 75 gel filtration column (GE Healthcare). Protein concentration was determined by absorbance at 280 nm using the calculated extinction coefficients for each domain (15470 $M^{-1}cm^{-1}$ and 12490 $M^{-1}cm^{-1}$ for canonical C2A and

C2Av1 domains, respectively). The eluted protein was tested for purity by SDS PAGE electrophoresis, and the mass of the both constructs were confirmed by matrix-assisted laser desorption/ionization time-of flight mass spectroscopy (MALDI-TOF). The protein was then concentrated to 10 mg/ml for crystallization.

Structure solution and refinement of C2A and C2Av1

The structure of the canonical C2A domain was solved by molecular replacement using Phaser (McCoy, 2007). The C2A domain from myoferlin (1DMH) was used as the search model. Initial molecular replacement attempts were inconclusive because of the large number of molecules in the ASU, so our initial efforts to determine the position of dysferlin monomers failed. Inspection of the self-rotation function using GLRF (Tong and Rossmann, 1997) showed the presence of a strong non-crystallographic peak at κ=120°, suggesting that the asymmetric unit possessed a trimer. Due to the large size of the unit cell, the Matthews coefficient predicted 5-6 monomers in the asymmetric unit of this crystal form. With this information, Phaser determined the location of the two stacked trimers that made up the entire asymmetric unit. Upon correctly finding the position of the two trimers, the initial R-factor was 47%. Refinement of the structure to 2.0 Å resolution was completed using TLS refinement in Phenix, and subsequence rounds of model building was done using Coot. Ten percent of the data was randomly chosen for cross validation. The structure was validated using MolProbity as implemented in Phenix. The structure of C2Av1 was determined by molecular replacement using a monomer of the canonical C2A (4IHB) as the search model. Phaser determined the position of each of

the three molecules in the asymmetric unit with an initial R factor = 45%. Refinement of the structure to 1.8 Å resolution was completed using TLS refinement in Phenix, and subsequence rounds of model building was done using Coot. Ten percent of the data was randomly chosen for cross validation. The structure was validated using MolProbity as implemented in Phenix.

Construction of the C2Av1 expression construct

The C2Av1 sequence was amplified from human muscle cDNA using a forward primer that included an EcoRI site immediately before the ATG start codon of the C2Av1 isoform, and a reverse primer encompassing the SbfI site at position 729. The PCR product was subcloned into a pTOPO2.1 shuttle vector and sequenced. A positive clone was digested with EcoRI and SbfI and subcloned into EcoRI/SbfI digested pcDNA4-EGFP dysferlin$_{MycHis}$ (generously provided by Prof. Bushby, Newcastle University, United Kingdom). This construct was then digested with SbfI, and the dysferlin SbfI fragment 729 – 1861 subcloned to regenerate the full-length dysferlin cDNA bearing the alternate C2Av1.

ITC Supplemental Methods

All titrations were run using protein concentrations varying from 80-110 μM of the dysferlin C2A constructs. For experiments in which one ligand was titrated into the protein in the presence of the second ligand (i.e. Ca2+ into protein with a phospholipid background; Fig 4C), precautions were taken such that the background ligand was

present in the same protein-saturating concentration in both the syringe and sample cell so that it would remain constant throughout the titration. This ensures that only the enthalpy of binding between the protein and the titrant was measured. The Ca2+ stock concentrations used in the experiments were verified using a BAPTA fluorescence assay (Invitrogen/Molecular Probes). BAPTA is a Ca2+ specific chelator, with a K of 0.2uM that changes absorbance upon Ca2+ binding. It is similar to the less specific EDTA, which cannot be used to sponge Ca2+ from our titrations due to its large enthalpy of binding that would dwarf any heats associated with ligand binding to protein. For titrations using phospholipids, the acidic phospholipid content of all liposomes used in the titrations was kept at 40% of the total phospholipid content to provide the signal necessary to deconvolute the complex binding isotherms in the presence of lipid. The possibility exists that a fraction of the heat of dilution for the titration of Ca2+ into protein with a phospholipid background are due to interactions between Ca2+ and membrane. However, the association constant of divalent cations for acidic phospholipid is about 10 M-1, so contributions from Ca2+ and membrane interactions are negligible (Lehrmann and Seelig, 1994). Furthermore, the resulting heats of dilution of these titrations were small and comparable to that observed previously. Heats of dilution were conducted by repeating each titration with the same concentrations of titrant and background species in the absence of macromolecule. These were then subtracted from the corresponding protein titration's data in order to obtain the correct binding parameters for each fit.

For all experiments, the ITC stir speed was 250 rpm and the interval between injections was 300 seconds. In addition, all solutions were thoroughly degassed prior to loading both the titration syringe and sample cell. All solutions were injected into the sample using a 1 µL initial injection point to displace air from the syringe followed by 27 x 9 µL injection points. The initial 1 µL injection point has been omitted from the data for clarity. The injections were set up in such a way that when injecting titrant the effective titrant concentration within the sample cell would slowly increase with each injection over a range in which saturation could be reached. For example, when injecting 11 mM Ca2+ into the sample cell using the previously stated injection volume pattern, by the third injection point the effective Ca2+ concentration within the sample cell would be approximately 0.22 mM and by the last injection point the effective Ca2+ concentration would be 2.5 mM.

Between experiments, the sample cell was cleaned by rinsing 5 times with 250 mL of an aqueous solution of 15% Contrad-70 and 15% methanol, followed by 5 L of exhaustive rinsing with Milli-Q water to remove any contaminating lipids. Titration and injection syringes were rinsed with methanol, followed by extensive rinsing with de-ionized water to remove any protein or lipid contaminants. Syringes were dried under N2 gas prior to storing.

DSC Supplemental Methods

To ensure that only the enthalpy of denaturation was monitored during the DSC experiments the lipid composition used was designed to undergo a gel state to fluid phase

transition with a transition midpoint at roughly 14°C, well below the transition temperature of the protein. To ensure that only the denaturation process was captured in the presence of lipids, scans were run on the lipids alone in the presence and absence of Ca2+, both of which show no transition in temperature range in which the data was collected. Excess ligand was intentionally used to characterize a specific subset of conformers (only conformers that have the ability to bind Ca2+, for instance) and not a heterogeneous population of conformations (a mixture of ligand-bound and unbound C2A). To obtain only the enthalpy of the denaturation process, a baseline scan was conducted using only the buffer and subtracted from the protein containing scans.

2.4 Results

2.4.1 Canonical dysferlin C2A is a type 2 C2 domain

We solved the X-ray structure of the canonical human dysferlin C2A domain to 2.0 Å resolution (Fig. 2a) by molecular replacement using the C2A domain of myoferlin (2DMH) as the search model. Human dysferlin C2A crystallized in 2.8 M Sodium Formate as two stacked trimers (Table 1). The overall topology of the canonical C2A domain is a Type 2 C2 domain (Fig. 2b) similar to the myoferlin C2A domain (2DMH) [28] and the otoferlin C2A domain (3L9B) [29]. Primary sequence alignment between dysferlin C2A and myoferlin C2A revealed that the two proteins share 66% sequence similarity between their C2A domains. The root mean square deviation (RMSD) between the C2A domains of myoferlin (1DMH) and dysferlin is 0.832 Å over all Cα atoms. Otoferlin C2A is structurally similar to dysferlin C2A; however, its vestigial Ca^{2+} binding loop 1 is significantly shorter than the homologous loop in either myoferlin or dysferlin [29].

The variant of C2A shows fundamental structural differences in the Ca^{2+}-binding pocket compared to canonical C2A. A comparison of the primary sequences of the canonical C2A domain and C2Av1 shows significantly more basic residues present within the variant C2A domain (Fig. 1c). At pH 7.4, the calculated isoelectric point (pI) for the canonical C2A domain is 7.66, while the calculated pI for C2Av1 is 10.4 [30]. The increase in the pI is due to five additional basic residues encoded by the alternate exon. To understand the impact of the alternate residues on the C2 structure, we solved the X-ray crystal structure of C2Av1 to 1.8 Å resolution using a monomer of our dysferlin C2A structure (4IHB) as the search model (Table 1). Like the canonical C2A crystal structure,

the C2Av1 domain crystallized with three molecules in the asymmetric unit (Fig. 3a). The overall structure of C2Av1 is similar to that of the canonical C2A domain as the RMSD between both isoforms is 0.493 Å over all Cα atoms (Fig. 3b). The resulting primary sequence substitution affects β-strand 1, loop 1 and β-strand 2. The most significant changes occur in Loop 1, which typically possesses the residues for Ca^{2+} and lipid binding in C2 domains. In addition, loop 1 of C2Av1 is one amino acid longer (Arg-20) than the homologous loop in the canonical C2A domain. Upon solving the crystal structure of the C2Av1 isoform, it became clear that the additional arginine residues form salt-bridges to each of the remaining Ca^{2+} binding residues (Fig. 3c). Arg-20 forms a salt-bridge interaction with Glu-75, Arg-21 coordinates with Asp-23, and Arg-81 with Asp-73. Interestingly, Asn-72 contributes to Ca^{2+} binding in the canonical C2A domain, but it is sterically blocked by the aliphatic chain of Arg-21. Therefore, we predict C2Av1 to have reduced potential for Ca^{2+} binding relative to that of the canonical C2A domain.

2.4.2 Ca^{2+} and phospholipid binding of the canonical C2A versus C2Av1

In the crystal structure of the canonical C2A domain, one of the six molecules in the asymmetric unit coordinates a single divalent cation that was scavenged from the crystallization solution (Fig. 2a,c). The residues that coordinate this cation have an average cation:ligand distance of 2.6 Å; therefore, we modeled and refined it as a calcium ion [31]. The position of this cation and its coordinating residues superimpose with the homologous X-ray structure of the Ca^{2+} bound C2 domain of phospholipase C-δ

(Grobler et al., 1996) (Fig. 2c). Given the structural homology between dysferlin C2A and phospholipase C-δ, we can infer the position of an additional cation-binding site. Therefore, Asp-18, Ile-19, Asp-21, Asn-40, Asp-71, His-72, and Glu-73 could contribute either side chain or main chain oxygen atoms to coordinate two divalent cations.

To quantify the ligand binding properties of the two isoforms, we measured the Ca^{2+} binding affinity of the canonical C2A and the C2Av1 using isothermal titration calorimetry (ITC). The canonical C2A domain possesses two distinct classes of Ca^{2+} binding sites; a single, high-affinity Ca^{2+} binding site with nanomolar binding affinity (K_D) (Fig. 4a, Table 3, Supplementary Fig. 2), and a set of independent sites with micromolar affinity, which dominate the binding isotherm (Table 2). The independent binding model used to fit the ITC isotherm for the canonical C2A domain predicts *n = 1* high affinity binding site and *n = 5* low affinity binding sites. However, from the structural analysis of the canonical C2A domain, only two Ca^{2+} binding sites can be accommodated by dysferlin C2A. We report a large error associated with the ITC data that corresponds to the high affinity Ca^{2+} binding events. Accurate characterization of these data are limited by the extreme steepness of the resulting titration curve [32], and by the amount of residual Ca^{2+} that can be removed from the system by Chelex-100 (BioRad). Any residual Ca^{2+} left in the buffers reduces the number of accessible titration points in the front of this titration curve. In addition, the measured value for the high affinity binding site is at the lower range for simple ITC (K_D ~ 1 – 10 nM) [32,33], so accurate measurements of Ca^{2+} binding affinity would be difficult. Interestingly, under similar experimental conditions, we do not observe Ca^{2+} binding by C2Av1 (Fig. 4a).

On measuring Ca^{2+} and phospholipid binding for both dysferlin C2A constructs, the Ca^{2+} binding affinity for the lower-affinity class of sites in canonical C2A domain increased from 53 μM to 15.5 μM in the presence of phospholipid PC:PS (60:40) as measured by ITC (Table 2) [34]. The ITC binding model fit to n = 2.1 Ca^{2+} sites. While C2Av1 has no substantial Ca^{2+} binding affinity in solution, it does show a robust avidity for negatively charged phospholipids (Fig. 4b). Once this domain binds phospholipids, a single, latent high-affinity Ca^{2+} binding site is uncovered (Fig. 4c, Table 3). When the affinity of the C2Av1 for membrane was measured in the presence of Ca^{2+}, a significant decrease was found (Fig. 4d). Thus, the high affinity Ca^{2+} in the C2Av1 domain stabilizes the domain in a similar manner as in the canonical C2A domain. This is required since the stabilization provided by salt-bridging is lost on membrane binding.

Conformational plasticity in the dysferlin C2A domain should be reflected in a low free energy of stability and concomitant stabilization by ligand as monitored by changes in the T_M (transition midpoint) determined from Differential Scanning Calorimetry (DSC) (Table 2). In the case of the canonical dysferlin C2A domain, the T_M in the presence of 5 mM EGTA was 42.2 °C. Occupancy of the high-affinity binding site of the canonical C2A domain in 1 μM Ca^{2+} showed only a slight increase in the T_M. In the presence of saturating Ca^{2+} (5 mM), the T_M increased to 54.9 °C. This net increase in T_M of C2A in the presence of saturating Ca^{2+} is consistent with ligand-dependent stabilization of the canonical C2A domain. With the C2Av1, we measured a T_M of 55 °C with or without Ca^{2+}, suggesting that Ca^{2+} does not bind or impart stability to C2Av1.

This is consistent with our ITC results, which show no significant Ca^{2+} binding by C2Av1 in solution (Fig. 4a).

2.4.3 Protein stability on the order of thermal energy (*k*T)

Conformational flexibility has been suggested as a mechanism for binding the wide variety of effectors in the C2A domain of synaptotagmin [23]. If the dysferlin C2A domains share this property, it should be reflected by an increase in the calculated stability of the domain upon ligand binding, as monitored by changes in the enthalpy (ΔH^o) and the transition midpoint (T_M) determined by Differential Scanning Calorimetry (DSC). In the case of the canonical dysferlin C2A domain, the T_M in the presence of 5 mM EGTA was 42.2 °C (Table 3). In the presence of saturating Ca^{2+}, the T_M increased to 54.9 °C. The net increase in T_M of C2A in the presence of saturating Ca^{2+} is consistent with ligand-dependent stabilization of the canonical C2A domain. With the C2Av1, we measured a T_M of 55 °C with or without Ca^{2+}, suggesting that Ca^{2+} does not bind or impart stability to C2Av1 in solution. This is consistent with our ITC results, which show no significant Ca^{2+} binding by C2Av1 in solution (Fig. 4a).

The free energy of stability ($\Delta G°$) is a measure of the energy barrier that limits a protein's ability to sample various conformations. For most proteins, $\Delta G°$ ranges from 5 to 20 kcal/mol; however, the stability of the C2A isoforms of dysferlin was found to be markedly lower than these typical values. In the absence of ligands, the $\Delta G°$ was measured to be 0.17 kcal/mol and 0.33 kcal/mol for the canonical C2A and C2Av1, respectively (Table 3). These low free energies are indicative of rapidly interconverting

folded to unfolded transitions. Assuming that the two-state model of unfolding is valid in this case (Supplemental), at 37 ˚C, 57% of the canonical C2A and 63% of the C2Av1 molecules would exist in a folded state in the absence of ligand. For comparison, in a protein solution with a ΔG° of 5 kcal/mol, 99% of all the protein molecules are in the folded state at this temperature.

The canonical C2A domain of dysferlin possesses a single high-affinity Ca^{2+} binding site that would likely be completely occupied at the resting muscle Ca^{2+} concentrations of ~50 nM [1]. To test the function of this high affinity site, we measured the stability of the canonical C2A domain in the presence of 1μM Ca^{2+}. Under these sub-saturating conditions, we observed only a slight increase in the T_M, but a marked increase in the measured enthalpy (Table 3). The increase in the enthalpy in the presence of 1 μM Ca^{2+} correlates with an increase in the stability (Fig. 5b, Table 3), and decrease in the plasticity of the domain. Therefore, we propose that the nanomolar Ca^{2+} binding site in the canonical dysferlin C2A domain predominantly serves a structural role. In the presence of saturating Ca^{2+}, we measure a further increase in ΔG° for the canonical C2A domain to 0.66 kcal/mol, which was also accompanied by a 12.7 °C increase in the T_M (Table 3). Interestingly, ΔG° for the C2Av1 domain also increased in the presence of Ca^{2+} (ΔG° = 0.73 kcal/mol), albeit not to the same extent as that measured in the canonical C2A domain.

The canonical C2A domain showed no significant increase in stability in the presence of phospholipids alone (PC:PS 60:40, Large Unilamellar Vesicles) (0.18 kcal/mol). However, with Ca^{2+} *and* phospholipid, the ΔG° for the canonical C2A

increased to 1.03 kcal/mol, consistent with Ca^{2+}-dependent phospholipid binding activity. In contrast, we measured a marked increase in ΔG° for C2Av1 in the presence of phospholipid (1.08 kcal/mol) (Fig. 5c, Table 3), but a decrease in the presence of Ca^{2+} *and* phospholipid (ΔG° = 0.45 kcal/mol) (Fig. 5d, Table 3). Regardless, both the canonical C2A and C2Av1, irrespective of ligation state, have exceptionally weak stabilizing interactions that sum to no more than twice thermal energy (*k*T or ~600 cal/mol at ambient temperature).

2.4.4 Electrostatic surface potential defines membrane interactions of the C2A domains of dysferlin

For well-characterized C2 domains, interaction with membrane occurs via an electrostatic switch (Fig. 6 e,f) and hydrophobic anchors located on loops 1 and 3. Since these loops also shape the Ca^{2+} binding pocket of the C2 domains of synaptotagmin, Ca^{2+} and lipid binding are effectively linked. Both isoforms of dysferlin C2A possess a single methionine residue (Met-75) on loop 3, but they lack a hydrophobic residue on loop 1. In addition, the surfaces of both the canonical C2A and C2Av1 possess a prominent positive electrostatic feature that could attract the domain to negatively charged phospholipids (Fig. 6). This feature is accentuated upon occupancy of the μM affinity Ca^{2+} binding sites (Fig. 6b), consistent with the Ca^{2+}-dependent phospholipid binding activity observed in other C2 domains. A strongly basic electrostatic surface appears to be a constitutive property of C2Av1 (Fig. 6c) and is consistent with the ability of the C2Av1 to interact with the membrane in the absence of Ca^{2+} (Fig. 4b).

2.4.5 C2A and C2Av1 co-localize in cultured C1C12 cells

In human muscle tissue, the ratio of canonical C2A to C2Av1 is roughly 4:1 [22]; however, the relative amount of each isoform varies among other tissues (Supplementary Fig. S-5). To determine the differences between the plasma membrane localization of full-length canonical C2A-dysferlin or C2Av1-dysferlin, we monitored the localization of transfected EGFP-dysferlin fusion constructs bearing each isoform in cultured C2C12 myoblasts by confocal microscopy. The efficiency of plasma membrane targeting of each isoform was assessed by flow cytometry. Transfected myoblasts were incubated with antibodies that selectively recognise an extracellular epitope, but are unable to cross the plasma membrane. Labelling experiments were performed at < 10 °C, to prevent vesicular trafficking and endocytosis of the surface-bound antibodies. These surface-binding experiments (immunohistochemistry, IHC and Fluorescence-activated cell sorting, FACs) showed that both constructs bear a similar intrinsic capacity to target the plasma membrane (Fig. 7a). Confocal microscopy shows similar levels of surface-expressed dysferlin, and similar subcellular localization of both isoforms as revealed by the auto-fluorescence of the EGFP fusion protein (Fig. 7a). Flow cytometry verified similar levels of plasma membrane expression for both C2A and C2Av1 isoforms by quantifying levels of surface-labelled dysferlin, relative to total levels of EGFP fluorescence (Fig. 7b).

2.5 Discussion

The ferlin proteins have been implicated in various cellular processes ranging from vesicle fusion to membrane repair. Dysferlin is the only member of this family that has been specifically adapted for Ca^{2+}-dependent membrane repair [35]. Over time, the first C2 domain (C2A) became the sole Ca^{2+}-dependent phospholipid binding domain in the dysferlin protein [36]; however, the alternative exon 1a exists within the *DYSF* gene, which encodes a C2A domain that utilizes Ca^{2+} differently. Alternate first exons in the *DYSF* gene are evolutionary preserved within the genomes of fish and mammals (data not shown), indicative of an essential role in the physiological function of dysferlin in eukaryotic cells. Further, the genomic sequences of otoferlin and myoferlin do not possess a homolog to exon 1a, despite their evolutionary relatedness with dysferlin. While myoferlin is structurally similar to dysferlin and is co-expressed in the same tissues, over-expression of myoferlin does not fully rescue the *dysferlin*-null phenotype [37]. These findings highlight the uniqueness of the dysferlin protein and the importance of examining the role of C2Av1 in membrane repair. To lay the groundwork for understanding the function of mixed canonical C2A-dysferlin and C2Av1-dysferlin proteins in the cell, we conducted extensive biophysical and thermodynamic analysis of both domains.

The crystal structure of dysferlin C2A together with structural homology to other cation-bound C2 domains argues for two discrete Ca^{2+} binding sites within the divalent cation-binding pocket of the canonical dysferlin C2A. However, our ITC binding model fits to two independent classes of binding sites instead of two discrete binding sites. The

first class corresponds to a single calcium ion with nanomolar affinity. This high affinity site is a unique feature of the C2A domain of dysferlin since C2 domains typically bind Ca^{2+} with micromolar affinity. The other class of sites in the canonical C2A domain of dysferlin binds with micromolar affinity and corresponds to five calcium ion sites. In total, our ITC analysis fits to six binding sites. This is clearly inconsistent with the cation binding data collected on other Ca^{2+} binding C2 domains. Our DSC analysis suggests that both dysferlin C2A domains have remarkably low stability. Such low stability is indicative of highly flexible structures, which can explore multiple conformational states [23,38]. Further, the Ca^{2+} binding loops may be in a receptive conformation to coordinate calcium ion, whereas the remainder of the domain may undergo rapid folded to unfolded transitions that could form additional Ca^{2+} binding sites (Fig. 8).

Unlike the Ca^{2+}-dependent canonical C2A domain, the alternative loop 1 sequence in C2Av1 effectively mimics the Ca^{2+}-bound canonical C2A dysferlin molecule in the cytosol. Indeed, the guanidino groups of Arg-20 and Arg-21 in the C2Av1 crystal structure may approximate the positions of the two calcium ions in the canonical C2A domain. While the C2Av1 domain does not binding Ca^{2+} in solution, it is nonetheless affected by Ca^{2+}. C2Av1 possesses a single high affinity Ca^{2+} binding site that is exposed upon binding membrane. The ITC data does not correlate to fully occupied binding sites in C2Av1 (Table 2); however, the thermodynamic parameters from the DSC experiments show evidence of C2Av1 Ca^{2+} interaction (Table 3). Interestingly, the thermodynamic stability of C2Av1 decreases upon Ca^{2+} binding proximate to a phospholipid surface; whereas, the canonical C2A domain gains stability under similar experimental conditions.

This suggests that C2Av1 is still sensitive to Ca^{2+} concentrations at the membrane surface, but it utilizes the Ca^{2+} signal differently. Therefore, the canonical C2A domain utilizes increasing cytoplasmic Ca^{2+} to initiate membrane binding, while the C2Av1 isoform uses high Ca^{2+} to alter its conformational ensemble to interact with membrane less efficiently (Fig. 5d).

Membrane binding model for dysferlin C2A isoforms

For other C2 domains, membrane binding involves electrostatic localization followed by membrane anchoring [39]. Comparison of the electrostatic surface potential of the two C2A domains of dysferlin suggests the initial phospholipid binding response is predominantly electrostatic in nature, due to the preponderance of basic charge distributed across their molecular surfaces (Fig. 6). This seems to be the case for both the canonical and C2Av1 domains of dysferlin as they show a clear preference for acidic phospholipids, but have no avidity for uncharged, PC-only membranes (Supplementary Fig. ##). (Fig. 8). It is therefore likely that the canonical C2A domain of dysferlin relies on a Ca^{2+}-dependent electrostatic switch mechanism. In contrast, C2Av1 cannot independently bind Ca^{2+}; therefore, the membrane-binding model for C2Av1 must be different. One possibility is that C2Av1 associates with membrane similar to the nPKC-ε C2 domain. Similar to C2Av1 it possesses membrane-binding properties that are not dependent on the surrounding Ca^{2+} concentration [40]. Loop 1 of the nPKC-ε C2 structure possesses two arginine residues that are predicted to snorkel into the membrane, while loop 3 anchors to the membrane via hydrophobic interactions from Ile-89 and Tyr-91 [40].

In dysferlin C2Av1, Met-77 on loop 3 could penetrate and anchor the domain to the acyl chains of the phospholipid, while the three basic residues on loop 1 (Lys-18, Arg-19 and Arg-20) could snorkel and associate with the acidic head group of the phospholipid (Schow et al., 2011).

Sensors of membrane damage

One of the most remarkable aspects of our thermodynamic analysis has been the exceptionally low stability of these domains. While we are not suggesting that the C2A domains of dysferlin are intrinsically disordered, they do share characteristics that classify them as weakly stable, but folded protein domains [41]. It is likely that the low stability is a key feature of these domains that accentuates dysferlins ability to mediate lipid fusion, or to interact with other molecules that assist in the membrane repair process. This is similar to the conclusion drawn concerning synaptotagmin function [23], as well as other membrane interacting domains [42]. We also predict that pathogenic mutations that occur within both isoforms of dysferlin C2A would be expected to perturb the ensemble distribution, thereby altering the functional response in a non-predictable manner. This also suggests that experiments to test the properties of dysferlin C2A using mutagenesis should be interpreted carefully.

The inverted ligand preference, ligand binding complexity, and thermodynamic uniqueness that we measure for both isoforms of the dysferlin C2A suggest the potential for diverse effector interactions that range from constitutive membrane interaction to Ca^{2+}-regulated interaction. The canonical C2A domain in dysferlin binds at least two

calcium ions, each with a specific function (Fig. 8). The high affinity site measured in the canonical C2A domain would be fully occupied at the resting, intracellular Ca^{2+} concentration of ~50 nM. Therefore, this site likely stabilizes the domain, while the lower affinity Ca^{2+} binding site mediates phospholipid binding and environmental sensitivity. At basal Ca^{2+} concentrations, C2Av1-dysferlin mimics Ca^{2+}-bound canonical C2A, and would dominate the initial interactions with the membrane and possibly the interactions with the C2A-dependent repair proteins. However, at high intracellular Ca^{2+} concentrations following membrane damage, canonical C2A-dysferlin could be recruited to the membrane, pooled from both canonical and variant isoforms, to assemble the repair complex rapidly. The mixed population of canonical and variant C2A isoforms that are present within cells could allow for graded-responses to membrane damage depending on the Ca^{2+} concentration and the ratio of C2A-dysferlin to C2Av1-dysferlin in any given cell type, enabling the cell to respond more effectively to membrane damage under a wide range of conditions.

Table 1: Crystallographic parameters

	Dys C2A	Dys C2Av1
Data Collection		
Space Group	I 1 2 1	$P3_121$
Cell Dimensions		
a,b,c (Å)	102.4, 70.7,118.3	71.2, 71.2, 137.5
α,β,γ (°)	90,113.4,90	90,90,120
Resolution (Å)	30-2.04	30 – 1.8
R_{sym}	7.3% (41.5%)	7.5% (53.5)
I/σI	11.1 (3.1)	26 (3.7)
Completeness (%)	99.3 (99.5)	95.7 (98.9)
Redundancy	3.6 (3.6)	6.6 (7)
Refinement		
Resolution (Å)	33.9 – 2.04	30 – 1.8
No. reflections	48842	36605
R_{work}/R_{free}	20.0/24.0	19.2/21.5
No. atoms		
Protein	5959	5515
Formate ions (FMT)	41	--
Ca^{2+}	1	--
Water	261	612
B factors (Å^2)		
Protein	49.27	26.8
Solvent	48.0	34.6
FMT/Ca^{2+}	43.5/65.9	--
R.M.S. deviations		
Bond lengths (Å)	0.008	0.024
Bond angles (°)	1.347	1.816

Table 2: Thermodynamic parameters for Ca^{2+} binding of the canonical dysferlin C2A and C2Av1 constructs in both the presence and absence of 60:40 POPC:POPS lipid vesicles. Fit assuming two sets of independent binding sites

	Ca^{2+} Only		Ca^{2+} in Lipid Background	
	C2A	**C2Av1**	**C2A**	**C2Av1**
n_1	0.9 ± 0.1	---	1.9 ± 0.2	0.5 ± 0.04
K_{d1}(μM)	0.006 ± 0.008	---	0.0010 ± 0.003	0.0020 ± 0.0006
K_1 (μM^{-1})	170 ± 240	---	1000 ± 300	500 ± 100
ΔH_1(kcal/mol)	-1.8 ± 0.6	---	-4.1 ± 0.4	0.1 ± 0.03
$T\Delta S_1$ (kcal/mol)	151.3 ± 0.7	---	7.8 ± 0.2	11.5 ± 0.1
ΔG_1(kcal/mol)	-10.9 ± 0.8	---	-11.9 ± 0.2	-11.4 ± 0.2
n_2	4.8 ± 0.2	---	2.1 + 0.4	0.1 ± 0.05
K_{d2} (μM)	53.2 ± 0.1	---	15.5 ± 2.1	375 ± 22
K_2 (μM^{-1})	0.019 ± 0.004	---	0.064 ± 0.017	0.0027 ± 0.002
ΔH_2(kcal/mol)	-19.3 ± 0.8	---	-2.2 ± 0.5	2.59 ± 0.09
$T\Delta S_2$ (kcal/mol)	14.8 ± 0.06	---	4.2 ± 0.4	7.11 ± 0.05
ΔG_2(kcal/mol)	-5.6 ± 0.1	---	-6.3 ± 0.8	-4.51 ± 0.03

Table 3: Summary of the DSC results. Dys C2A refers to the canonical C2A isoform, and DysC2Av1 the variant isoform. Where ΔG represents the free energy at 37°C, and n represents the number of replicates.

No Ligand(EGTA)						
	ΔH (kcal/mol)	**ΔC_P(kcal/mol)**	**T_M(°C)**	**ΔG(kcal/mol)**	**TΔS(kcal/mol)**	**n**
DysC2A	12.6±0.90	0.97±0.10	42.2±0.60	0.17±0.02	12.4±0.9	4
DysC2Av1	18.3±0.04	1.32±0.02	55.6±0.01	0.33±0.03	17.9±0.04	4
1 μM Ca^{2+}						
DysC2A	27.8±0.5	0.97±0.01	44.7±0.8	0.58±0.04	27.2±0.5	4
5 mM Ca^{2+}						
DysC2A	20.9±0.30	0.97±0.01	54.9±0.30	0.66±0.010	20.3±0.30	4
DysC2Av1	25.4±0.30	1.32±0.02	55.7±0.80	0.73±0.02	24.7±0.30	4
Phospholipid						
DysC2A	11.0±1.00	0.97±0.01	44.0±1.00	0.18±0.04	11.0±1.00	4
DysC2Av1	34.3±0.70	1.32±0.02	51.0±0.40	1.08±0.008	33.2±0.60	4
Phospholipid + Ca^{2+}						
DysC2A	27.4±0.30	0.97±0.01	55.0±1.00	1.03±0.03	26.4±0.40	4
DysC2Av1	19.9±0.20	1.32±0.02	52.2±0.01	0.45±0.008	19.5±0.20	4

Table-S1- Related to Table 2
Ratios between the calorimetrically determined and the Van't Hoff enthalpies ($\Delta H_{cal}/\Delta H_{vH}$).

	No Ligand	**Ca^{2+}**	**Lipid**	**Lipid and Ca^{2+}**	**1µM Ca^{2+}**
DysC2A	0.21	0.53	0.16	0.91	1.03
DysC2Av1	0.29	0.56	1.06	0.35	

Table-S2-Related to Table 2
Comparison of experimentally determined and predicted ΔCp values.

	$\Delta Cp_{(Experimental)}$ (kcal/molK)	**$\Delta Cp_{(Calculated)}$ (kcal/molK)**
DysC2A	0.97±0.10	1.62
DysC2Av1	1.32±0.02	1.61

Table-S3-Related to Table 2
Comparison of enthalpies (ΔH) and melting temperatures (T_M) obtained from DSC scans done at scan rates of 1.0°C/min. and 1.2°C/min.

No Ligand (EGTA)		
DysC2A	**ΔH (kcal/mol)**	**T_M (°C)**
Scan Rate 1.0°C/min	12.5±0.8	42.2±0.7
Scan Rate 1.2°C/min	12.52±0.01	44.0±1.0
DysC2Av1	**ΔH (kcal/mol)**	**T_M (°C)**
Scan Rate 1.0°C/min	18.3±0.5	55.6±0.01
Scan Rate 1.2°C/min	19.0±1.0	47.3±0.2
5mM Ca^{2+}		
DysC2A	**ΔH (kcal/mol)**	**T_M (°C)**
Scan Rate 1.0°C/min	20.9±0.3	54.9±0.3
Scan Rate 1.2°C/min	21.8±0.8	57.0±0.1
DysC2Av1	**ΔH (kcal/mol)**	**T_M (°C)**
Scan Rate 1.0°C/min	25.4±0.3	55.7±0.8
Scan Rate 1.2°C/min	25.7±0.3	50.0±0.2
Phospholipid		
DysC2A	**ΔH (kcal/mol)**	**T_M (°C)**
Scan Rate 1.0°C/min	11.0±1.0	44.0±1.0
Scan Rate 1.2°C/min	10.936±0.004	44.6±0.9
DysC2Av1	**ΔH (kcal/mol)**	**T_M (°C)**
Scan Rate 1.0°C/min	34.2±0.7	51.0±0.4
Scan Rate 1.2°C/min	34.2±0.7	50±2
Phospholipid and Ca^{2+}		
DysC2A	**ΔH (kcal/mol)**	**T_M (°C)**
Scan Rate 1.0°C/min	27.5±0.4	56.0±1.0
Scan Rate 1.2°C/min	28.3±0.2	57.6±0.3
DysC2Av1	**ΔH (kcal/mol)**	**T_M (°C)**
Scan Rate 1.0°C/min	19.9±0.1	52.2±0.1
Scan Rate 1.2°C/min	19.2±0.6	52.8±0.3

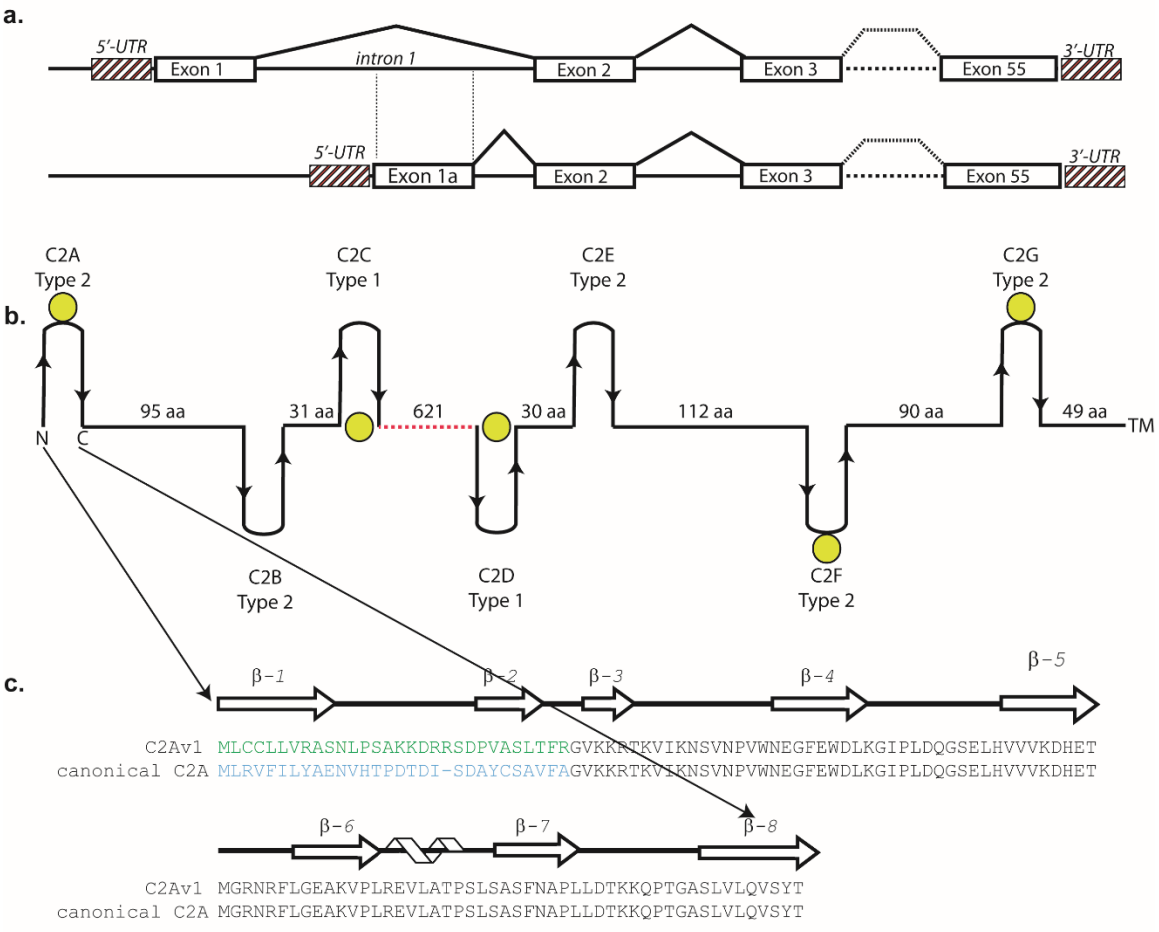

Figure 1: (a) Schematic of the partial exon structure of *dysferlin* C2A (Pramono et al., 2009) highlighting the position of the alternative exon 1a. The entire genomic DNA sequence possesses 55 exons. **(b)** Overall modular organization of the full-length dysferlin protein. The spacers between C2 domains have been scaled according to the predicted distances between C2 domains. Yellow spheres correspond to predicted Ca^{2+}-binding C2 domains in dysferlin based on conserved residues in the primary sequence alignments of our own domain alignments as well as those of Therrien, et al.(Therrien et al., 2009). If the N- and C- termini of the domain are on the same side of the domain as the Ca^{2+} binding pocket, then the domain is Type 1; if the N- and C- termini are in opposition to the Ca^{2+} binding pocket, then the domain is Type 2. The dotted red line corresponds to the DysN/DysC domain. **(c)** Primary sequence alignment of C2A variant 1 versus the canonical C2A domain of dysferlin. The arrows above the sequence correspond to residues that possess β-strand secondary structure, while the helical cartoon corresponds to residues with α-helical secondary structure.

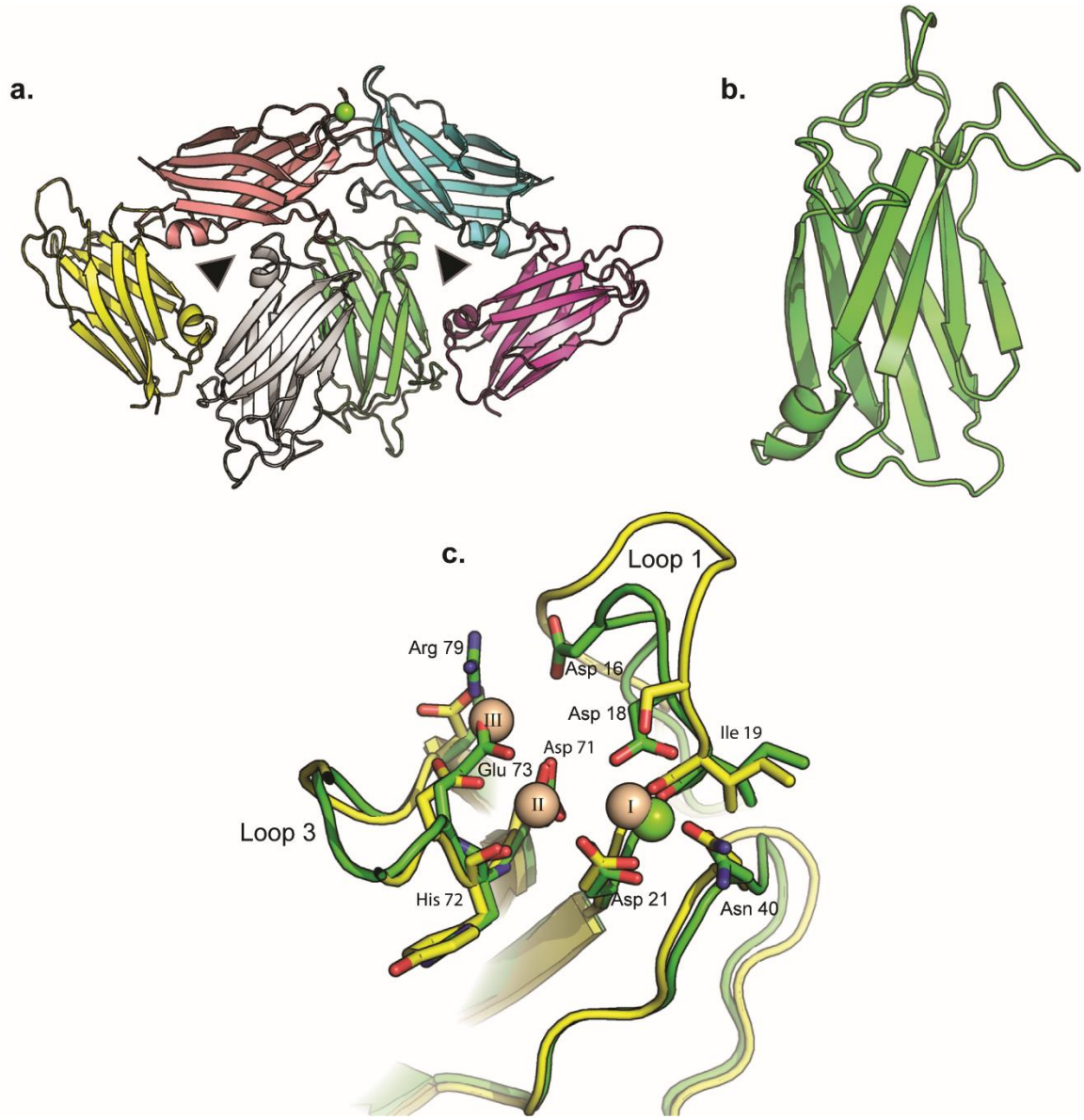

Figure 2: (a) Ribbon diagram of the stacked trimeric arrangement of the asymmetric unit of human dysferlin C2A. The green sphere is a single Ca^{2+} coordinated to one of the six domains in the asymmetric unit. Non-crystallographic three-fold symmetry operators are represented as triangles. **(b)** An isolated canonical C2A domain is shown in green. **(c)** Ca^{2+} binding sites in dysferlin C2A. The green sticks correspond to the dysferlin C2A structure. The green sphere corresponds to the high affinity Ca^{2+} found in the crystal structure. The yellow sticks correspond to the three La^{3+} described in the phospholipase C-δ1 C2 domain (Essen et al., 1997).

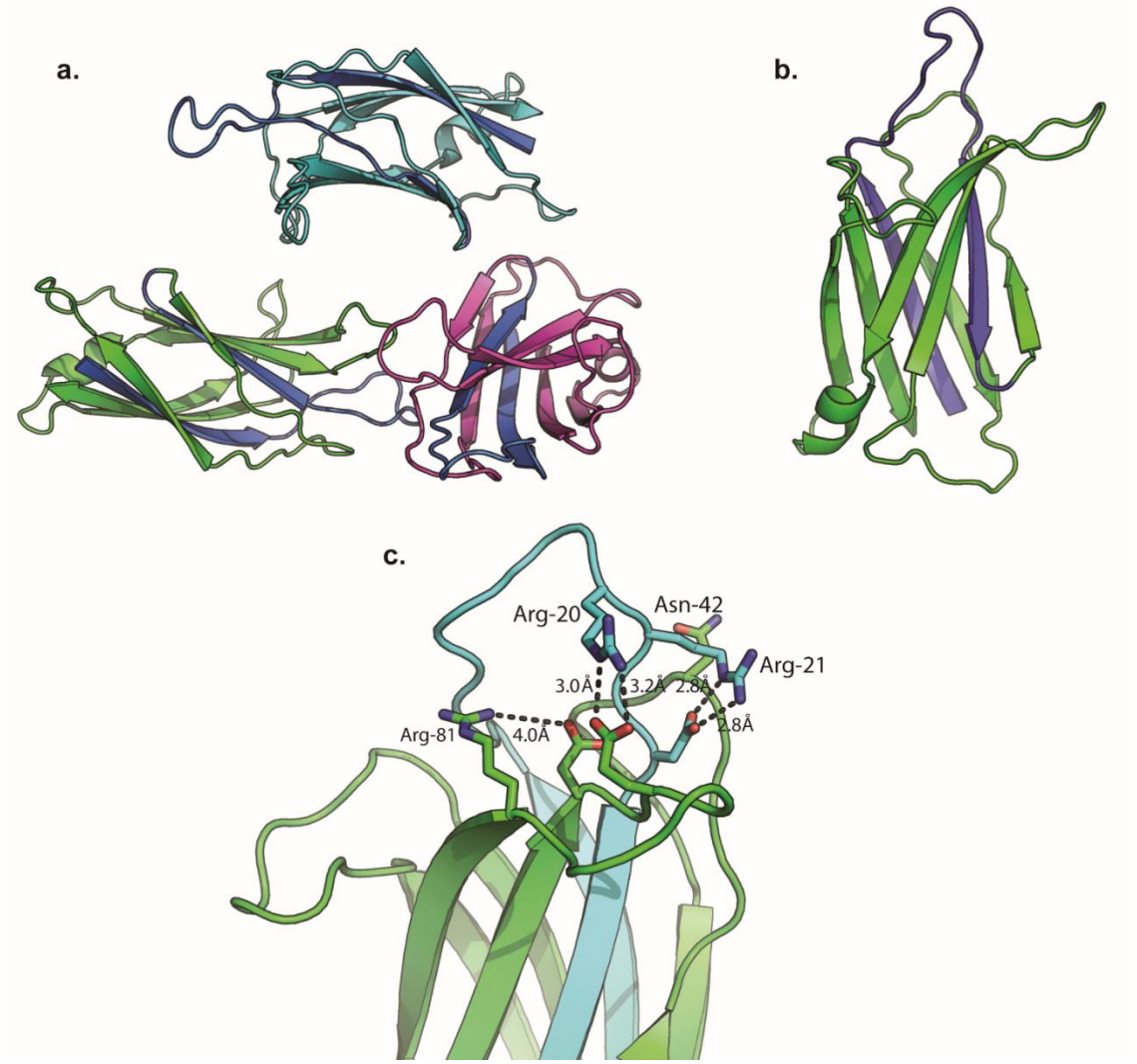

Figure 3: (a) Asymmetric unit of C2Av1. The variant residues are shown in blue. **(b)** Single C2Av1 domain. The variant residues are shown in blue. **(c)** Cation binding pocket of dysferlin C2Av1. The variant residues are shown in blue.

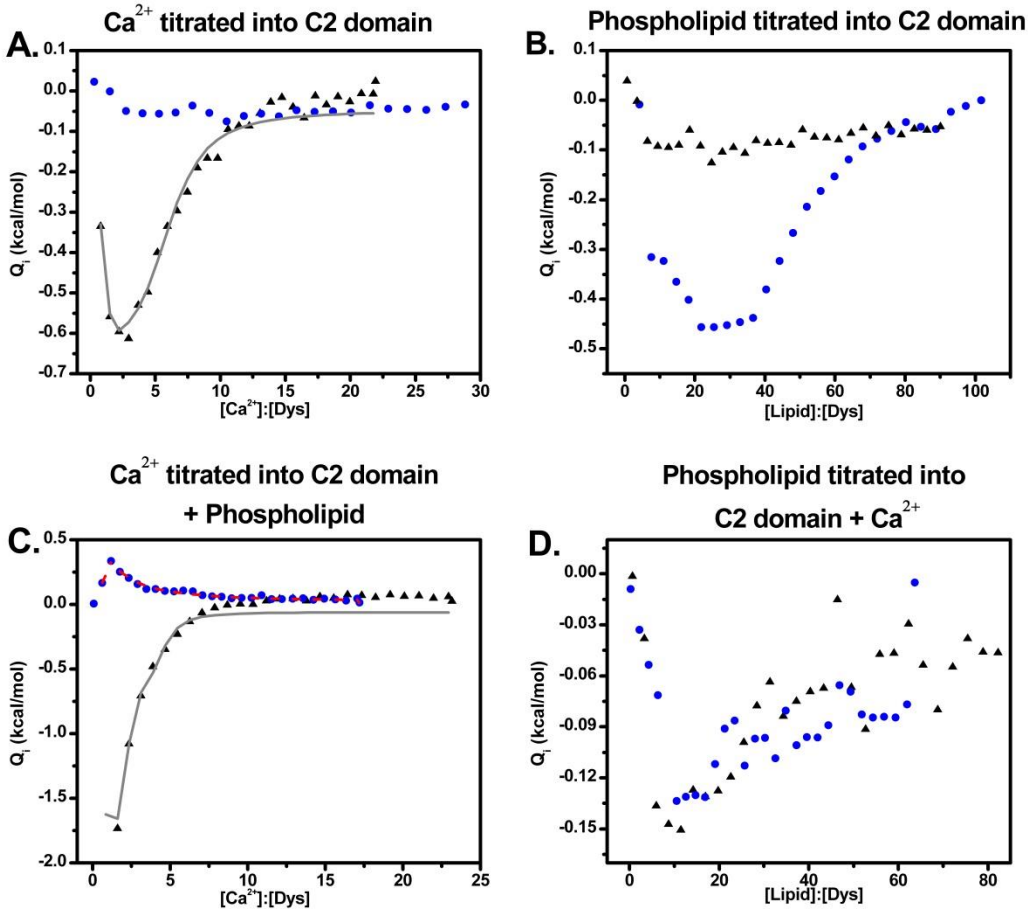

Figure 4: Binding profiles for the canonical dysferlin C2A and the C2Av1 domains. The canonical construct is shown above as open black squares while the C2Av1 construct is shown as blue circles. The fits of the canonical C2A data are shown as a grey line, while the fits of the C2Av1 data are shown as a dashed red line. All heats were normalized to the concentration of protein in the sample cell at each injection. **(A)** titration of 102 µM dysferlin C2A and the titration of 103 µM C2Av1 with Ca^{2+}. **(B)** titration of 50 µM dysferlin C2A and the titration of 56 µM C2Av1with LUVs made of a 60:40 mixture of POPC:POPS. **(C)** titration of 80 µM dysferlin C2A and the titration of 108 µM dysferlin C2Av1 with Ca^{2+} in the presence of 5 mM total lipid composed of LUVs made of a 60:40 mixture of POPC:POPS. **(D)** titration of 47 µM dysferlin C2A and the titration of 90 µM dysferlin C2Av1with LUVs made of a 60:40 mixture of POPC:POPS in the presence of 2 mM Ca^{2+}.

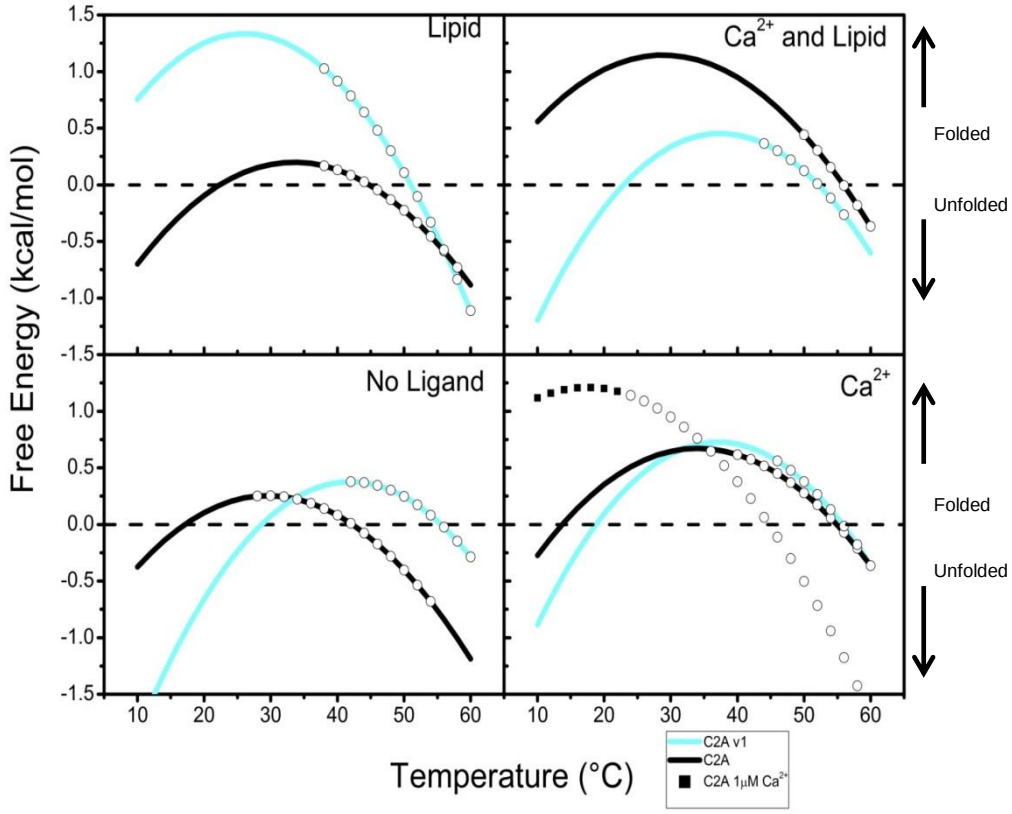

Figure 5: Free energy diagrams of dysferlin C2A domains in the absence of ligand (EGTA), Ca^{2+}, phospholipid, and phospholipid and Ca^{2+}. At any point along the curve the protein is found in both the native and denatured states, as the temperature changes so does the ratio between the two states. Where the curve crosses 0 kcal/mol on the y-axis the population of protein in the native and denatured states are equal to one another, below this the protein is found predominantly in the denatured state and above this is predominantly in the native state.

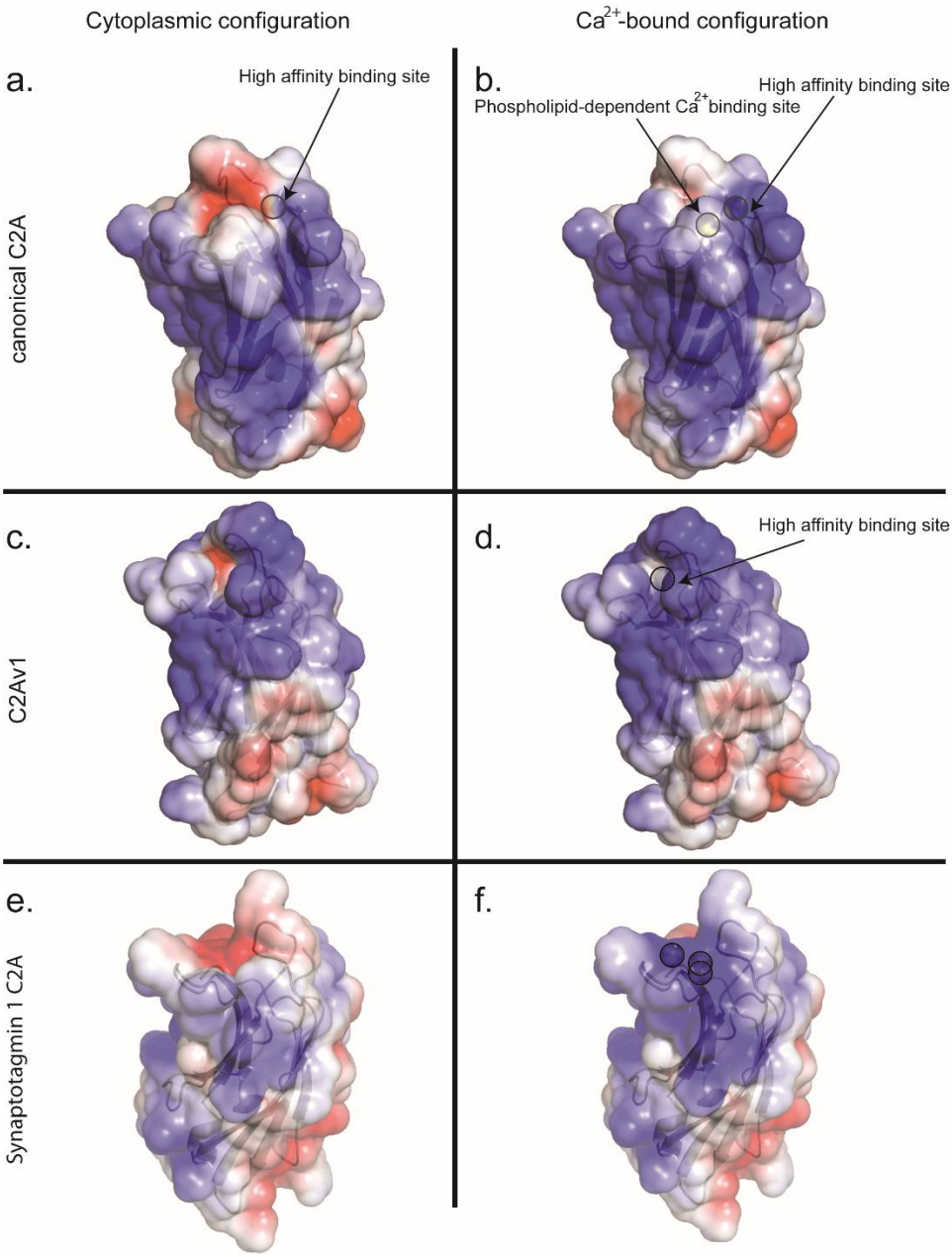

Figure 6: Electrostatic surface potential of the canonical C2A domain with a single, structural Ca^{2+} (top) and two Ca^{2+} and (bottom) C2Av1 with a single structural Ca^{2+}. Solvent accessible surface is colored by the calculated electrostatic potential and displayed at ± 3 *k*T/e. Calcium ions are highlighted by a circular outline. The electrostatic surface potential representation of synaptotagmin 1 C2A with and without Ca^{2+} (1byn) is shown for comparison.

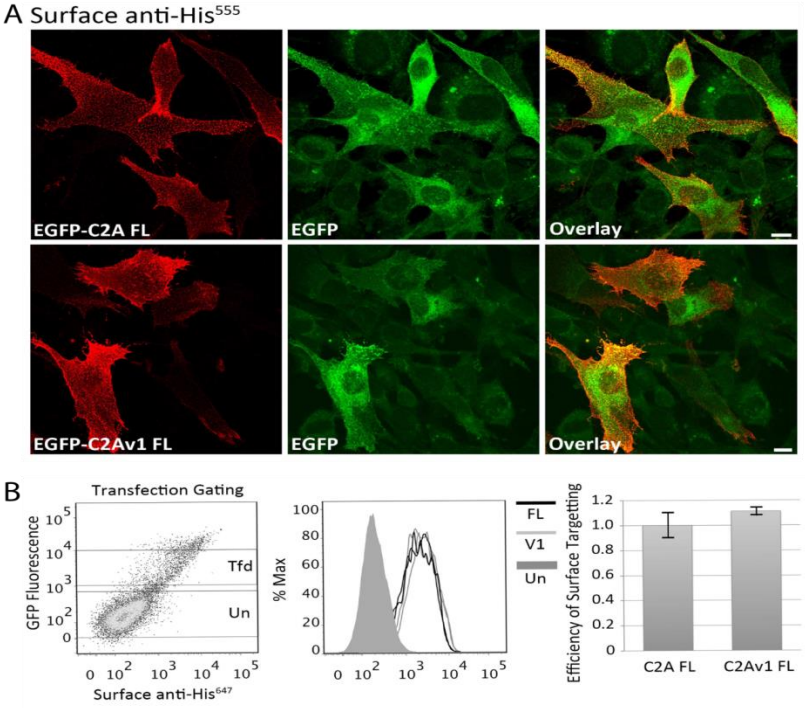

Figure 7: Full-length dysferlin proteins bearing alternately spliced canonical C2A or C2Av1 show similar intrinsic capacity to target the plasma membrane. **(A)** Representative confocal images showing surface expressed EGFP-$FL_{C2A}Dysferlin_{MycHis}$ (upper panels) or EGFP-$FL_{C2Av1}Dysferlin_{MycHis}$ (lower panels). Transfected C2C12 myoblasts were incubated with mouse anti-His to selectively label the extracellular His epitope. Labeling was performed on live cells at <10 ^{o}C to prevent endosomal internalization of surface-bound antibody. Cells were then washed, fixed, and labeled with goat anti-mouse^{555} (shown in red). Scale bar 10 μM. **(B)** Flow cytometry quantifies similar levels of surface expressed EGFP-$FL_{C2A}Dysferlin_{MycHis}$ or EGFP-$FL_{C2Av1}Dysferlin_{MycHis.}$ Transfected C2C12 myoblasts were dissociated from the culture dish and labeled as live cells at <10 ^{o}C with mouse anti-His followed by an anti-mouse^{alexa647} secondary antibody. Live cells were gated based on impermeability to propodium iodide (not shown). *Left panel*; Shows increasing levels of surface-labelled anti-His^{alexa647} (x-axis) is proportional to the levels of EGFP autofluorescence (y-axis). Gates for transfected (Tfd) and untransfected (Un) cells is shown; very highly transfected cells often show signs of toxicity and were excluded from analysis. *Middle panel*; Histogram showing similar normal distributions of surface bound anti-mouse^{alexa647} in populations of transfected cells expressing FL_{C2A} or FL_{C2Av1} constructs, from duplicate samples labeled on the same day. *Right panel*; Pooled data from three experiments performed in duplicate showing similar levels of surface-labeled anti-His^{alexa647} relative to EGFP autofluorescence for both FL_{C2A} or FL_{C2Av1} constructs. To allow comparison between constructs transfected and labeled on the same day, values derived from canonical C2A were normalized to 1.

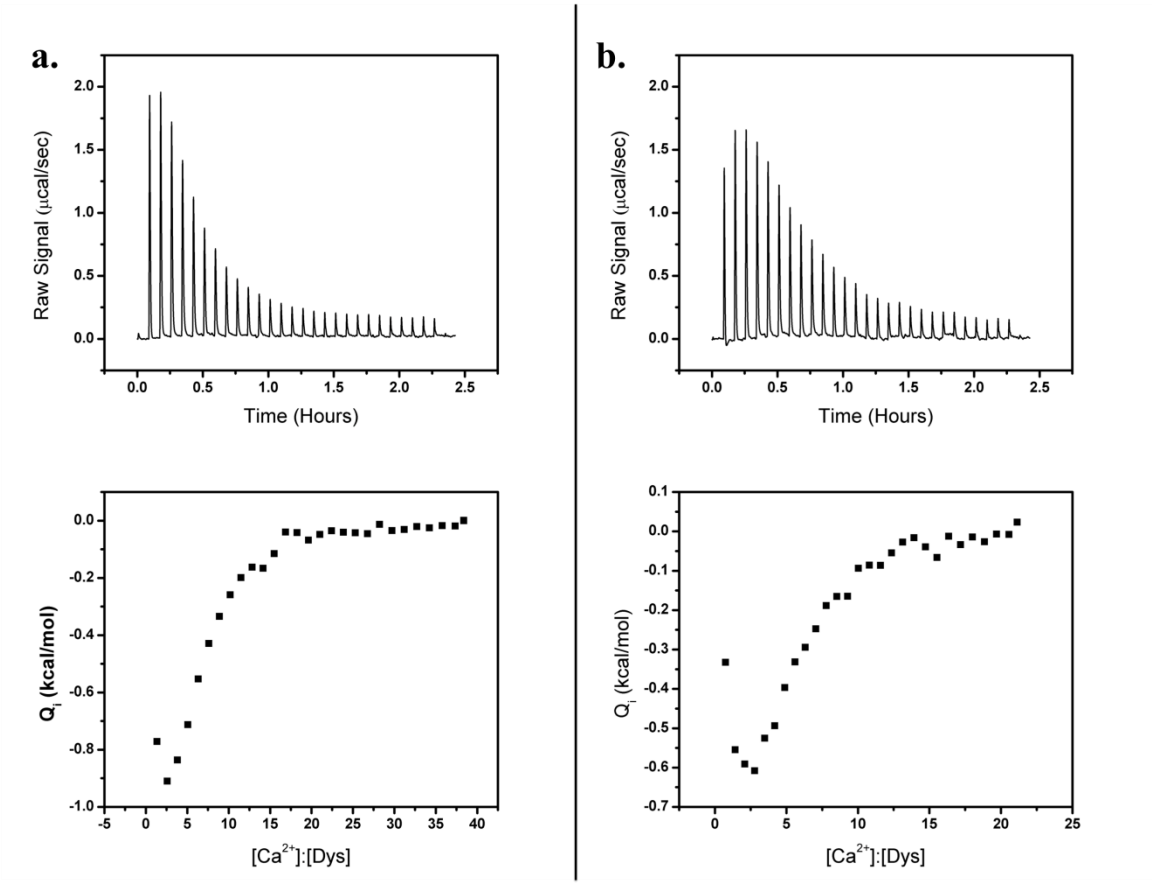

Figure -S1-Related to Figure 4

Replicate titrations of Ca^{2+} injected into canonical C2A. The upper panels show the raw heat rate for the titration while the lower panels show the integrated heats for each injection point. The titration shown in (b) was run at a lower ligand to protein ratio than the titration in (a) to attempt to better characterize the curve at the beginning of the titration that describes the high affinity Ca^{2+} binding sites.

a. 83 uM C2A titrated with 10.82 mM Ca^{2+} in the titration syringe.

b. 103 uM C2A titrated with 7.4 mM Ca^{2+} in the titration syringe.

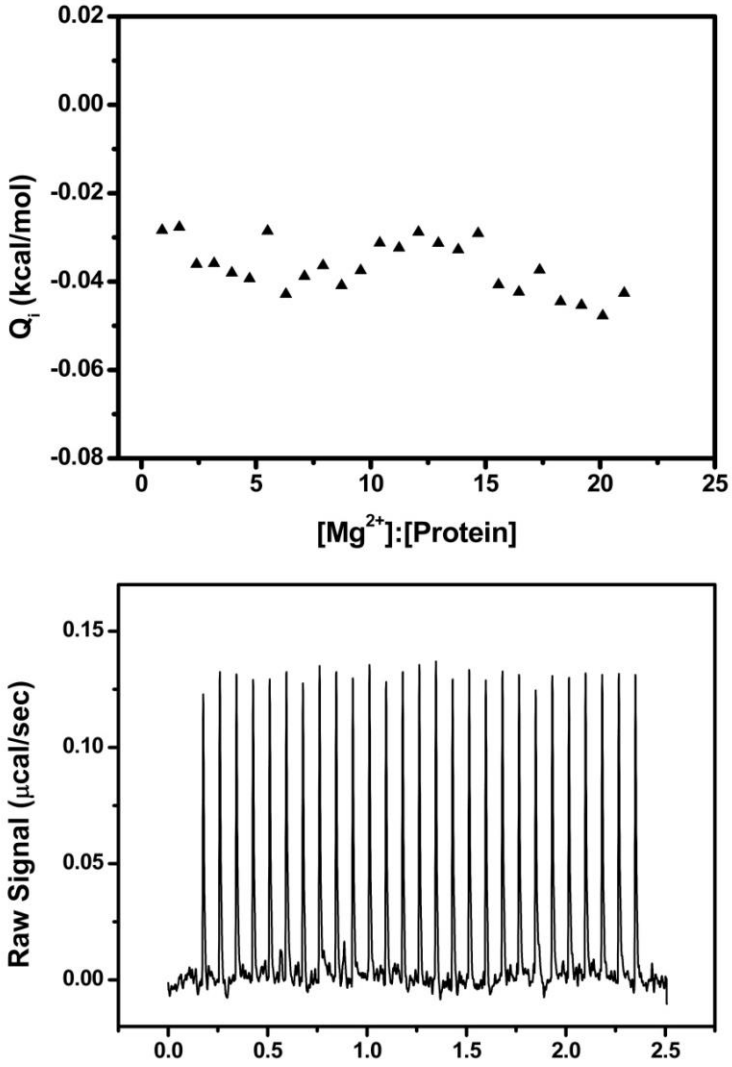

Figure-S2-Related to Figure 4.
Mg2+ binding of Canonical C2A domain[43]. Results of the ITC titration of 10 mM Mg^{2+} into 100 μM canonical C2A. The upper panel shows the integrated heats of each injection point, while the lower panel shows the raw heat rate. No appreciable binding is measured**.**

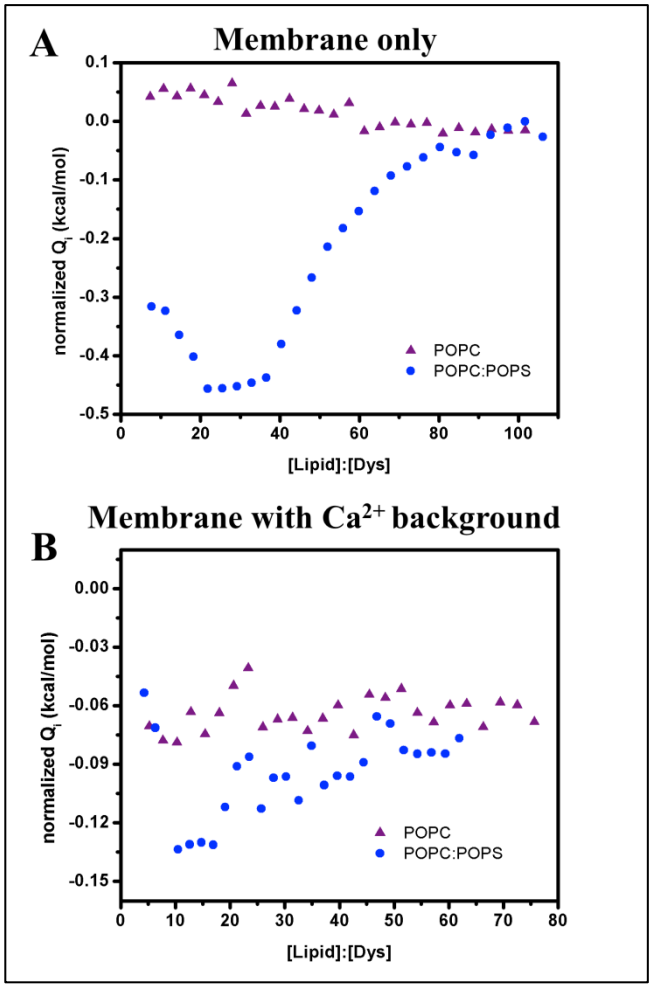

Figure-S3-Related to Figure 4. Phospholipid preference for C2Av1.

ITC binding profiles of C2Av1 with 60:40 POPC:POPS lipid vesicles (blue circles) and POPC lipid vesicles (purple triangles) in both the absence (A) and presence (B) of calcium ions. All heats were normalized to the concentration of protein in the sample cell at each injection.

A. Titration of 60 µM C2Av1 with POPC and the titration of 57 µM C2Av1 with 60:40 POPC:POPS.

B. Titration of 90 µM C2Av1 with POPC in the presence of 2 mM Ca^{2+} and the titration of 90 µM C2Av1 with 60:40 POPC:POPS in the presence of 2 mM Ca^{2+}.

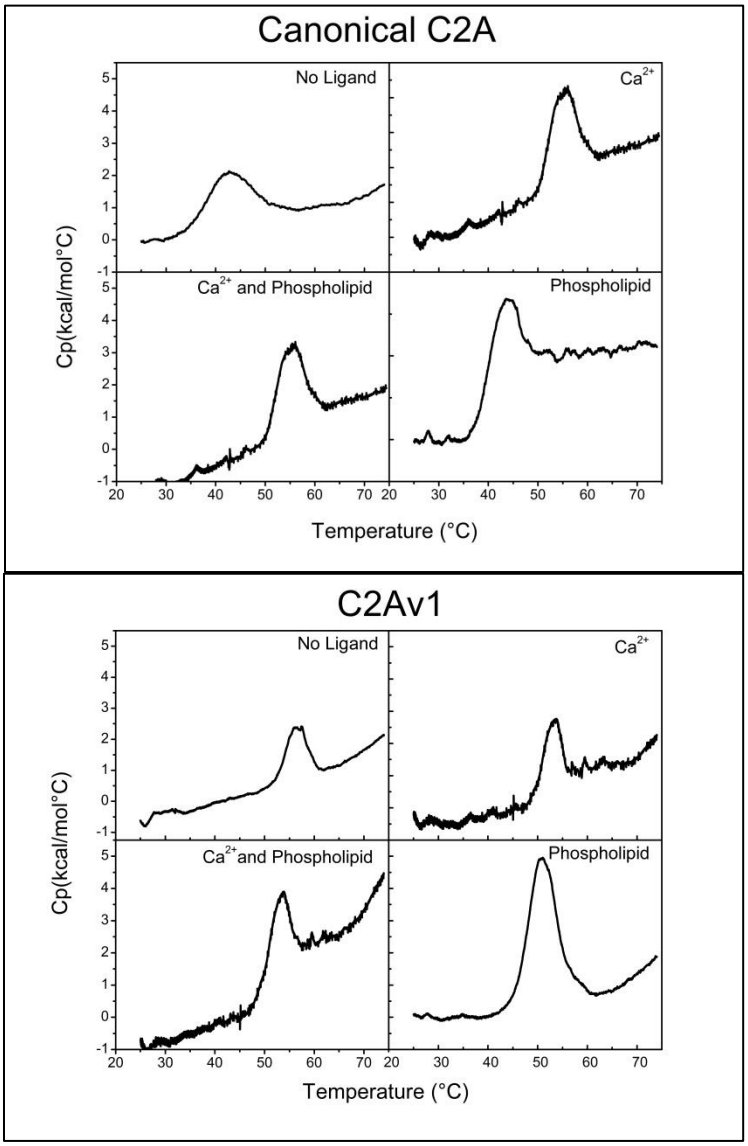

Figure-S4-Related to Table 2

Denaturation profiles of the canonical C2A (upper panels) and C2Av1 (lower panels) domains obtained from DSC. The high amount of noise present in the baselines of the scans is likely result of the low signal received throughout the denaturation of the domains.

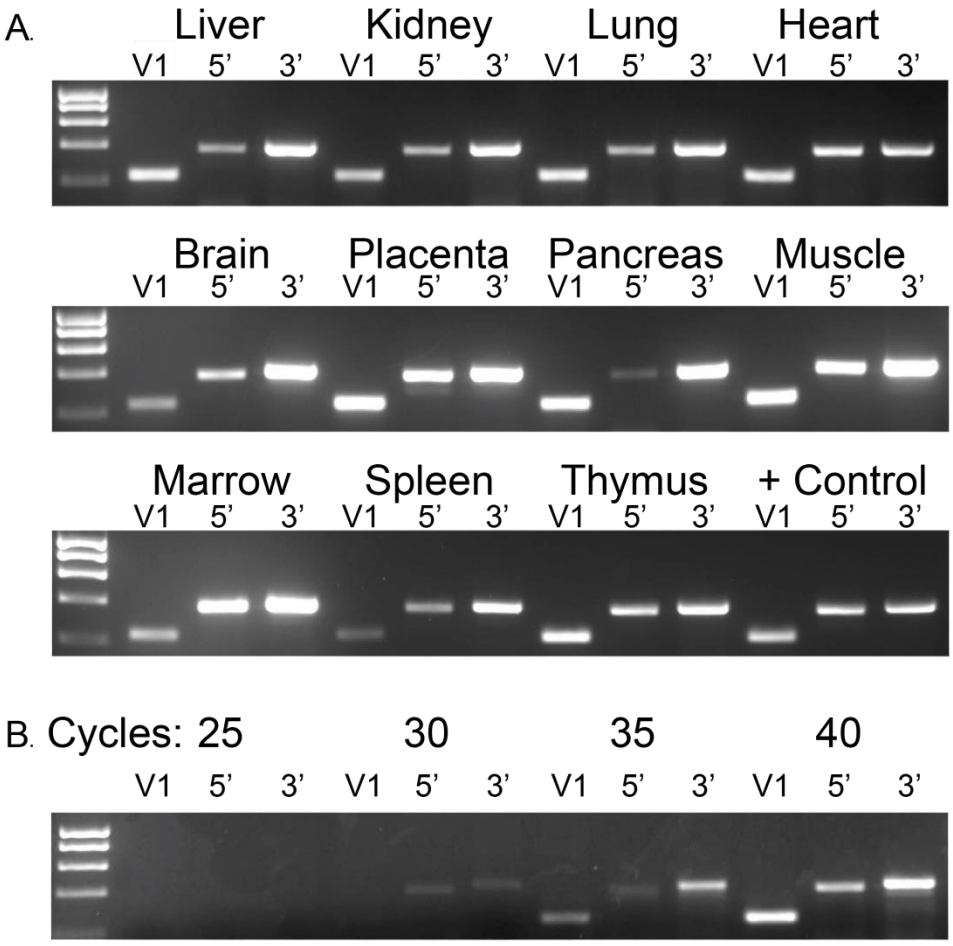

Figure-S5-Related to Figure 7. Tissue expression of dysferlin C2A and C2Av1

a) C2Av1 and canonical C2A are co-expressed in most tissues.

Specific primers were used to amplify canonical C2A and C2Av1 from human cDNA panels (Human Multiple Tissue Panels I and II, Clontech). Canonical C2A: Forward (5'UTR) 5`-GGTGGAAGATGAGCAGAAGC-3`, Reverse (Exon 6): 5`-TTCTTCACCCCTGCAAACAC-3'. C2Av1: Forward (5'UTR) 5`-AAGGCGACAGCTCTCTTGG-3`, Reverse (Exon 3): 5` CTTCTTCACCCCTCGGAAAG 3`. PCR products were isolated using Qiaex II beads (Qiagen) and verified by sequencing (Australian Genome Research Facility). PCR was performed using Premix buffer D (Illumina) and Taq polymerase (Invitrogen). Products were electrophoresed on a 2% agarose gel (Amresco) with hyperladder I (Bioline) to determine size. **V1**: PCR fragment from 5'UTR of C2Av1 to exon 3. **5'**: PCR fragment from 5'UTR of canonical C2A to exon 6. **3':** PCR fragment from Exon 53 to the 3'UTR.

b) Standard curve showing non-saturation of PCR amplification conditions.

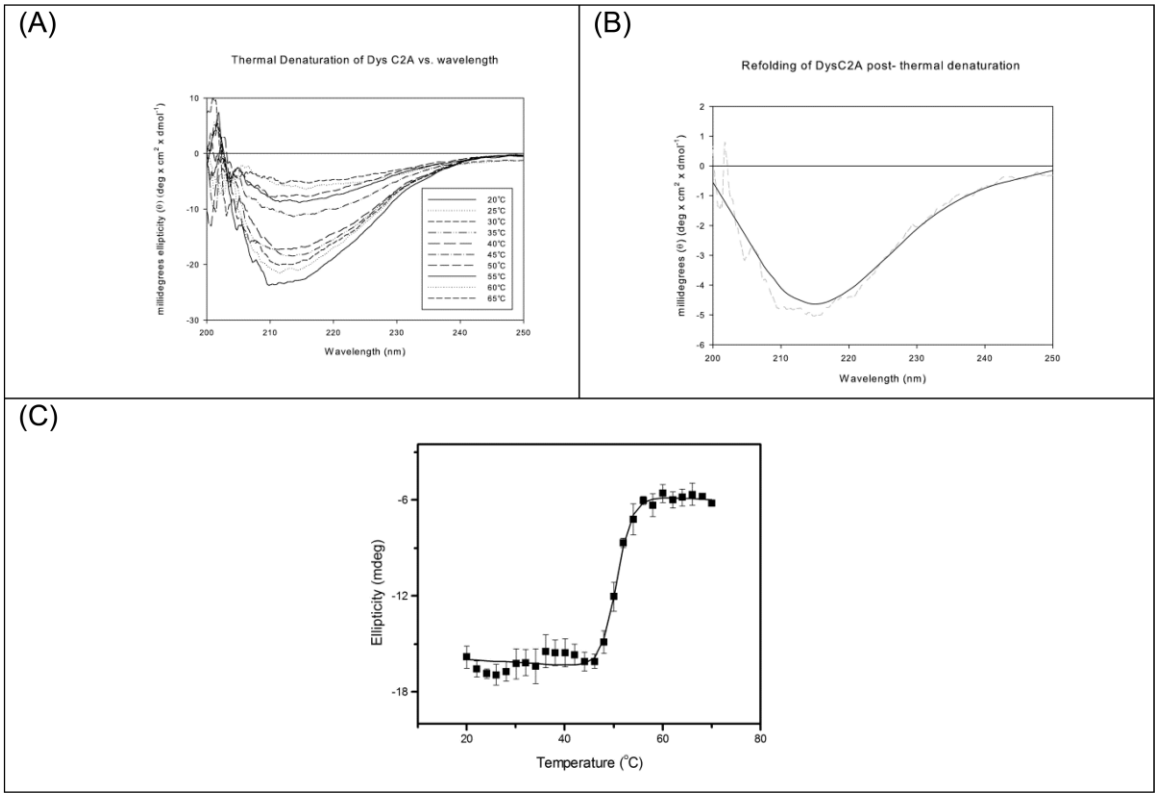

Figure-S6-Related to Figure 5 and Table 2b

A more classical approach to demonstrate refolding in C2A, albeit very inefficiently, is to analyze the circular dichroism (CD) signal indicative of β-sheet secondary structure vs. temperature.

Figure (A) shows the raw, un-smoothed CD signal (200 nm – 250 nm) from 30 μM of purified dysferlin C2A in 5 mM CaCl2, 20 mM MOPS, pH 7.4, 200 mM KCl vs. a temperature gradient from 20 °C to 65 °C. While the buffer composition is not ideal for high-resolution CD measurements, it is consistent with the buffer conditions used in our DSC experiments. The melting of C2A is consistent with the denaturation of the protein vs. temperature. After the protein fully denatured at 65 °C, the protein sample was cooled to 20 °C, centrifuged to remove all precipitated C2A, and then re-measured. Figure (B) shows the raw CD signal as a grey dashed line, and the smoothed signal as a solid, black line. (C) CD signal monitored at 212 nm vs. temperature to illustrate the transition from fully folded to fully unfolded canonical dysferlin C2A protein

Chapter 3: Randomly Organized Lipids and Marginally Stable Proteins: A Coupling of Weak Interactions to Optimize Membrane Signaling*

*Note: The following chapter was reproduced in its entirety in accordance with rights given to authors by Elsevier publications from the following article: Rice, A. M., Mahling, R., Fealey, M. E., Rannikko, A., Dunleavy, K., Hendrickson, T., Lohese, K. J., Kruggel, S., Heiling, H., Harren, D., Sutton, R. B., Pastor, J., and Hinderliter, A. (2014). Randomly organized lipids and marginally stable proteins: A coupling of weak interactions to optimize membrane signaling. *Biochimica et Biophysica Acta*, *1838*(9), 2331–40. doi:10.1016/j.bbamem.2014.03.005

With contribution of this author being the differential scanning calorimetry, tryptophan fluorescence and circular dichroism studies of the C2A domain of cotton Synaptotagmin I, and the C2A domain of human synaptotagmin I construct containing residues 96-265.

3.1 Introduction

A cell membrane is a pliable and responsive surface. Changes in the local environment of a given lipid are propagated in all directions within a leaflet by the weak cooperative interactions between each lipid molecule and its six nearest neighbors [44] . This type of propagation behavior suggests that the membrane has great signaling potential. Another key facet to consider with regard to biological membranes and signaling is the high degree of lipid species diversity. The distribution and diversity of lipids in eukaryotic membranes is thought to maintain the system in a nearly random distribution which, according to information theory [45], maximizes the amount of information that can be cooperatively propagated in a signaling event because it is not biased in any one direction as in a more ordered system. Together, the weak cooperatively of lipid molecules and their nearly random distribution suggest the membrane constitutes a major information transducer in the cell.

To transduce the vast array of information encoded within the mosaic membrane

into the cell interior requires both transient organization of the signaling lipid species and a recipient protein that further senses and propagates the message. A lipid mixture near a critical point, teetering on a phase boundary between random distribution and restricted domain, could fulfill the first requirement. Domain formation can increase the probability of a particular signaling event, for instance, by providing platforms for protein-protein interactions that initiate the intracellular portion of a signaling cascade. In this sense, transient order in lipid organization allows for a discrete message to be propagated at levels above background thermal noise, or in other words, above the milieu of all other possible messages encoded in the membrane lipid distribution.

Subsequent detection and propagation of such a wide range of membrane-encoded messages would seem to require a protein with complementary features; the protein would need to have a tendency towards random distributions so as to maximize the amount and diversity of information that can be recognized and propagated. Intrinsically disordered proteins are one well-known class of proteins with this tendency. Intrinsically disordered proteins are natively unfolded and have significant structural and conformational plasticity making them uniquely sensitive to differences in local environment, not unlike the near random but pliable membrane surface. Moreover, intrinsic disorder can facilitate propagation of information within the body of a protein [46]. When we measured the stability of a specific class of proteins by thermal denaturation we found that these proteins, whose functional role is directly linked to membrane biology, have features of intrinsic disorder; these proteins retain some secondary structure, but are marginally stable or nearly disordered [23,47,48]. Specifically, this seems to be the case with

C2 domains of synaptotagmin I (Syt I) in neurons (involved in exocytosis) and the C2 domains of dysferlin (Dys) in muscle (responsible for sensing and repairing membrane damage). Currently, there are 14496 C2 domains annotated in 9258 protein sequences within the SMART non-redundant database [49]. It is unknown if this marginally stable behavior is a general feature of C2 domains, but denaturations carried out previously on various C2 domains from protein kinase C also converge on this finding [50]. Moreover, when we denatured the C2A domain of cotton Syt I, we found it had the same hallmarks as human Syt I, suggesting potential conservation across phylogenetic kingdoms.

A new potential rule for membrane signaling emerges when we simultaneously consider the near disordered nature of membrane lipids as well as membrane-sensing proteins, namely maximum flow of signaling information through the membrane and into the cell is optimized by the cooperation of the two near-random distributions of membrane lipids and proteins. Indeed, when lipid species diversity and protein intrinsic disorder are compared, both increase with organism complexity [51,52]. While at first glance, this hypothesis may seem to imply uni-directionality of information flow (a marginally stable protein only decodes the information of the membrane), the mechanism applies in both directions. Protein interactions with membranes can induce membrane domain formation (order) if the protein has specificity for some of the lipids and these lipids are distributed non-ideally [53,54]. If, however, the protein's interaction with the membrane depends on intracellular signals (such as calcium ion), then the protein becomes a means to relay intracellular conditions back to the membrane potentially for amplification via weak cooperative lipid-lipid interactions. The end result is reciprocal

exchange of information.

Here we explore our hypothesis that the distribution of lipids within the eukaryotic membrane is coupled to interactions with weakly stable but structured proteins to transduce and modulate signaling information. We first use experimental data from the literature on membrane phospholipid compositions in stimulated and unstimulated mast cells to calculate information content encoded within different lipid compositions (excluding cholesterol as a component) as well as their associated acyl chains and head groups [55]. We then complement these findings with recent and new measurements of protein stability and membrane disruption in which membrane lipid composition (and thus information content) is a variable. We find that C2 domain stabilities are highly sensitive to the information content of lipid compositions and undergo correlated changes with membrane information content.

3.2 Materials and Methods

3.2.1 Protein Constructs

The C2 domains studied were constructs derived from human Syt I, cotton Syt I, and Dys. The only C2A construct of human Syt I used for experiments in this study contained residues 96-265. In the top half of Table 3, thermodynamic parameters are reported for a shorter human Syt I C2A construct containing residues 140-265. Additional residues in the 96-265 C2A construct correspond to the region between C2A and Syt I's single transmembrane helix. The human Syt I C2B domain included residues 272-422. Of the two C2 domains in cotton Syt I, only the C2A domain was studied. Purification of these constructs was carried out as previously described [23,47,48].

3.2.2 Preparation of lipid samples

All lipids were purchased from Avanti Polar Lipids (Birmingham, AL). Samples without cholesterol were prepared as previously described [23]. Cholesterol-containing samples were prepared by aliquoting lipid stocks into a 4:1 mixture of chloroform:methanol followed by rotary evaporation using a Buchi R-215 at a temperature between 50-60°C. The lipid films were then placed under vacuum for a minimum of 8 hours to remove excess solvent and hydrated with the appropriate buffer. LUVs were prepared by hand extrusion using a 0.1μm filter. SUVs were prepared through multiple rounds of extrusion with filters of gradually smaller pore sizes ending with a 0.03μm pore size.

3.2.3 Differential Scanning Calorimetry (DSC)

DSC experiments as well as both scan rate and concentration dependent controls were performed on a NanoDSC (TA Instruments, New Castle, DE) as described previously [23,47,48]. All scans were conducted in chelexed 20 mM MOPS, 100 mM KCl, pH 7.5 using saturating ligand concentrations. All scans with lipid contained one of the following: 1) LUVs of 60:40 POPC:POPS; 2) LUVs of (80:20):30 (POPC:POPS):cholesterol; 30 mole percent cholesterol was doped on top of a mixture POPC:POPS (80:20) 3) LUVs with the mixture shown in Table 4 plus 45 mole percent cholesterol doped in; or 4) SUVs of 3). The concentration of the calcium stock solution used for all scans was verified using both a calcium ion selective electrode (ThermoScientific) and a BAPTA chelating assay (Invitrogen/Molecular Probes, Eugene, OR). The concentration of all lipid stock solutions was confirmed through a phosphate assay according to standard protocols [23]. For the experiments reported in this study the human Syt I C2A construct was found have an average reversibility of 93% except in the presence of LUVs composed of the membrane domain forming mixture in which the reversibility was found to be 46%. For a comparison between consecutive denaturation scans see figure 8. For a justification of the thermodynamic parameters reported for the other domains discussed please see references 4-6.

3.2.4 Tryptophan Fluorescence (TF)

TF experiments were performed on a Lifetime Spectrometer (Fluorescence Innovations, Bozeman, MT) using nanomolar protein concentrations as previously

described [23,47,56]. No time-resolved measurements were made; instead the integrated intensity of the lifetime decay was used to monitor intrinsic tryptophan fluorescence (excitation and emission wavelengths of 295 and 340 nm, respectively). Buffers, Ca^{2+} stocks, and lipid samples used were identical to that described above in section 2.4. Percent reversibility was measured by comparing the integrated fluorescence lifetime intensity of the sample before heating and after cooling. Due to the exceptionally low stability of the cotton Syt I C2A domain, no change in tryptophan fluorescence could be detected for these constructs. As a result, only the Syt I C2 domains were studied using this method.

3.2.5 Determination of Denaturation Parameters

All denaturation parameters were determined through either fitting the denaturation profiles as described in reference [47] or through direct determination of the enthalpy of denaturation (ΔH), change in heat capacity (ΔC_p) and melting temperature (T_m) from the DSC denaturation profiles as previously described. For an in-depth explanation on the determination of the denaturation parameters please see references [47] and [48]. The need to use two methods for determining the denaturation parameters arises because at the lower enthalpy values the model fails to accurately recapitulate the experimentally obtained data, the fits presented in figure 9 are obtained for the human synaptotagmin I C2A construct containing residues 96-265 under several different conditions. However, the denaturations done in the presence of the membrane domain forming mixture were unable to be accurately recapitulated by the model as a result of

their complexity, however, this unique shape of these curves is reproducible as can be seen in figure 10. As such the parameters reported for those conditions were determined as described in reference[48].

3.2.6. Circular Dichroism (CD)

CD experiments were performed on a Jasco CD Spectrometer (Annapolis, MD), using 15µM of the Syt. I C2A domain (residues 96-265) with 700µM LUVs composed of POPC:POPS (60:40) and 1mM Ca2+ in a 0.1 cm quartz cuvette. The spectrum was obtained in the same buffer system described in sections 2.3 and 2.4. Data points were collected in 1 nm increments and averaged over 5 acquisitions. Spectra collected were corrected for any buffer contributions by subtracting a buffer scan from the corresponding protein scan.

3.2.7. Carboxyfluorescein (CF) Release Assay

LUVs containing carboxyfluorescein dye were prepared as previously described [57 23]. To determine the effect of protein binding on membrane leakage, the dye signal was monitored with excitation and emission wavelengths of 492 nm and 515 nm, respectively, as a function of time and temperature, with one addition of ligand and one addition of protein. In the absence of ligand or protein, 20mM MOPS, 100mM KCl, 0.02% NaN_3 was added to obtain constant increases of volume at each addition of solution. All fluorescence measurements were performed on a Fluorolog 3 double excitation and double emission monochromoter (Horiba Jobin Yvon) in a 500µL quartz cuvette.

Appropriate temperatures were chosen to enhance membrane transition and perturbation of the LUV lipid compositions listed in Table 4, on which the experiments were performed [58]. Time and temperature dependent experiments were performed for a period of 60 minutes using a temperature controlled water bath (Pharmacia Biotech Multitemp III). The cuvette contained 300µL of liposome sample at the start of the fluorescence scan, 100µL of buffer or Ca^{2+} solution titrated in after 15 minutes, and 85µL of buffer or protein titrated in after 30 minutes. The cuvette was placed in the fluorometer and the scan was immediately started at constant temperature (20.4°C). Buffer or Ca^{2+} solution was added at 15 minutes, followed by buffer or protein at 30 minutes. At the time of the second injection, the temperature was set to increase to 75°C and the change in CF fluorescence was monitored in order to confirm consistency between experiments as well as dye release. Within the cuvette the concentration of liposome was 200µM and concentration of Ca^{2+} ion solution was 3mM after its addition at 15 minutes. A 50.6µM stock sample of the Syt I C2A domain (encoding residues 96-265) was added in one increment of 85µL to obtain a concentration of 13.33µM. Triton X-100 detergent was added after each scan to completely disrupt the membrane and confirm the presence of CF within the liposome as well as determine the maximum efflux.

3.3 Information Theory for Membranes

Information theory provides a means to study the amount of information contained within a data set [59]. Information theory applies to information content of a signal rather than its meaning. When we receive a signal, we receive information. Meaning is what we then do with the signal after we receive it. Information is the uncertainty in the identity of the next signal; when the uncertainty of the next signal is high, then we gain a large amount of information. In contrast, if we are very certain of the identity of the next signal, then we gain little new information when it is received.

When applied within the context of a membrane surface, information theory could have the ability to quantify and predict a membrane's signaling potential. The information content of a variable is calculated in terms of informational entropy, which measures the predictability or uncertainty of that variable. A higher calculated entropy means a given variable is less certain, and therefore when it is detected (by us or by the molecule which interacts with it) a larger amount of information is transmitted [45]. The entropy $H(x)$ of any discrete variable within a distribution can be calculated in units of bits using:

$$H(x) = -\sum p(x_i)*\log_2(p(x_i)) \qquad (1)$$

where $p(x_i)$ is the probability of event x occurring relative to all other events in the system such that the sum of all probabilities $p(x_i)$ equals 1 (ie. $\sum p(x_i) = 1$). For example, when calculating entropy associated with the head group composition of a lipid surface $H(h)$,

$p(h_i)$ represents the mole fraction of all lipids containing the i^{th} type head group within the membrane composition. Similar calculations were made regarding the acyl chain composition as well as designated $H(a)$. Because a phospholipid is composed of both an acyl chain as well as a head group, the mole fraction of a given lipid within a membrane composition is the joint probability of its two independent variables such that $p(l) = p(h,a) = p(h)* p(a)$. Thus the entropy associated with a membrane's lipid composition is reported as the joint entropy $H(h,a)$ of its two variables. Continuing with the statistical nomenclature $H(h)$ and $H(a)$ can then be described as marginal entropies of the joint lipid distribution. Several possible relationships between the joint entropy ($H(h,a)$) and marginal entropies ($H(a)$ and $H(h)$) of the system are described in Fig.8.

In a system containing multiple randomly distributed variables, the marginal entropy of each variable is the uncertainty/information content contained within the composition of that variable, independent of any other variable in the system. The joint entropy of the same system is the novel information content contained within the sum of the marginal entropies of all variables within the system (Fig. 8). The mutual information, $H(h;a)$, is the interdependence of two variables, and is the amount of common information content shared between the marginal entropies of the variables in the system. For instance, if you know that a particular acyl chain of a lipid in a given membrane composition associates with head groups with vastly different probabilities, knowing the acyl chain composition of a lipid automatically narrows the field of possibilities for the head group composition. In other words mutual information $H(h;a)$ is how much information you have automatically learned about one variable by knowing the other

variable. (See Figure 11 for a graphical explanation of the inter-relatedness of marginal entropy, joint entropy, and mutual information of various systems.)

Through the use of equation 1, by determining the mole fraction of each lipid component in a membrane, the marginal entropies $H(a)$ and $H(h)$, joint entropy $H(h,a)$ and mutual information content $H(h;a)$ of the lipid distribution can be calculated for both the relationship between the acyl chain and head group distributions as well as the relationship between the information stored within and across both leaflets of the plasma membrane. Here we use the bit as an absolute unit of measurement of the entropy/information content stored within the lipid composition of a membrane. Because it is calculated using the mole percentages of lipid species in the membrane it is independent of membrane or lipid concentration as long as membrane composition remains constant. In terms of the Shannon Information Index (Eq. 1) the entropy of the system (calculated in bits) can be described as the predictability of a component on the membrane surface [59]. The lower the entropy of the lipid composition, the more easily the distribution of the lipid on the surface may be predicted. A higher entropy equates to a more random membrane composition and hence more information transferred by a particular realized state.

If it is assumed that the lipid composition of the entire membrane does not change over the course of a signaling event, upon domain formation the calculated entropy or information content of the entire membrane surface will remain the same. This is because the entropy of the membrane only depends on the membrane's lipid composition and not the lipid's physical distribution across the membrane surface. It is feasible, however, that

due to a non-random distribution of lipids across the membrane surface local regions of the membrane such as lipid rafts would have lower entropies due to the restriction of the lipid composition in those regions. This means that though the storage capacity of the membrane will remain the same if the relative ratios of lipids composing the membrane are constant, any event in which lipids are de-mixed would locally reduce entropy in the domains. In this way the joint entropy of a membrane can also be viewed as a unit of the maximum potential change that a local region of the membrane can undergo upon lipid de-mixing/domain formation. A membrane with 10 equally probable types of lipids undergoing domain formation to form localized domains which predominantly contain only 2 of the 10 different types of lipids underwent a larger local change in entropy than a membrane that underwent the same domain formation but only had 5 different types of lipids to begin with regardless of the fact that in both cases the entropy of the resultant domains would be the same. Thus, a more complex membrane with higher entropy can induce larger changes in local membrane compositions which could allow for a discrete lipid signal to be either sensed or induced by membrane associated proteins above the level of random noise within a membrane's lipid distribution.

3.4 Results

3.4.1 Information content of a cell membrane surface

To determine the capacity of the membrane to encode information for signaling events, experimentally derived lipid compositions from the literature were analyzed using information theory. In the context of information theory we calculated the entropy (uncertainty) of various membrane isolates including the total lipid extract (TLE), plasma membrane blebs (PM), and detergent resistant extracts from either unstimulated (DRMu) or stimulated (DRMs) mast cells [55]. Each of the membrane isolates encodes between 5.6 to 5.8 bits of information in the joint distributions of their acyl chains and head groups (Table 5) with more information residing in the distribution of the acyl chains than in the distribution of the head groups.

To assess the relative information content of the inner and outer leaflets in the mast cell membrane, calculations were performed on each data set assuming an asymmetry of the bilayers in which the outer leaflet was composed mainly of PC and SM head group-containing lipids while the inner leaflet contained an assortment of PE, PS, PG, PI, and PA containing head groups [60,61]. The literature values used for the entropy calculations were tested against our assumption using geometric constraints based on the minimal curvature of the plasma membrane bilayer and the subsequent required parity of the number of molecules in each leaflet due to the hydrophobic effect. Our calculations indicate that PC, SM lipids represent 55% of the lipids in the bilayer, while the PE, PS, PG, PI, and PA lipids represent the remaining 45%, supporting (to a first approximation) our assumption of the bilayer asymmetry. We found that the joint entropy between the

acyl chains and head groups of the inner leaflet of the membrane is approximately 1 bit higher than that of the outer leaflet (Table 5). For membrane associating proteins, this finding suggests more information content is potentially presented to (and decoded by) those inside the cell than those outside the cell.

In addition to analyzing the joint entropy contained within the inner and outer leaflets of the membrane-isolates, the marginal entropies of the head groups and acyl chains within each leaflet were calculated. The inner leaflet contains higher entropy and more uncertainty in the head groups than the outer leaflet, while the outer leaflet contains more uncertainty in the acyl chains than the inner leaflet. Additionally, the marginal entropy of the head groups of the outer leaflet is entirely contained within the marginal entropy of its acyl chains. This implies that the PC and SM of the outer membrane have mutually exclusive subsets of acyl chains meaning the joint entropy of the system is entirely dependent on the acyl chain composition (Fig. 8). Knowing the acyl chain composition of a lipid in the outer leaflet of the PM determines the head group associated with it by default. This result is less surprising when considering the difference in the synthetic pathway of SM and PC, but might have interesting implications in the packing and distribution of the outer membrane.

When we calculated the information content of a mast cell's total plasma membrane extract as well as stimulated and non-stimulated detergent-resistant membrane extracts, we found more information resided in the marginal entropy of the acyl chains than the head groups (Table 5). This is due, in part, to the large degeneracy of acyl chain unsaturation. This was not solely a consequence of simply having a greater number of

possible acyl chains than head groups but because there are a greater number of significantly populated distinct chemical species and therefore more possible combinations in the former than the latter. Mass spectrometry is unable to resolve between each of the two acyl chains per phospholipid. Because of this the entropy of the system could be higher than what was calculated due to undercounting of the possible chemically distinct acyl chain combinations. Overall we found that the joint entropy between the acyl chains and head groups of the inner leaflet of the membrane is approximately 1 bit higher than that of the outer leaflet (Table 5). This increase is due, primarily, to the novel information content (ie. non-zero conditional entropy) of the head group distribution of the inner leaflet. The mutual information $H(x;y)$ of two variables represents the redundant or shared information between the variable's marginal entropies (Fig. 8) and is a measure of the dependence of those two variables. In this way, the 3.4 to 3.8 bits of mutual information shared between the two leaflets of the membrane can be viewed as the extent of the interdependence of the bilayers.

Though the stimulation of the mast cells (DRMs) does not increase or decrease the joint entropy of the membrane isolates compared to the unstimulated (DRMu) it does increase the marginal entropies of the head groups, the acyl chains, and the mutual information shared between the two leaflets of the membrane isolates (Table 5). This result then, is consistent with the migration of polyunsaturated lipids into these detergent resistant membrane fractions resulting in increased shared information content between the domains, and a change in the distribution of information within the membrane. The higher information content of the inner leaflet, along with the changes in the information

of the membrane brought upon by the redistribution of lipids through domain formation, presents the membrane as a highly responsive surface having the capacity to encode and propagate information.

3.4.2 C2 domains at neuronal, muscle, and plant membranes are weakly held together

C2 domains are functional modules exploited by numerous proteins in membrane trafficking and signaling events[62,63]. As such, they are likely candidates for the decoding and propagation of information stored within the membrane's changing lipid distribution as discussed above. Currently, there are 39 unique crystal structures of C2 domains that have been assigned via SCOP classification [64]. Of these structures most share a similar overall fold such as those in human synaptotagmin I, the canonical and variant forms of Dys, cytosolic phospholipase A_2 α, protein kinase C, and extended synaptotagmins (Fig. 12) [56,62,63,65]. No crystal structure is available for *Gossypium* (cotton) Syt I; however, a good quality homology model can be computed based on its similarity with human Syt I. While the C2 domain structures of human and cotton Syt I as well as the canonical and variant forms of Dys C2A are highly similar, their free energies of stability at 37 °C ($\Delta G_{37°C}$) are not, spanning from 0.017-2.32 kcal/mol (Fig. 13, lower panels; Table 6). Despite this range, these different C2 domain stabilities are similar in the sense that all are at the lower limit of what constitutes a folded protein and all have features of protein disorder. Given that marginal stability is found in C2 domains from tissues of different embryonic origin (neurons and muscle) as well as different eukaryotic organisms (humans and plants), it brings up the question of whether or not this is a conversed

feature of membrane associated C2 domains. The initial data presented here suggests this may be the case and earlier DSC denaturation work on the α-, β-, and γ-isoforms of protein kinase C, wherein all C2 domains were found to have a $\Delta G_{37°C}$ of ~1 kcal/mol, further supports this hypothesis [50].

3.4.3 Membrane composition and curvature set the protein ensemble

The marginal stability of the C2 domains tested above suggested that each would be sensitive to changes in their local environment, particularly the membrane surface (and encoded information content) with which they interact [66,67]. To test this hypothesis, a C2 domain construct of human Syt I was denatured in the presence of vesicles of varying lipid composition and the resulting data was used to calculate $\Delta G_{37°C}$. Human Syt I C2A (encoding residues 96-265) in the presence of non-domain forming LUVs (60:40 mixture of POPC:POPS) was found to be weakly stable with a $\Delta G_{37°C}$ of 2.18 kcal/mol (Fig. 13, upper left panel; Table 6). Such a membrane composition has low information content as determined with information theory as done above for mast cell membranes; the total stored information only amounts to 0.97 bits of information. When the composition includes cholesterol ((80:20):30 mixture of (POPC:POPS):chol as LUVs with an information content of 0.72 bits), this basal stability decreases to 1.67 kcal/mole (Fig. 14, middle panel; Table 6).

When the LUV membrane complexity mimics the heterogeneity of the plasma membrane (Table 4) and thus has greater information content (2.50 bits), C2A's stability and unfolding profile undergo additional dramatic changes (Fig. 14, middle panel). This

plasma membrane mimic is based upon the distribution and mole percents of lipid species found in a synaptic vesicle, specifically the cytosolic face with which Syt I interacts *in vivo* [68]. In the presence of this synaptic vesicle mimic and saturating Ca^{2+}, human Syt I C2A has a stability of 5.75 kcal/mol. If, however, physiological unsaturated PS and PI lipids are replaced with PS and PI containing saturated acyl chains, a lipid mixture is made; the composition of which still replicates the general characteristics and distributions found in a synaptic vesicle, but also weakly forms domains as suggested by the subtle DSC transition seen with LUVs alone (Fig. 14, left panel). Using this LUV chimera, the calculated $\Delta G_{37°C}$ in the presence saturating Ca^{2+} was 7.09 kcal/mol and increased further still to 7.6 kcal/mol using SUVs of identical composition. In the case of the chimera, the replacement of unsaturated PS and PI with saturated versions does not globally change the calculated information content of the membrane as discussed above. On a local level, however, the slight phase separation of saturated lipid would decrease information content allowing for a discrete phospholipid signal to be propagated above background membrane noise. Indeed, human Syt I C2A's $\Delta G_{37°C}$ increases 23% (5.75 to 7.09 kcal/mol) in response to this local change in lipid distribution and increases an additional 7% (7.09 to 7.6 kcal/mole) in response to increased curvature. This latter observation is of particular importance to human Syt I because vesicles undergoing exocytosis and subsequent recycling experience a broad range of positive and negative curvatures both of which can change lipid distributions [69,70]. If Syt I senses these changes, as suggested by the change in $\Delta G_{37°C}$ presented here, it will have ramifications on the protein's conformational ensemble.

The same rule of membrane composition sensitivity seen for C2A alone seems to extend to the C2AB fragment of human Syt I, which includes both C2 domains of the protein [47]. The C2A and C2B domains are stabilized by different lipid species, where C2A is stabilized by phosphatidylserine (PS) and C2B by phosphatidylinositol (PIP_2) [47]. Because one domain becomes destabilized when the other is stabilized, both C2 domain ensembles are set by interactions with either lipid type. This is best illustrated in the TF denaturations of C2AB which have a strong fluorescence contribution from the C2B core tryptophan (Fig. 14, right panel). In the presence of 60:40 POPC:POPS LUVs, C2A is stabilized and C2B is destabilized (green). However, addition of Ca^{2+} drives C2A into a PS-bound state which makes the destabilization of C2B more prominent (orange and red). In contrast, when C2AB is in the presence of 95:5 POPC:PIP_2 LUVs, C2B is stabilized and C2A is destabilized (blue). As with PS-containing membrane, Ca^{2+} accentuates this effect (purple). The denaturations reveal a strikingly broad range of stabilities that highlight the ability of the membrane to broaden or narrow the conformational ensemble of C2B within the C2AB fragment using the lipid binding ability of either domain. Just as in membrane domain formation, the narrowing C2 domain ensemble decreases information content and allows for the reception of a discrete message; however, the allosteric coupling that exists between C2A and C2B allows for further transformation of the initial membrane message. Allostery, in this case, enhances the inherent plasticity of C2 domains and their ability to coordinate membrane information [71].

The responsiveness of human Syt I C2 domains is further exemplified by a few

peculiar changes in the baseline heat capacity (ΔC_p) (Fig. 13, top left panel). C2A and C2B have a very large ΔC_p under some membrane conditions. As can be seen in Table 6 the large ΔC_p values can have a dramatic effect on the calculated stability of the domain, as it narrows the temperature range over which the protein appears stable and consequently can give rise to a negative $\Delta G_{37°C}$. While we are not concluding that the C2A domain is unfolded under these conditions (indeed at 25 °C, a temperature well below the calculated cold denaturation threshold, C2A is still folded; (Fig. 13 top right panel), the changes in ΔC_p provide another metric for the protein's sensitivity to the local membrane environment. Both C2 domains of human Syt I are known to have partial membrane insertion capabilities [72,73]. Moreover, structural orientation modeling of C2 domains bound to PIP_2 suggests a fairly large surface area of contact between protein and membrane [74]. Since one contribution to the change in baseline heat capacity is the change in solvation of the protein in native and denatured states, partial insertion into the 60:40 POPC:POPS (for C2A) or 95:5 POPC:PIP_2 (for C2B) membranes, or significant reduction in solvent accessibility due to surface adherence could alter solvation of the native C2 domain. If in the unfolded form of the protein, hydrophobic residues partially partitioned into the membrane, solvation could also be altered leading to a change in ΔC_p. This latter example, however, would result in a reduced ΔC_p because hydrophic residues would be protected from aqueous solution and not be surrounded by water cages that differentially absorb heat. Since this is the opposite of our data, the large ΔC_p's point instead to unique membrane modifications of the native state. Regardless of the root cause, the behavior of the C2 domain is membrane composition and condition-dependent.

3.4.4 Unique Syt I C2A conformers invoke distinct membrane-disruption responses in a synaptic vesicle mimic

From the cumulative denaturation studies above, it appears that these C2 domains (from human Syt I, in particular) are acutely sensitive to membrane environment and are capable of adopting numerous conformations. This intrinsic plasticity leads to a question similar to that discussed for membrane lipid diversity and encoded information. Just as different lipid-lipid pairs constitute different potential signals, so too should C2 domain conformers. In this context, noise comes from the breadth of the C2 domain's conformational ensemble (determined by the free energy of stability). The signal is a particular subset of conformers that are simultaneously selected from the ensemble and more heavily weighted by binding of ligand (such as membrane and Ca^{2+}). The resulting conformer subset mediates molecular events that fulfill a biological function of the C2 domain as a means to propagate the given signal [71].

To test this definition of function, we applied our recently developed carboxyfluorescein efflux assay to human Syt I C2A using vesicles that had either the domain forming or non-domain forming synaptic vesicle compositions listed in Table 4. From human Syt I C2A's change in stability shown above, it appears that the membrane domain forming mixture selects a smaller set of conformers from the ensemble (as suggested by the 23% increase in $\Delta G_{37^{o}C}$ compared to non-domain forming mixture). When looking at the change in efflux as a function of time, the C2A conformers selected by the domain forming mixture reduce release. This can be seen by the downward

inflection at ~37 °C (where the phase transition occurs). However, when the lipid mixture mimics the synaptic vesicle, the extent to which C2A limits efflux increases; the downward inflection has a larger magnitude. In both cases, however, when the sample temperature increases beyond the melting temperature of C2A, the rate of efflux increases dramatically. Thus, the distinct C2A conformers selected by each lipid mixture send unique signals back to the membrane, resulting in differential efflux outcomes that may relate to function (Fig. 15) [71].

3.5 Discussion

Eukaryotic lipids are numerous. If each lipid combination is regarded as a potential signal, the eukaryotic membrane becomes a repository of information, highly diversified by chemical variation in head group and acyl chain. Indeed, when information content is calculated with information theory, it scales with lipid diversity as there are an increasing number of possible lipid-lipid combinations. These signals likely have specificity, suggested by both the unique lipid distributions found amongst compartments and leaflets as well as the numerous proteins that selectively bind to, partition into, or enzymatically target them. Within this context, a non-random distribution of lipids (like those found in membrane domains) could reduce information in a local region of the membrane. Membrane domains are non-ideal mixtures of lipids. As such, domains could have fewer potential combinations of lipids and consequently less information. This reduction of information can be conceptualized as an increase in the signal-to-noise ratio (S/N) of the membrane. The frequency of the lipid-lipid combination(s) that constitutes the domain (signal) increases at the expense of other lipid-lipid combinations (noise). In this scenario, predictable signaling outcomes come about from restricting available combinations of lipids either in a signaling domain or upon protein binding. While the DRM isolates of this study paradoxically showed an increase in information content, this likely resulted from detergent capture of multiple domains with varying lipid compositions; as the method of extraction cannot isolate one specific domain [75]. The information theory calculations, when applied to the much simpler 60:40 POPC:POPS mixture, indicate that indeed, fewer lipid components result in decreased information

content (information content decreased from 5.6 bits in DRMs to 0.97 in 60:40 POPC:POPS mixture) consistent with domain formation being a means for increased lipid S/N.

Much like the membrane, C2 domains that associate with or are tethered to the membrane also seem to be dominated by weak interactions. This marginal stability imparts these proteins with a membrane-responsive character, where the conformational distribution of the protein is set by the lipid composition and information content. This selection/restriction of the protein conformational ensemble by the membrane can be viewed as a decrease in the informational entropy of the protein, which in turn reciprocally affects the membrane (Fig. 15). If lipid diversity is a means to store information (Table 5) and weakly stable membrane-associated proteins conformationally respond to membrane composition (Fig. 13 and Fig. 14) while simultaneously affecting membrane distribution (Fig. 15), then these weak interactions provide a means for translating and transducing membrane-encoded information to downstream effector molecules whether they be proteins required for membrane repair (Dys) or for regulated release of neurotransmitter (human Syt I). In both cases, noise that manifests as non-functional combinations of lipids or non-functional protein conformers is unrecognized by the cell; the cell cannot make sense of the information presented in these non-signaling states. However, when a particular signal is to be transmitted, the near randomness of both lipid distribution and protein structure condense into a particular configuration associated with the signal allowing for its propagation.

Table 4: Phospholipid components in the membrane domain forming mixture (left columns), as well as the phospholipid components of the synaptic vesicle mimic mixture, where FA1 and FA2 represent the acyl chains attached to the glycerol backbone. These lipid compositions are based off of those presented in [68], and are designed to capture the essence of the lipid diversity of the synaptic vesicle outer leaflet. The percentages listed for each phospholipid species represent the mol percent of that species within the total phospholipid mixture, while the percent given for cholesterol represents the mol percent found within the total mixture.

Membrane Domain Forming Mixture				**Synaptic Vesicle Mimic Mixture**			
PE ratio	*FA1*	*FA2*	*% Total Phospholipid*	*PE ratio*	*FA1*	*FA2*	*% Total Phospholipid*
3	16:0	18:1	38	3	16:0	18:1	38
2	18:0	18:1	25	2	18:0	18:1	25
1	18:0	22:6	13	1	18:0	22:6	13
PI ratio	*FA 1*	*FA2*	*% Total Phospholipid*	*PI ratio*	*FA 1*	*FA2*	*% Total Phospholipid*
2	18:0	18:0	1	-	-	-	-
1	18:1	18:1	0.5	1	18:1	18:1	0.5
2	16:0	18:1	1	2	16:0	18:1	1
1	18:0	20:4	0.5	1	18:0	20:4	0.5
PS ratio	*FA 1*	*FA2*	*% Total Phospholipid*	*PS ratio*	*FA 1*	*FA2*	*% Total Phospholipid*
3	16:0	16:0	7	-	-	-	-
1	18:0	22:6	2	1	18:0	22:6	12
2	18:0	18:1	5	2	18:0	18:1	10
3	16:0	18:1	7	-	-	-	-
Cholesterol	-	-	45%	Cholesterol	-	-	45%

Table 5: The information content or entropy (*H)* of membranes isolated from RBL-2H3 mast cells calculated in bits of information. Membrane samples included the total lipid extract (TLE), plasma membrane blebs (PM), and detergent resistant extracts of cells from both unstimulated (DRMu) and stimulated (DRMs) mast cells [55]. Information content was analyzed in terms of the total membrane isolate of each membrane sample as well as the information content of the inner and outer leaflets of the samples. DRM are detergent resistant membranes and correlate with membrane domain compatible lipid mixtures. Estimations of the 95% confidence intervals for the joint entropy calculations of each composition are shown with the exception of DRMs which lacked replicate analysis in the literature. Confidence intervals for other entropy calculations could not be completed due to constraints of the literature.

Bits of Information:	**Total isolate**				**"Outer leaflet"**			**"Inner leaflet"**		
	TLE	PM	DRM u	DRM s	PM	DRMu	DRMs	PM	DRM u	DRM s
Joint entropy: $H(h,a)$	5.6 ± 0.36	5.4 ± 0.18	5.7± 0.23	5.7± n/a	4.2 ±0.15	4.0± 0.14	4.2± n/a	4.9 ±0.11	5.1± 0.18	5.3± n/a
Marginal entropy head groups: $H(h)$	2.3	2.1	2.5	2.4	0.7	0.9	0.8	1.6	1.9	1.9
Marginal entropy acyl chains: $H(a)$	4.2	4.2	4.2	4.4	4.2	4.0	4.2	3.6	3.6	3.9
Mutual info. of head groups and acyl chains: $H(h;a)$	0.8	0.9	1.1	1.0	0.7	0.9	0.8	0.3	0.5	0.5
Mutual info. of leaflets: $H(outer;inner)$	--	3.8	3.4	3.7	--	--	--	--	--	--

Table 6: Stability parameters obtained for C2 domains of Syt I and both isoforms of the C2A domain in dysferlin (Dys). The top portion of the table includes human Syt I and Dys data summarized from previous denaturation studies [23,47,56], as well as new measurements for cotton Syt I C2A. The parameters reported for the human Syt I C2A domain, in the top half of the table, were collected with the construct containing the amino acids 140-265. The lower portion of the table shows the stability parameters for the human Syt I C2A construct containing residues 96-265, in the presence of phospholipid bilayers of different compositions and size. All ΔG values reported represent free energy of stability at 37°C, and n is the number of replicates obtained under each condition.

Previously Studied C2 Domains in Absence of Ligand						
	ΔH(kcal/mol)	**ΔCp(kcal/mol·K)**	**T_m(°C)**	**$\Delta G_{37°C}$(kcal/mol)**	**ΔS(kcal/mol·K)**	**n**
Syt I C2A	58.7±0.3	1.92±0.09	55.99±0.04	2.32±0.05	0.178±0.006	4
Syt I C2B	69.6±0.6	2.19±0.04	46.4±0.1	1.74±0.09	0.22±0.01	4
Cotton Syt I C2A	2.5±0.1	0.37±0.09	39.5±0.1	0.017±0.01	0.008±0.004	4
Dys C2A	12.6±0.8	0.97±0.01	42.2±0.6	0.17±0.02	0.040±0.002	4
Dys C2Av1	18.3±0.4	1.32±0.01	55.6±0.1	0.33±0.02	0.058±0.001	4
Human Syt I C2A (96-265) in Presence of Lipid						
	ΔH(kcal/mol)	**ΔCp(kcal/mol·K)**	**T_m(°C)**	**$\Delta G_{37°C}$(kcal/mol)**	**ΔS(kcal/mol·K)**	
POPC:POPS(60:40)	59.2±0.2	1.91±0.04	53.32±0.03	2.18±0.02	0.181±0.004	4
POPC:POPS(60:40) and Ca^{2+}	58.6±0.4	4.50±0.03	68.96±0.06	-1.50±0.01	0.171±0.007	4
(POPC:POPS):cholesterol (80:20):30	67.9±0.2	3.08±0.02	68.04±0.04	1.67±0.01	0.199±0.003	4
Membrane Domain LUV and Ca^{2+}	135.7±0.5	3.58±0.01	68.6±0.6	7.09±0.06	0.413±0.02	4
Membrane Domain SUV and Ca^{2+}	140.8±0.6	3.60±0.02	75.3±0.6	7.60±0.02	0.429±0.01	4
Synaptic Mimic and Ca^{2+}	107.0±0.1	2.75±0.06	67.36±0.01	5.75±0.02	0.315±0.001	4

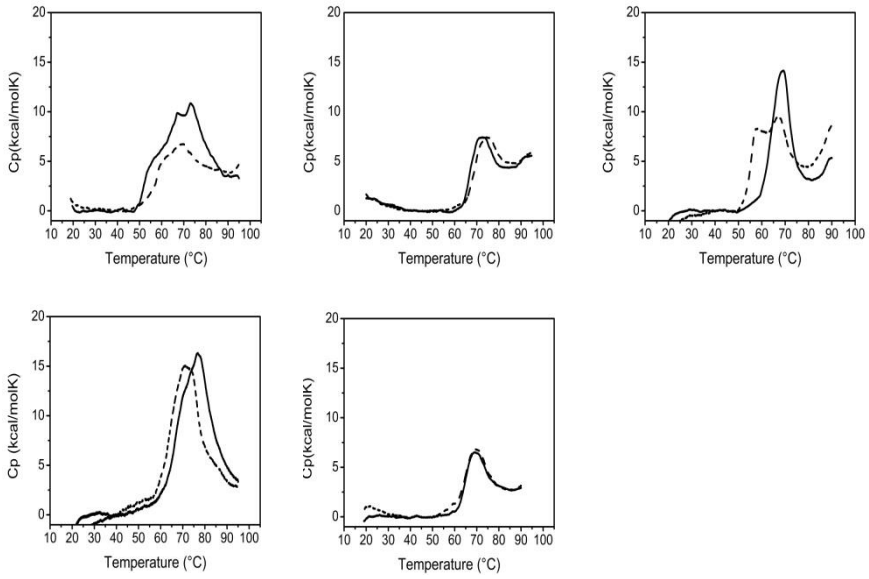

Figure 8: Comparison between the first (solid black line) and second (dashed black line) denaturation scans of the human Syt I C2A in the presence of 1mM of the membrane domain forming mixture as LUVs (upper left panel), 1mM of the membrane domain forming mixture as SUVs (lower left panel), 1mM LUVs composed of POPC:POPS (60:40) (upper center panel), 1mM LUVs composed of (POPC:POPS):cholesterol (80:20):30, (lower center panel), and 1mM synaptic vesicle mimic (upper right panel). All scans were conducted in the presence of 1mM Ca^{2+} and a buffer composed of 20mM MOPS 100mM KCl at a pH of 7.5 at a protein concentration of 13µM.

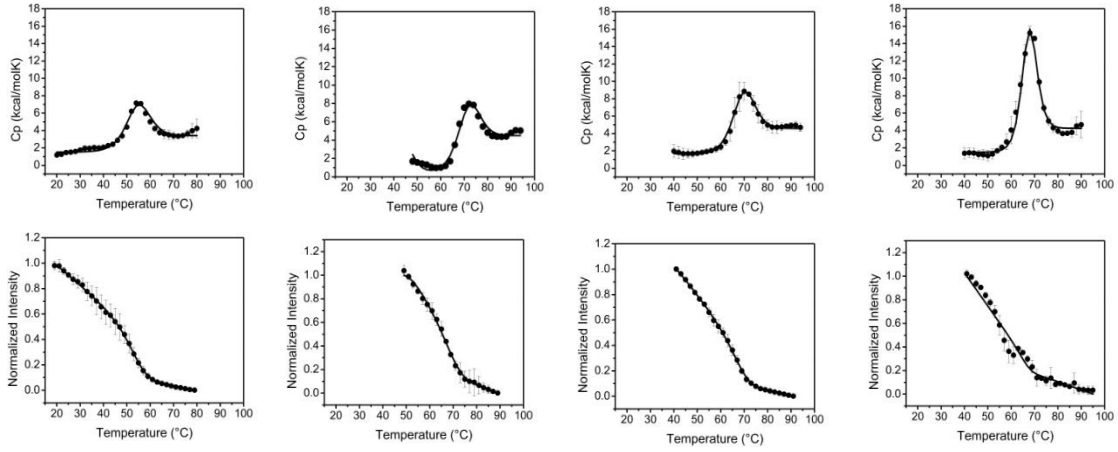

Figure 9: Fits of denaturation data obtained for the human synaptotagmin I C2A domain construct containing residues 96-265 from DSC (upper panels) and TF (lower panels), where the solid line represents the fitted model and the black dots the data obtained in the presence of 1mM LUVs composed of POPC:POPS (60:40) and 1mM EGTA (outer left column), 1mM LUVs composed of POPC:POPS (60:40) and 1mM Ca^{2+} (inner left column), 1mM LUVs composed of POPC:POPC:Cholesterol (80:20):30, and 1mM Ca^{2+} (inner right column), and 1mM of the synaptic vesicle mimic and 1mM Ca^{2+} All DSC scans were conducted at a [C2A]=13μM, and all TF denaturations were done at a [C2A]=1μM. Through the TF experiments the C2A domain construct was found to have reversibility ranging from 90%- 43%.

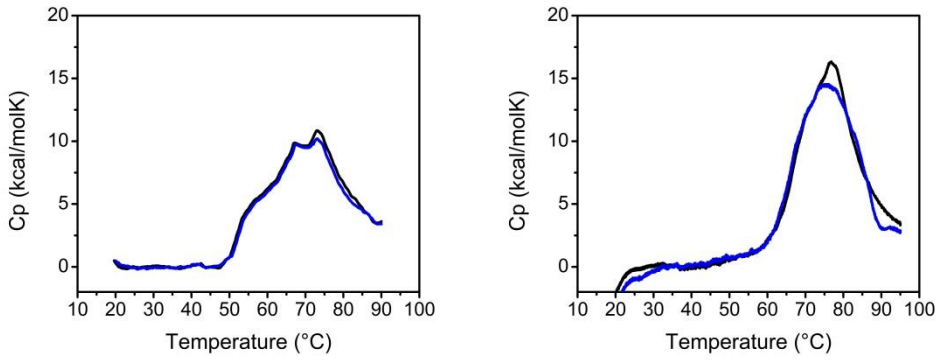

Figure 10: Comparison between different DSC experiments run with the human Syt I C2A domain containing residues 96-265, in the presence of 1mM membrane domain forming LUVs (left panel) and 1mM membrane domain forming SUVs. All scans were conducted in the presence of 1mM Ca^{2+}, at a [C2A]= 13µM, and in a buffer composed of 20mM MOPS, and 100mM KCl at a pH of 7.5. The two experiments are depicted in different colors, with one experiment being represented with the solid black line, and one the solid blue line

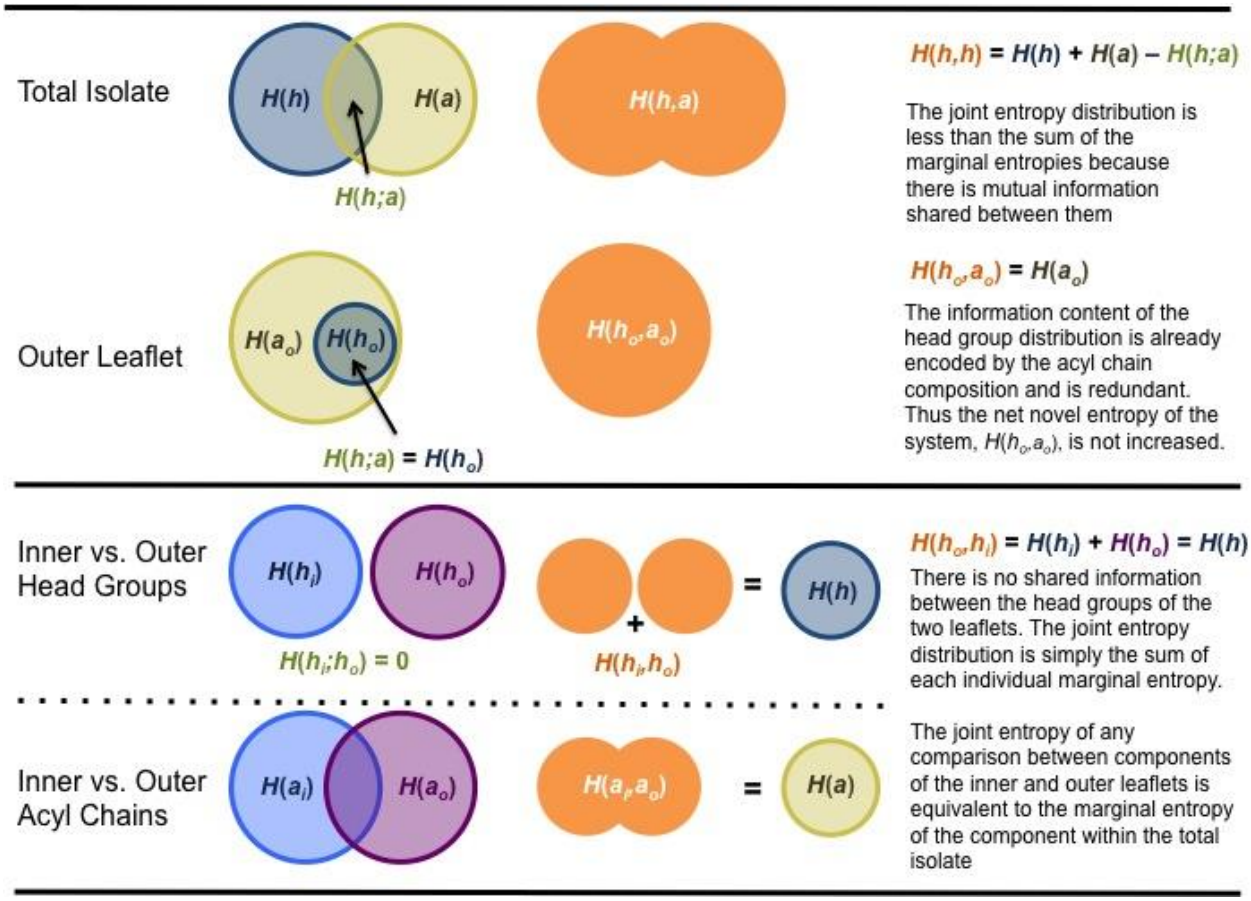

Figure 11: Examples and explanations of the overlap of marginal entropies of variables within their joint entropy where the marginal entropy is $H(x)$, joint entropy is $H(x,y)$ and mutual information content is $H(x;y)$

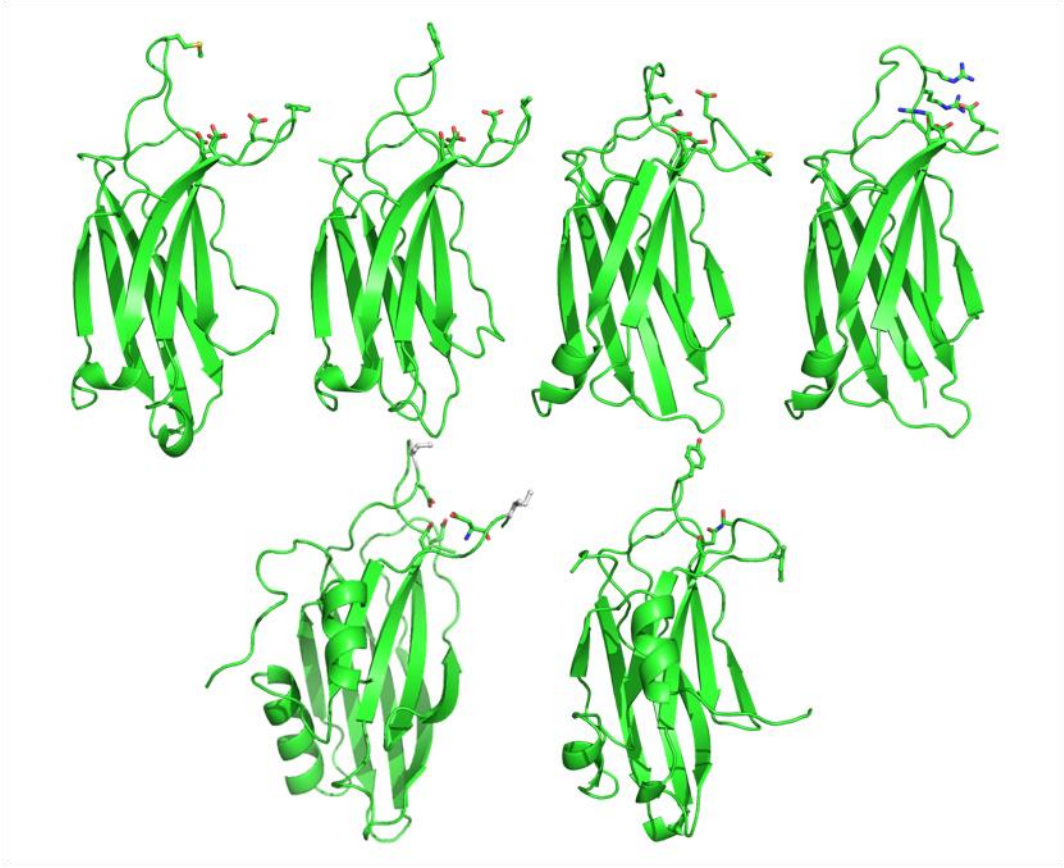

Figure 12: Structures of various C2 domains. The top row of structures correspond to C2A domains (from left to right) of human Syt I, cotton Syt I, human canonical Dys, and human variant Dys. The bottom row of structures are C2B domains (from left to right) from human and cotton Syt I. The calcium binding residues are shown and the putative lipid interacting residues are in white balls-and-sticks. Note the high level of structural similarity.

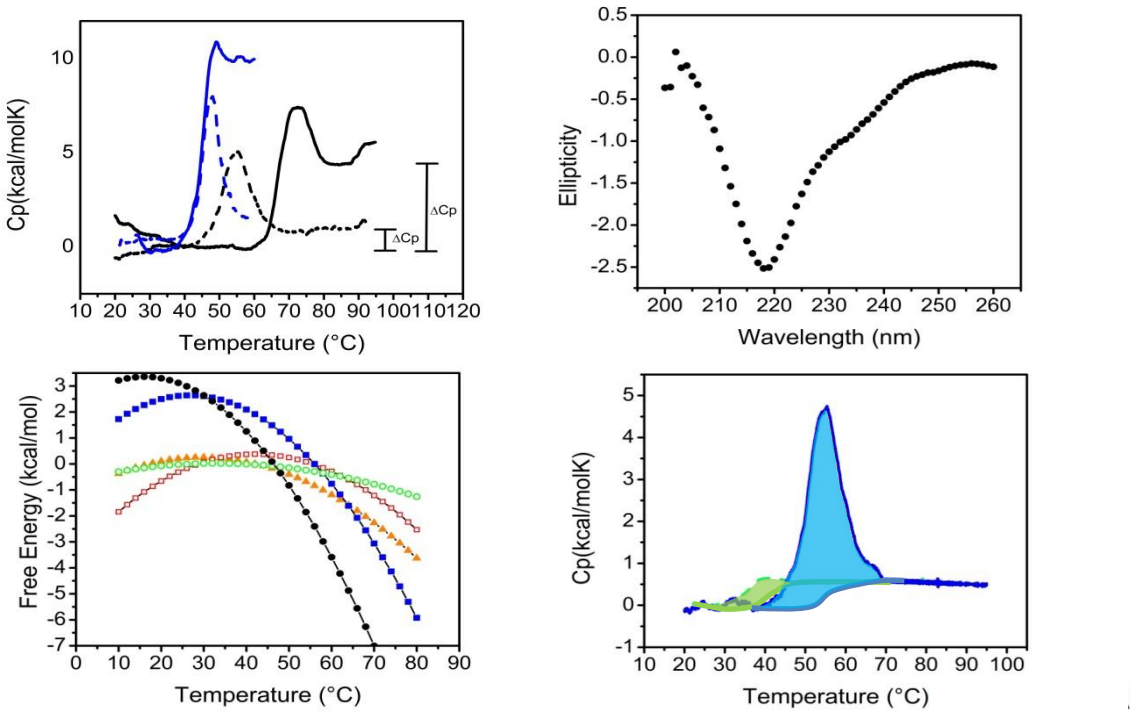

Figure 13: *Upper Panels:* The left panel shows the denaturation profile of human Syt. I C2A (residues 96-265) at 13µM in the presence of 1mM LUVs composed of POPC:POPS (60:40) and with either 1mM EGTA (dashed line) or 1mM Ca2+ (solid line). Also shown is 11µM C2B in the presence of 490µM LUVs composed of (95:5) POPC:PIP2 (solid blue line), 13µM C2B in the presence of 0.5 mM EGTA (dashed blue line). The large ΔCp differences are highlighted for the C2A domain with brackets (left panel). The right panel is the CD spectrum obtained for the C2A domain (residues 96-265) in the presence of 700 µM LUVs composed of POPC:POPS (60:40) and 1mM Ca2+. *Lower Panels:* The left panel shows the free energies stabilities of several C2 domains, in the absence of ligand, over a range of temperatures. These stabilities were calculated through the use of the Gibbs-Hemholtz equation, utilizing the ΔH, ΔCp, and T_m obtained from the thermal denaturation profiles of the domains. The orange triangles, red squares, blue squares, green circles, and black circles represent canonical C2A Dys, C2Av1 Dys, human Syt I C2A (residues140-265), cotton Syt I C2A, and human Syt I C2B, respectively. The right panel show the denaturation profile of the cotton C2A domain [Cotton C2A] = 175µM) with that of the human Syt I C2A domain construct containing the amino acids 140-265 (blue; [Human C2A] = 13µM) in the presence of 1mM EGTA. The blue and green lines under the curves represent the baselines used for integration and the shaded regions under the curves represent the area which is the enthalpy of denaturation.

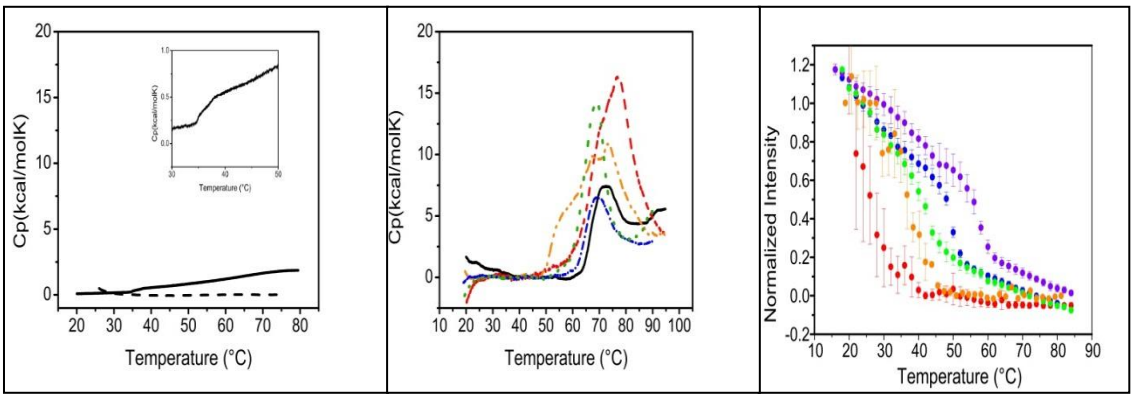

Figure 14: *Left Panel*: Thermograms obtained for LUVs of the membrane domain forming lipid mixture, at a phospholipid concentration of 3.3mM(solid line) and the synaptic mimic mixture at a phospholipid concentration of 1mM (dashed line). The inset in the upper right is a close-up of the phase transition. *Middle Panel*: Denaturation profiles of 13 µM human Syt I C2A (residues 96-265) in the presence of 1 mM LUVs (unless stated otherwise) of different lipid compositions and 1mM Ca^{2+}. The solid black line (▬) represents the denaturation with POPC:POPS (60:40); the blue dashed and dotted line(▬ · ▬ · ·) represents the denaturation with (POPC:POPS):cholesterol (80:20):30; the yellow dashed and dotted line (▬ · · ▬) represents denaturation with the membrane domain forming lipid mixture from Table 1; the red dashed line (▬ ▬) represents the denaturation with the membrane domain forming lipid mixture as SUVs; and the green dotted line (· · ·) represents the denaturation with the synaptic vesicle mimic from Table 1.All DSC scans were conducted in a buffer composed of 20mM MOPS and 100mM KCl at a pH of 7.5. *Right Panel*: FLT denaturation of C2AB fragment of Syt I in the presence of membrane with or without Ca2+. Red: 0.75 µM C2AB, 5.1 mM Ca2+, 110 µM LUVs (60:40, POPC:POPS). Orange: 0.9 µM C2AB, 600 µM Ca2+, 1.2 mM LUVs (60:40, POPC:POPS). Green: 0.75 µM C2AB, 110 µM LUVs (60:40, POPC:POPS), 500 µM EGTA. Blue: 0.75 µM C2AB, 210 µM LUVs (95:5, POPC:PIP2), 500 µM EGTA. Purple: 0.75 µM C2AB, 5.1 mM Ca2+, 210 µM LUVs (95:5, POPC:PIP2). Right panel adapted from [47].

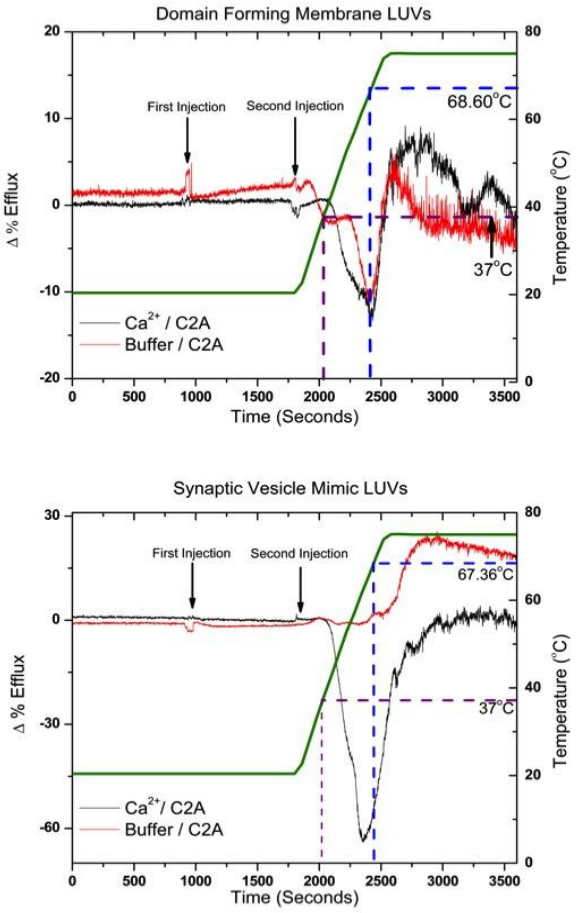

Figure 15: Change in the percent efflux of carboxyfluorescein from 200µM LUVs composed of a synaptic vesicle mimic lipid mixture (below) and LUVs composed of domain forming lipid mixture (upper) injected with Ca^{2+} at 15 min and human Syt C2A domain (residues 96-265) at 30 min to final concentrations of 3mM and 13.33µM respectively. Δ%Efflux was calculated by subtracting control titrations in which no protein was added during the second injection. Arrows indicate the addition of Ca^{2+} (1^{st} injection), or protein (2^{nd} injection) during the course of equilibration. For titration controls in which Ca^{2+} or protein were not present the injections were made with buffer composed of 20mM MOPS, 100mM KCl, 0.02% NaN_3, pH of 7.5. For all titrations the temperature was held constant at 20.4C until equilibration of the second injection when it was set to increase to 75˚C. The green line represents the temperature change over time, while the blue and purple dashed lines represent the temperatures (and corresponding titration times) at which the membrane phase transition occurs (purple) and the bound-protein denatures (blue). The efflux conditions for both plots were as follows: the **Black** solid line represents the Δ%efflux in the presence of both the human Syt C2A (residues 96-265) and Ca^{2+}, and the **Red** represents the Δ%efflux of the domain in the absence of Ca^{2+}.

Chapter 4: Marginal Stability in Annexin A2

4.1 Introduction

Calcium ion (Ca^{2+}) influx into the cell provides a means of signaling for a multitude of events, initiating the activity of a plethora of proteins. If unregulated, the influx of this broadly regulating ion can lead to Ca^{2+} induced apoptosis [1]. One cell type that is at a particularly high risk of succumbing to this type of apoptosis is myocytes. This is due to the fact that the force generated through their normal function results in the formation of micro-lesions within the membrane leaving the cell open to an influx of extracellular Ca^{2+}. In order for these cells to survive, these lesions must be effectively and rapidly repaired. The repair process is completed by a finely tuned system that relies on the concerted action of dysferlin, TRIM 72 (MG53), caviolen 3, and several annexin isoforms [2,3]. One of these components, dysferlin, has recently gained much attention as mutations within this protein have been shown to cause multiple types of muscular dystrophies including Limb-Girdle type 2B, Myoshi Myopathy, and Distal Compartment Myopathy [4,5]. Dysferlin is a large protein containing 2,020 amino acids and is structurally composed of seven linked C2 domains. Currently, there have been over 500 mutations within dysferlin that have been linked to these dystrophies [6]. When the locations of these mutations are examined no hotspots are found, but rather, they are spread throughout the dysferlin molecule [7]. This includes not only folded regions but also the disordered regions that link the domains together suggesting these mutations result in more than the inability to bind Ca^{2+} and membrane.

Interestingly, the exact same mutation within dysferlin has been shown to cause different types of muscular dystrophies in different patients [8]. These mutations often lead to a deficiency of dysferlin within the cell, which has been found to result in an inability of intercellular vesicles to fuse with the plasma membrane despite their localization at the wound site [9]. Additionally, it has been shown that the localization of several proteins involved in the membrane repair process is much slower in dysferlin deficient zebra fish cells [10]. Together these findings suggest that dysferlinopathies represent a complex category of disease which seems to affect more than just dysferlin. Given that dysferlin interacts with a number of proteins during the repair process, it appears that mutations within dysferlin may also impact the ability of these other proteins to function. One of these proteins is annexin A2 (A2) which has been shown to interact with dysferlin throughout the membrane resealing process [11]. Annexin A2 has been found to be up regulated in the muscle tissue of individuals suffering from dysferlinopathies [12]. Despite the discovery that A2 and dysferlin act together during membrane resealing over a decade ago, the significance of their interaction remains unclear.

Recent work performed on dysferlin has found that the C2A domain is marginally stable [13]. The work of Hilser and colleagues has shown that marginal stability acts to maximize communication within a protein molecule as this allows for the protein to exist in a wide set of possible conformations in response to environmental cues [14]. We have recently shown this ability to communicate intra-molecularly is the basis for the function of synaptotagmin I, a protein structurally homologous to dysferlin [15]. The two C2 domains, which comprise the intracellular portion of synaptotagmin I, are energetically

linked allowing the information of ligand binding by one domain to propagate to the other domain [16]. Because the stability and structure of synaptotagmin I and dysferlin are similar, it is likely that dysferlin functions through a similar mechanism of information flow. However, given that dysferlin does not function alone in the membrane repair process but rather interacts with multiple effector proteins, it would seem that the ability to transduce information intra-molecularly alone is not enough. The implication of dysferlin as a sensor of membrane damage suggests that it has the ability to communicate this information throughout the proteins that it interacts with. This leads us to propose that the communication of information, such as ligand binding, extends beyond dysferlin itself and to the other components of the membrane repair machinery. Because of dysferlin's marginal stability, we hypothesized that annexin A2 must also be weakly stable in order to maximize the information transfer between the two proteins. Marginal stability would indicate that annexin A2 is able to exist in a wide set of conformations allowing it to respond acutely to signals from dysferlin. A high number of possible conformations would allow annexin A2 to change its shape to be specific to a given situation, thus information content is higher in a marginally stable protein than a less plastic protein. If both dysferlin and A2 are marginally stable, events such as ligand binding by either would be expected to be propagated to the other.

To test this, a combination of calorimetry and spectroscopy were used to investigate the stability and structure of A2 under a variety of ligand conditions. In order to determine if marginal stability may be unique to annexin A2, another annexin isoform also expressed in muscle tissue, annexin a5 (a5) of *Rattus norvegicus* (which shares 98%

of its sequence with its human counterpart), was used as a comparison (Fig. 16). While the two isoforms examined here contain highly similar sequences within their folded core domains, A2 was found to be less stable than a5 under all conditions examined and was observed to be more structurally responsive to its endogenous ligands of Ca^{2+} and acidic phospholipid. These results suggest that the membrane repair machinery functions as a cohesive unit with communication, via information flow, between participating proteins. Protein cross communication would provide a possible rationale for the wide phenotypic differences found between individuals suffering with dysferlinopathies. Every mutation within dysferlin will have a different result in protein communication and the ability to transmit information. Therefore if dysferlin acts to regulate the function of other components involved in membrane repair, changes such as mutations would result in the dysfunction of not only dysferlin but multiple components of this process.

4.2 Material and Methods

4.2.1 Protein purification

Wild type annexin a5, from *Rattus norvegicus,* was purified as previously described [57]. For human annexin A2, the cDNA was cloned into a p202 vector, and expressed in *E. coli* Bl-21 cells as a MBP 6Xhis tag fusion protein. Cells were grown at 37°C in one liter of LB broth containing ampicillin (0.1mg/mL). Overexpression of A2 was induced by the addition of 1mM isopropyl-β-D-thiogalactopyranoside once the cells reached an optical density between 0.6-0.8 at 600nm. Five hours after induction, cells were harvested by centrifugation. Following this, cells were lysed by sonication in a buffer composed of 20mM 4-(2-hydroxyethyl)-1-piperzineethanesulfonic acid (HEPES), 100mM NaCl, 1mM phenylmethanesulfonylfluoride and 1mM 2-mercaptoethanol (βME) at pH 7.5. The lysate was then centrifuged at 16,000 rpm, 4°C for 30 minutes. After centrifugation the supernatant was sterile-filtered through a 0.45 µm Millipore PES filter. The annexin A2 was then mixed with Ni-NTA column media (Qiagen) for 6 hours. The column was then washed with 800mL of lysis buffer to remove any contaminating proteins, followed by 600mL of wash buffer (identical to lysis buffer but also contains 30mM imidazole). This process was monitored through the A280 via a Nanodrop 2000 (Thermo Scientific). Following this, the A2 fusion protein was eluted by running 200mL of elution buffer (20mM HEPES, 100mM KCl, 250mM imidazole, pH 8) through the column. Tobacco Etch Virus nuclear inclusion a endopeptidase (TEV), was then added to the eluent, after which it was rocked for 8 hours at 4°C to allow cleavage of annexin A2

form the tag. Following cleavage by TEV, protein solution was then repassed over the nickel column to remove the TEV protease and MBP 6Xhis tag, after which the recombinant annexin A2 was dialyzed into a batch chelexed (Chelex-100) buffer composed of 20mM MOPS, 100mM KCl at a pH of 7.5. The purity of the protein was then confirmed through the use of an SDS-PAGE gel.

4.2.2 Preparation of lipid samples

All lipids were purchased from Avanti Polar Lipids (Birmingham, AL). Samples without cholesterol were prepared as previously described [23]. Cholesterol-containing samples were prepared by aliquoting lipid stocks into a 4:1 mixture of chloroform:methanol followed by rotary evaporation using a Buchi R-215 Rotovap at a temperature between 50-60°C. The lipid films were then placed under vacuum for a minimum of 8 hours to remove excess solvent and hydrated with the appropriate buffer. LUVs were then prepared by hand extrusion using a 0.1μm filter.

4.2.3 Differential Scanning Calorimetry (DSC)

DSC experiments including both scan rate and concentration dependent controls, were performed on a NanoDSC (TA Instruments, New Castle, DE) as previously described [56]. All scans were conducted in chelexed 20 mM MOPS, 100 mM KCl, buffer at pH 7.5. All DSC experiments in the absence of Ca^{2+} were done in 1mM EGTA. All scans conducted in the presence of Ca^{2+} were completed in the presence of 5mM Ca^{2+}, while all scans containing lipids were conducted in the presence of 4mM phospholipid as

LUVs. The concentration of the calcium stock solution used for all scans was verified using both a Ca^{2+} selective electrode (ThermoScientific) and a BAPTA chelating assay (Invitrogen/Molecular Probes, Eugene, OR). The concentrations of all lipid stock solutions were confirmed by a phosphate assay according to standard protocols [27]. As has been noted by others, we were unable to characterize any reversibility for the denaturation of annexin a5 [76]. However, annexin A2 was found to show reversibility ranging from 60-90% as determined by the comparison of enthalpies from consecutive denaturations.

4.2.4 Circular Dichroism (CD)

CD experiments were performed on a Jasco CD Spectrometer (Annapolis, MD), at a concentration of 5μM protein for all annexin constructs studied. All CD scans were conducted in a buffer composed of 20mM MOPS and 100mM KCl at pH 7.5. Spectra collected in the absence of Ca^{2+} were conducted with 500μM EGTA. In the presence of Ca^{2+}, all spectra were obtained with 5mM Ca^{2+} and those in the presence of lipid were obtained with 2mM phospholipid as LUVs. Data points were collected in 1nm increments and averaged over 5 acquisitions. Spectra collected were corrected for any buffer contributions by subtracting a buffer scan from the corresponding protein scan.

4.3 Results

4.3.1 Thermodynamic differences between annexins A2 and a5

Given that A2 and a5 share a high amount of both structural and sequential homology within their folded Ca^{2+} binding core (Fig 16 and 18), one would expect the stabilities of the isoforms to be similar as well, however the values obtained for the two isoforms are quite different. The free energy of stability (ΔG_{37}) of a protein is often interpreted simply as the energy barrier that must be overcome in order to denature the protein. However, the ΔG_{37} can be thought of as representing the energy barrier that must be overcome in order for a protein to transition from one state to another. The lower the free energy of stability, the more states are available to the protein in its native ensemble. Typically, a protein's free energy of stability is between 5 and 20 kcal/mol [21]. In the absence of ligand, the a5 isoform falls within this range with a ΔG_{37} of 6.36±0.06 kcal/mol. On the other hand, the A2 isoform was found to be significantly less stable with a ΔG_{37} of 3.0±0.1 kcal/mol, just under half of the ΔG_{37} of a5 under the same conditions. The lower stability of A2 indicates that this isoform is more structurally plastic than the a5. Evidence of this heightened plasticity can also be found when the CD spectra of the two isoforms are compared (Fig 19). While both maintain the α-helical fold typical of the annexin core, the broader and less intense spectra obtained for the A2 isoform is consistent with it being less ordered.

4.3.2 Differences in responsiveness to ligand

The A2 isoform was found to be less stable under all conditions examined, however, the stability parameters and CD spectra for the A2 were found to change significantly more in the presence of ligand than those of a5. In the presence of Ca^{2+}, a significant increase in the melting temperature (T_M) was found, rising from 53.3±0.3°C in the absence of ligand to 76.3±0.1°C. Coupled with the increase in melting temperature, the A2 isoform also showed an increase in its change in heat capacity (ΔCp) from 2.8±0.5 kcal/molK in the absence of ligand to 5.2±0.6 kcal/molK with Ca^{2+} accompanied by an increase in the enthalpy of denaturation (ΔH) (Fig 20, Table 8). In comparison, a5 showed a modest change in T_M from 50.38±0.04°C in the absence of ligand to 52.44±0.03°C in the presence of Ca^{2+}, and a comparatively minor increase in the ΔH with no significant change in ΔCp (Fig 20, Table 8). The differences found for A2 were further exaggerated in the presence of both Ca^{2+} and acidic phospholipid, while the enthalpy and T_M showed small changes, the ΔCp of the A2 isoform increased dramatically to 11.6±0.2 kcal/molK. For the a5 we found only an increase in enthalpy and T_M under these same conditions, but not in the ΔCp (Table 8). The ΔCp can be thought of as a metric for how buried the hydrophobic amino acids are within a protein in the folded state. The increase in the ΔCp of annexin A2, in the presence of Ca^{2+}, would suggest that these amino acids are significantly more shielded from solution when in the presence of this ligand, an observation consistent with a more well-structured protein. Support for this was also found through a comparison of the CD spectra in the absence and presence of Ca^{2+}. The increased intensity of the minima of the spectra in the presence

of Ca^{2+}, when compared to the spectra in the absence of Ca^{2+}, is consistent with a global ordering of A2 (Fig. 19, right panels). While the minima of the a5 spectra also showed an increased intensity under these conditions, the increase was not as substantial as that of A2. Taken together these data are consistent with both isoforms becoming more structurally ordered in the presence of Ca^{2+}. However, the ordering of A2 being more global than that of a5.

As seen in Table 8, the A2 isoform is reported to have a negative free energy of stability (ΔG_{37}) at 37°C when both Ca^{2+} and acidic phospholipid species are present. This would suggest that under these conditions the protein is denatured at physiologic temperature. However, from the A2 CD spectra taken at 25°C (well below the cold denaturation transition temperature), it was found that the protein is still folded under these conditions, showing a slight increase in intensity over the spectra obtained in the presence of Ca^{2+} alone (Fig. 19). This would indicate that a subset of the conformational ensemble is being selected for in which the hydrophobic core of the protein is more concealed from the aqueous environment. The negative free energy of stability under these conditions likely results from the large ΔCp value, which greatly narrows the temperature range over which the protein appears stable. The large increase in the ΔCp under these conditions may be the result of A2's ability to aggregate vesicles in the presence of Ca^{2+} [22]. Aggregation would cause a larger area of the protein to be hidden from solution only becoming exposed upon denaturation of the molecule.

4.3.2 Annexins and the muscle membrane

The differences between the A2 and a5 isoforms examined within this study suggest that these two isoforms behave uniquely within the cell. In order to more fully examine this possibility, the stabilities of both A2 and a5 were determined in the presence of a lipid mixture designed to mimic the complexity of the inner leaflet of the sarcolemma (Table 7). The muscle cell membrane was selected as both isoforms are expressed in muscle cells. Notable differences were found between the two isoforms when their stabilities in the presence of the muscle membrane mimic mixture were compared to those in the presence of a binary mixture of POPC:POPS (60:40). The A2 isoform exhibited a dramatic increase in stability in the presence of the muscle mimic mixture in both the presence and absence of Ca^{2+}, (Table 8, Fig. 20 and 21). The a5 isoform on the other hand showed a similar stability between both the muscle membrane mimic and POPC:POPS mixture in the presence and absence of Ca^{2+} (Table 8, Fig. 20 and 21). The changes found for the A2 isoform may be attributed to its ability to bind negatively charged lipids showing preference for those containing phosphoinositol or phosphoserine headgroups [23], while the a5 isoform has been shown to interact preferentially with lipids that contain a phosphoserine headgroup. The observed changes for the A2, and lack thereof for a5, is in line with the A2 isoform being more sensitive to its local environment, suggesting that A2 is better equipped to respond to changes in its environment as well.

4.4 Discussion

Unlike most pathologies that arise from mutations within a protein, the muscular dystrophies that result from mutations within dysferlin show a high degree of phenotypic variability [24,25]. Many studies have been performed to examine the action of dysferlin at the cellular level; but there is still no consensus on a mechanism to explain how mutations within it lead to the disease state. While there has been much work focusing on dysferlin itself, there has been relatively little emphasis on the proteins which dysferlin associates with during the membrane repair process. Since dysferlin does not function on its own during membrane repair, a complete understanding of dysferlinopathies must also include an understanding of the proteins with which dysferlin interacts. The purpose of this study was to investigate the hypothesis that annexin A2 is a marginally stable protein, allowing it to be an acutely sensitive system that is capable of responding to signals from its interaction partner dysferlin. To test this hypothesis, we have examined the stability and structure of annexin A2 under a variety of conditions, as well as annexin a5. In support of this, we find A2 to be a marginally stable protein that exhibits a much more responsive nature, as shown by changes in its stability and CD spectra, to the presence of its endogenous ligands. This is consistent with a protein that is highly sensitive to its environment. Given that communication is maximized through weak interactions, the low stability reported for the C2A domain of dysferlin and for annexin A2 is consistent with these two molecules being able to exchange information, such as the binding of ligand. Recognizing that these experiments were not conducted on

dysferlin itself, these results still shed light onto its nature within the cell. Since dysferlin interacts with a number of proteins during the membrane repair process, understanding the properties of these interaction partners will provide insights not only into their function, but into dysferlin's function as well.

When the spectra of the two annexin isoforms are compared, both are found to have an α-helical spectrum with two minima at roughly 222 and 208 nm. The differences between the two isoforms can be seen when in the presence of ligand. In the presence of Ca^{2+}, the A2 isoform showed a roughly 300% increase in the intensity of the minima of its spectra, while the a5 isoform exhibited an increase of roughly 167%. The much larger increase in the α-helical nature for A2 is consistent with a more global ordering for the A2 molecule than the a5. Considered at the molecular level, this suggests that the information of binding to Ca^{2+} is propagated to a much higher degree throughout A2 as compared to a5. This was recapitulated in the denaturation data, as a5 showed no increase in the change in heat capacity (ΔCp) and a modest increase of 6.5% in the enthalpy of denaturation (ΔH) under these conditions, compared to an increase of 35.9% in the ΔH for A2. The differences between the isoforms are apparent even in the presence of the muscle membrane lipid mixture, supporting that *in vivo* the two isoforms behave distinctly different despite their high homology.

The differences raise the question: what makes the annexin isoforms distinct? When our stability data is combined with reported stabilities of other annexins, it is found that each isoform has a distinct stability [20]. It is well known that the annexins primarily differ within their N-terminal domains, which show a variety of sequences and lenghs

[26,27]. This region has often been regarded as a regulatory domain since it contains sites for post translation modification, such as phosphorylation and proteolytic cleavage. Specifically in annexins A1 and A2, these modifications have been found to change the behavior of the protein [28–30]. However, because this is the only variable region in the isoforms, the N-terminal domains may in fact also act to determine the energetic properties of each isoform. From the data presented here, it appears that the N-terminal domains may also impact the stability of the folded core in an isoform specific manner, as while A2 is a larger molecule than a5 (suggesting more interactions) it is much less stable. This would represent a new possible mechanism by which this region is able to regulate the function of the different isoforms. Support for this comes from the examination of a chimeric annexin construct which contained the core of annexin a5 and the N-terminal tail of annexin a1. This chimeric construct was found to show properties which are associated with the a1 isoform but not the a5, such as the ability to aggregate vesicles [31], showing that this region is able to change the properties of the Ca^{2+} binding core even when unmodified. This new possible mechanism of annexin regulation could provide a physical basis for the broad range of intercellular functions different isoforms have been reported to participate in. However, further experimental work is needed to determine the true nature of this.

The free energy of stability is a measure of the amount of energy required to transition a protein from the native state to the denatured state. However, a more biologically relevant interpretation of this value is that it represents the ease with which the protein can transition from one conformation to another. If the energy barrier to

unfolding is high, then the energy barrier to converting between conformers will also be high. This idea is graphically represented in figure 22. Low stability within a protein molecule translates to a higher degree of sensitivity to changes within the protein's environment, as they have a more dramatic impact on a weakly stable protein's conformational ensemble than to that of a more stable protein. This is exemplified by comparing the stability of the two isoforms in the presence of the muscle membrane mimic and Ca^{2+}. Under these conditions, the A2 isoforms showed a considerable increase in stability while the stability of a5 is comparable to that in the presence of POPC:POPS (60:40) and Ca^{2+}. Interestingly while the A2 isoform showed a considerable gain in structure in the presence of solely Ca^{2+}, while the overall stability (ΔG_{37}) of A2 actually decreases under these conditions, as opposed to the increases seen for a5. At first this seems counter intuitive; however, when this observation is considered within the context of the multiple Ca^{2+} dependent interactions of A2, this result points to the need to maintain malleability even while bound to ligand. Annexin A2 functions in a myriad of seemingly unrelated processes; however, all have the common feature of information flow within the cell [32]. As such, the marginal stability of this isoform, even in the presence of ligand, may result from its need to integrate multiple cellular signals and respond appropriately. The response then would be synergistically determined by the multiple interaction partners of A2.

As stated the annexins are a family of proteins which are highly conserved at both the sequential and structural levels. However, the isoforms have been found to evolve at different rates, with the A2 isoform being identified as the slowest overall, [33]making this

isoform one of the most highly conserved. Much like the annexins the ferlin family of proteins (which includes dysferlin) also have highly similar sequences[34]. This would seem to suggest that the marginal stability that has been observed in the human forms of these proteins is a common feature. Given that both A2 and dysferlin are members of protein families which are highly conserved, it is not surprising that the mechanism of membrane lesion repair is also thought to be a highly conserved process throughout eukaryotes [35]. From this it seems likely that the properties of each, such as stability, are optimized for their function, and that even smalls changes in these (such as those that arise from a point muation) can have dramatic negative effects on an organism.

When this considered within the context of membrane repair, as well as the results presented here a picture emerges of system which functions as a unit. Dysferlin is often described as the Ca^{2+} sensor of membrane damage triggering the exocytosis of vesicles to patch the lesion [35,37]. As a sensor of this damage, it seems reasonable that dysferlin's ability to correctly propagate this information is critical for triggering the resealing of the damaged membrane. As would be expected with any finely tuned piece of machinery, even seemingly small errors can have deleterious consequences. Mutations within dysferlin, even those which would seemingly not impact dysferlin's ability to bind Ca^{2+} and membrane (for example those within the linker regions), would likely impact how the information of membrane damage is communicated throughout dysferlin itself. This would then change the ability to propagate this information to other components of the repair machinery. If this flow of information is considered in terms of a signal to noise ratio, where signal represents the appropriate information being propagated and

noise the propagation of information which is unable to be interpreted by the other components of the repair machinery, then mutations within dysferlin would likely change this ratio. Disease states would then be associated with an increase in the amount of noise. This would result in the inability of the repair machinery to function consistently. While the appropriate signal may still be transmitted, this occurs less often, leading to a degeneration of the tissue over time. The vast number of mutations within dysferlin and the resulting phenotypic variations indicates that each mutation impacts the flow of information in a unique manner. If information flow occurs less accurately over time, the ability to maintain the membrane integrity decreases, resulting in the muscular dystrophic disease states.

Table 7: The phospholipid components of the muscle membrane mimic mixture where FA1 and FA2 represent the acyl chains attached to the glycerol backbone. These lipid compositions are based off of those presented in [80] and are designed to capture the essence of the lipid diversity of the inner leaflet of the myocyte plasma membrane. The percentages listed for each phospholipid species represent the mol percent of that species within the total phospholipid mixture while the percent given for cholesterol represents the mol percent found within the total mixture.

Muscle Mix			
PE ratio	FA 1	FA2	% Total
3	16:0	18:1	18
2	18:0	18:1	12
1	18:0	18:2	6
1	16:0	16:1	6
PI ratio	FA 1	FA2	% Total
2	18:0	18:0	13
1	18:0	18:1	6
2	16:0	18:1	13
PS ratio	FA 1	FA2	% Total
3	16:0	16:0	9
3	16:0	18:1	9
1	18:0	18:2	3
2	18:0	18:1	5
Cholesterol			30

Table 8: Thermodynamic parameters obtained for annexins A2 and a5. All ΔG_{37} values reported represent the free energy of stability at 37°C, values reported represent the average of four denaturations and all error values are at the 95% confidence interval. All scans conducted in the absence of ligand were done at 1mM EGTA or in the presence of 5mM Ca^{2+}. Lipid containing scans were done with LUVs composed of either POPC:POPS (60:40) or the muscle membrane mimic mixture at concentrations of 2 and 4mM respectively. All scans were completed in a buffer composed of 20mM MOPS, and 100mM KCl at a pH of 7.5 at a protein concentration of 10µM or 8µM (scans with the muscle membrane mimic mixture) for both A2 and a5.

Annexin A2						
	ΔH(kcal/mol)	ΔCp(kcal/molK)	T_M (°C)	ΔG_{37}(kcal/mol)	$\Delta H_{Cal}/ \Delta H_{VH}$	n
No Ligand	82.7±1.0	2.8±0.5	53.3±0.3	3.0±0.1	1.00	4
Ca^{2+}	129.1±0.1	5.2±0.6	76.3±0.1	2.5±0.1	0.83	4
POPC:POPS (60:40)	78.9±0.4	2.5±0.1	53.16±0.7	2.89±0.04	0.98	4
POPC:POPS (60:40) and Ca^{2+}	131.5±0.5	11.6±0.2	78.7±0.3	-14.04±0.02	1.05	4
Muscle Mimic	232.0±0.5	7.0±0.4	51.6±0.8	8.1±0.3	1.32	3
Muscle Mimic and Ca^{2+}	314.7±0.4	12.9±0.7	65.7±0.9	10.4±0.1	1.52	3
Annexin a5						
No Ligand	162.2±0.8	1.5±0.5	50.38±0.04	6.36±0.06	0.99	4
Ca^{2+}	173.5±0.6	1.2±0.4	52.44±0.03	7.8±0.3	0.89	4
POPC:POPS (60:40)	144.8±0.7	1.2±0.4	51.07±0.05	5.9±0.3	1.01	4
POPC:POPS (60:40) and Ca^{2+}	259.5±1	1.4±0.1	83.18±0.01	29.1±0.5	0.89	4
Muscle Mix					1.24	4
Muscle Mix and Ca^{2+}	258.8±0.9	1.8±0.1	78.7±0.2	26.1±0.5	1.41	4

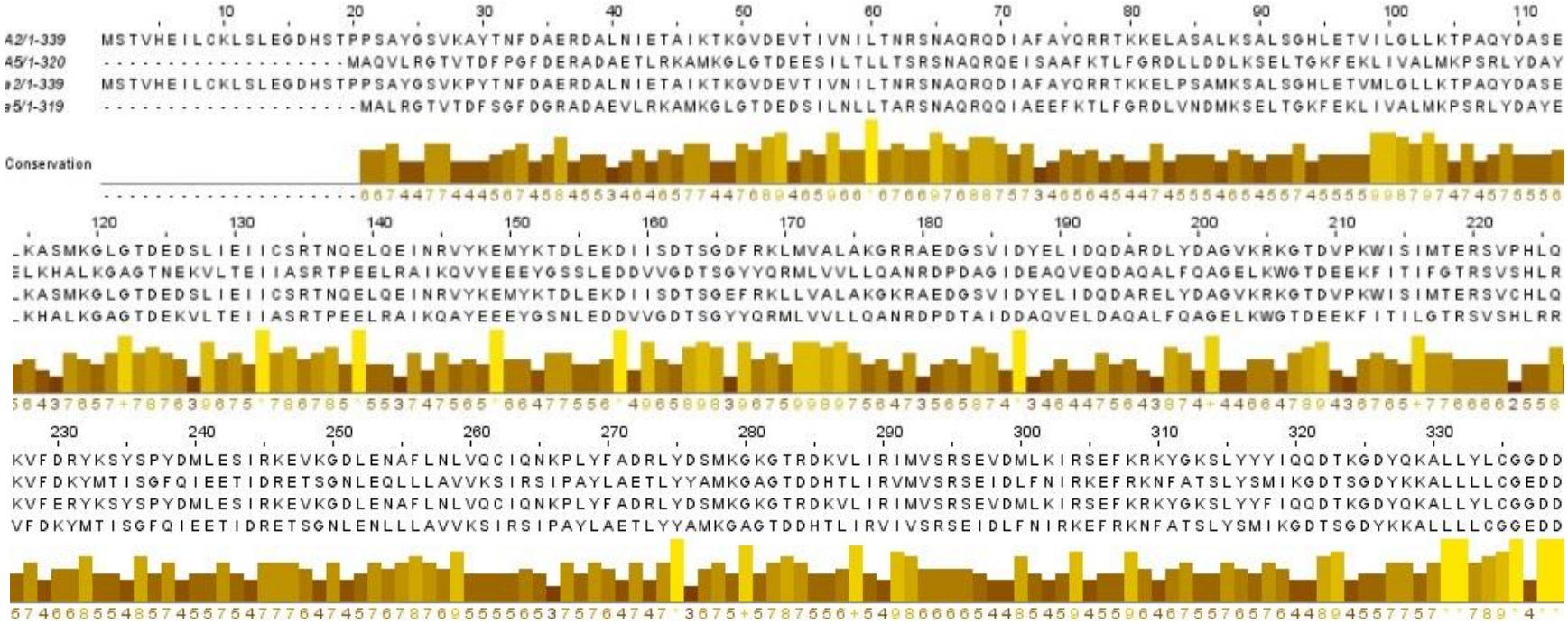

Figure 16: Sequence alignment of annexin A2 *(Homo sapiens)*, A5 *(Homo sapiens)*, a2 *(Rattus norvegicus*) and a5 *(Rattus norvegicus).* The upper portion shows the amino acid sequence for annexin A2 and A5 from *Homo sapiens* and a2 and a5 from *Rattus. norvegicus* respectively going from the top to the bottom. The lower portion depicts the conservation at each amino acid position for each of the four sequences

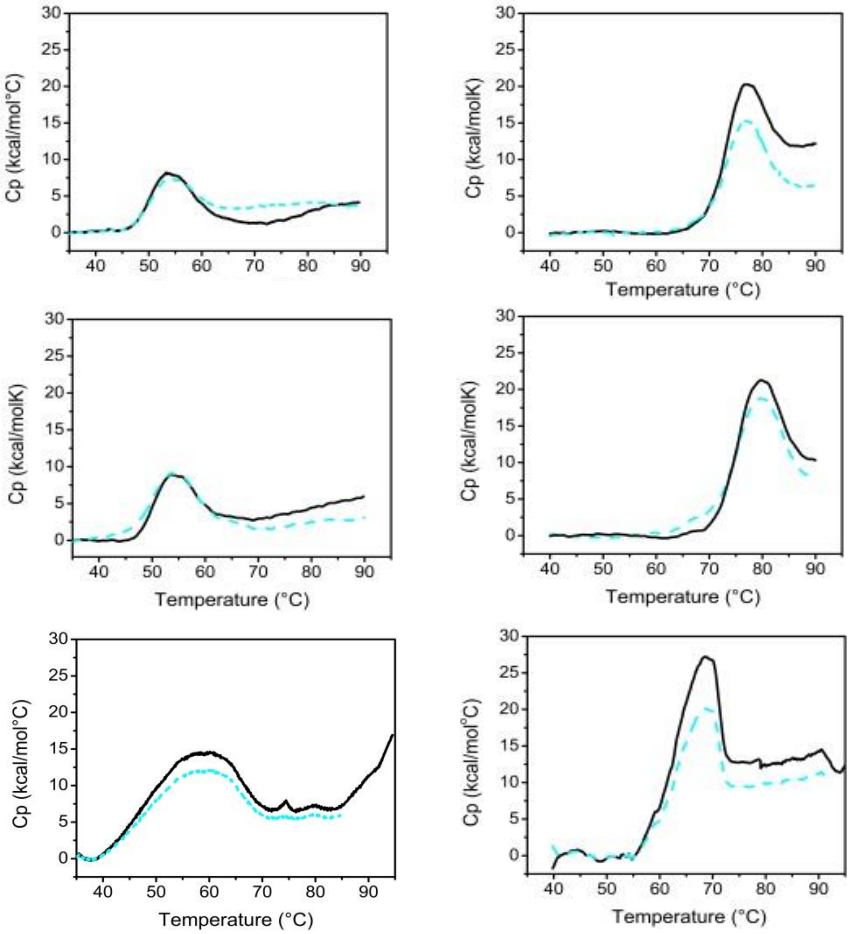

.

Figure 17: *Left column:* Comparison of consecutive denaturation scans of 10µM annexin A2 in the absence of ligand (*upper panel*), the presence of 2mM LUVs composed POPC:POPS (*middle panel*) and 8µM A2 in the presence of 4mM LUVs composed of the muscle mimic mixture. *Right column*: Comparison of consecutive denaturation scans of 10µM annexin A2 in the presence of 5mM Ca^{2+} (*upper panel*), the presence of 5mM Ca^{2+} and 2mM LUVs composed of POPC:POPS (60:40) and 8µM A2 in the presence of 5mM Ca^{2+} and 4mM LUVs composed of the muscle mimic mixture. In each panel the initial denaturation is shown as a black solid line and the second as a blue dashed line. All scans were conducted in a buffer composed of 20mM MOPS and 100mM KCl at a pH of 7.5. All scans in the absence of Ca^{2+} were run at 1mM EGTA.

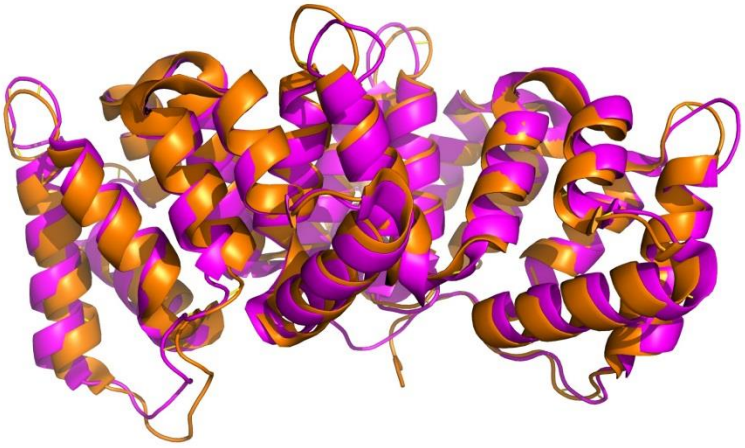

Figure 18: Crystal structure overlay of annexin a5 of *Rattus norvegicus* (orange) and annexin A2 of *Homo sapiens* (purple). Crystal structure files gathered from RCBS Protein Data Bank with accession numbers of 2HYW (A2 *Homo sapeins*) and 2H0K (a5 *Rattus norvegicus*), and developed using PyMOL

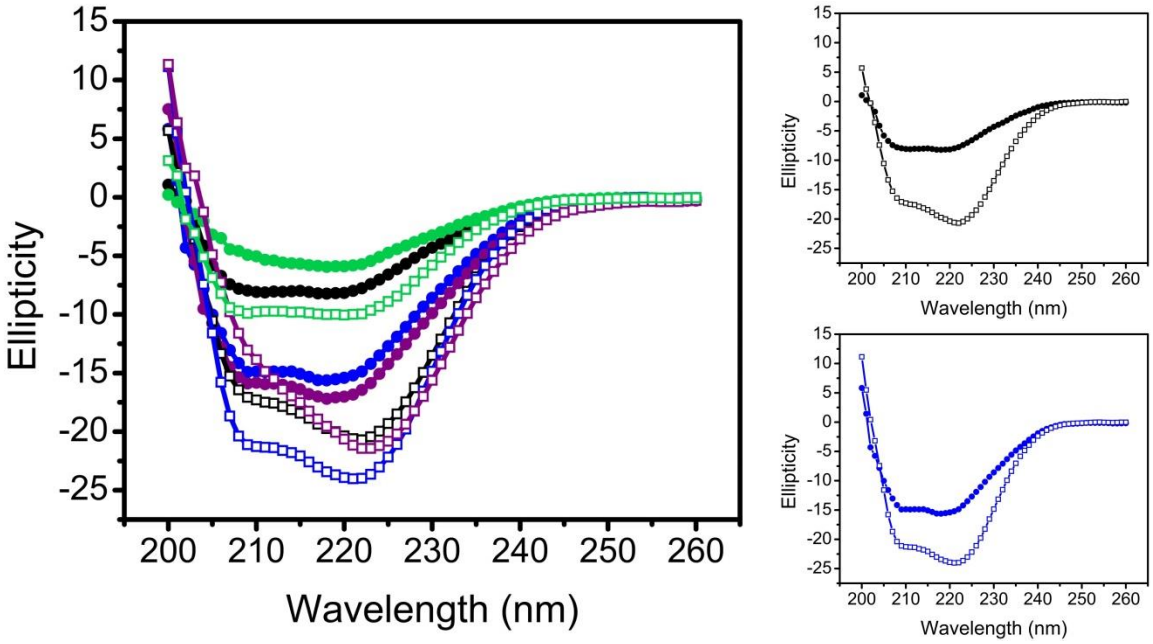

Figure 19: *Left:* CD spectra for annexins A2 (closed circles) and a5 (open squares), in the absence of ligand (**Black**), the presence of 5mM Ca^{2+} (**Blue**), the presence of 5mM Ca^{2+} and 1mM LUVs composed of POPC:POPS (60:40) (**Purple**), and the presence of 1mM LUVs composed of POPC:POPS (60:40) (**Green**). All spectra were taken at a protein concentration of 5µM, in a buffer composed of 20mM MOPS and 100mM KCl at pH 7.5. *Right:* The right panels highlight a comparison of the spectra of annexin A2 and a5 in the absence of ligand (top), and in the presence of Ca^{2+} (bottom).

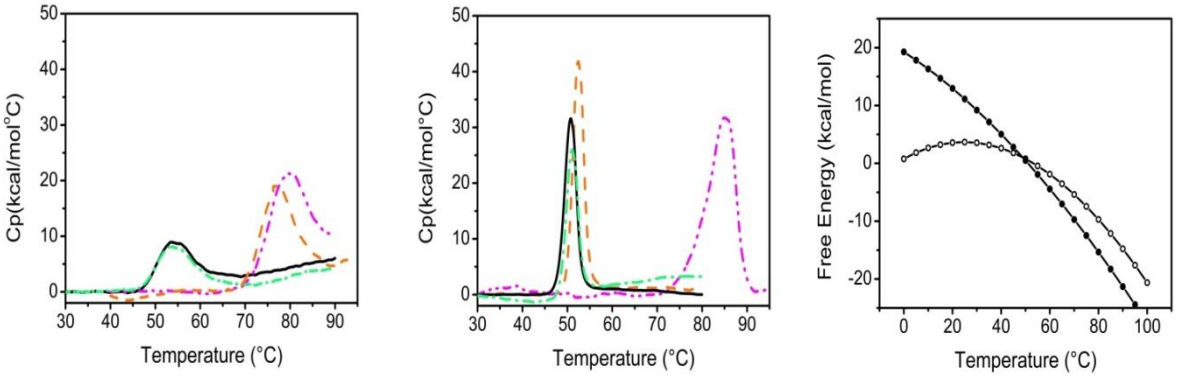

Figure 20: *Left panel:* Denaturation profiles obtained for 10µM annexin A2 in the absence of ligand, solid black line (━━━); presence of 5mM Ca^{2+}, dashed orange line (━ ━); 2mM LUVs composed of POPC:POPS (60:40), green dashed and dotted line (━ ┅); and 5mM Ca^{2+} and 2mM LUVs composed of POPC:POPS (60:40), purple dashed and dotted line (━ ┅ ┅). *Center panel:* Denaturation profiles obtained for 10µM annexin a5 in the absence of ligand, solid black line (━━━); presence of 5mM Ca^{2+}, orange dashed line (━ ━); 2mM LUVs composed of POPC:POPS (60:40), green dashed and dotted line (━ ┅); and 5mM Ca^{2+} and 2mM LUVs composed of POPC:POPS, purple dashed and dotted line (━ ┅ ┅). All scans were conducted in a buffer composed of 20mM MOPS, 100mM KCl at pH 7.5, for both the left and center panels. *Right Panel:* Comparison of the free energy of stability of annexin A2 (open black circles) and a5 (solid black circles) in the absence of ligand.

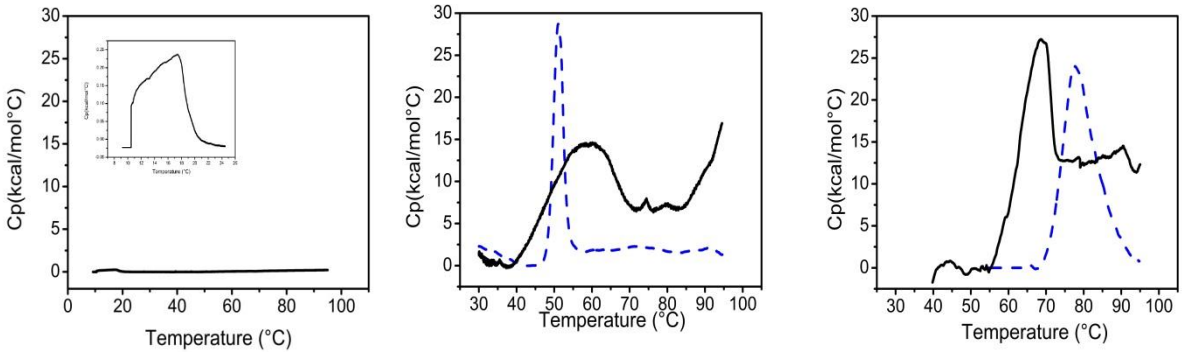

Figure 21: *Left panel:* Thermogram obtained with 4mM LUVs of the muscle mimic lipid mixture, the insert in the upper left is a close-up of the phase transition. *Middle panel:* Denaturation profile of 8µM A2, solid black line (━━━), and 8µM a5, dashed blue line (━ ━), in the presence of 4mM muscle mimic mixture lipids. *Right panel:* Denaturation profile of 8µM A2, solid black line (━━━), and 8µM a5, dashed blue line (━ ━), in the presence of 4mM muscle mimic lipids and 5mM Ca^{2+}. All scans were done in a buffer composed of 20mM MOPS and 100mM KCl at a pH of 7.5.

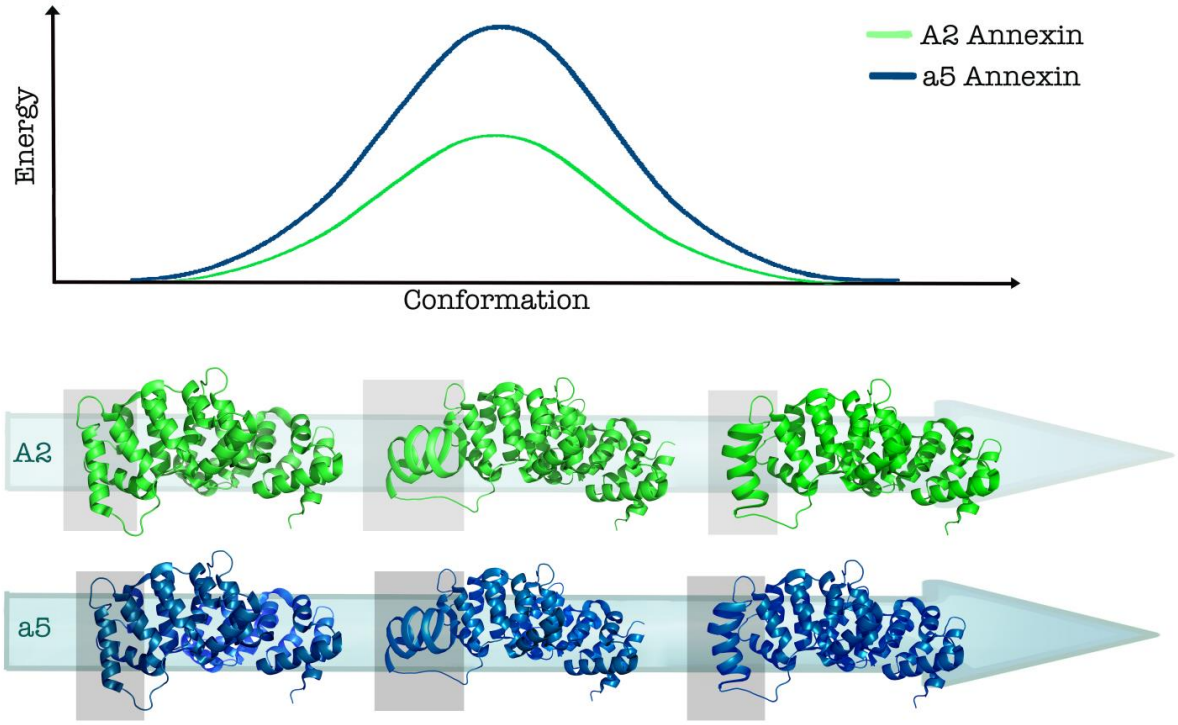

Figure 22: Graphical representation of the difference in the energetic barrier required for annexin A2 and a5 to transition between conformers.

Conclusion: The above studies support the hypothesis that mutations within dysferlin interfere with its ability to properly communicate with its interaction partners during membrane repair. Much like the C2 domains of synaptotagmin I both isoforms of the C2A domain of dysferlin were found to be weakly stable. Since information flow is maximized by weak interactions it appears that both of the proteins are well suited to responding to changes in their environment. The finding that annexin A2, is also marginally stable is also consistent with this as this would allow it to respond appropriately to signals from dysferlin. Based the data that is presented here it is hoped that this work will provide a foundation to further explore the role of dysferlin in information transmission and the impact mutations have on this ability.

References

1. Berchtold, M. W., Brinkmeier, H. & Müntener, M. Calcium ion in skeletal muscle: its crucial role for muscle function, plasticity, and disease. *Physiol. Rev.* **80,** 1215–65 (2000).

2. Aoki, M. *et al.* Genomic organization of the dysferlin gene and novel mutations in Miyoshi myopathy. *Neurology* **57,** 271–8 (2001).

3. Cagliani, R. *et al.* Mutation finding in patients with dysferlin deficiency and role of the dysferlin interacting proteins annexin A1 and A2 in muscular dystrophies. *Hum. Mutat.* **26,** 283 (2005).

4. Cacciottolo, M. *et al.* Muscular dystrophy with marked Dysferlin deficiency is consistently caused by primary dysferlin gene mutations. *Eur. J. Hum. Genet.* **19,** 974–80 (2011).

5. Liu, J. *et al.* Dysferlin, a novel skeletal muscle gene, is mutated in Miyoshi myopathy and limb girdle muscular dystrophy. *Nat. Genet.* **20,** 31–6 (1998).

6. McNeil, P. L. Repairing a torn cell surface: make way, lysosomes to the rescue. *J. Cell Sci.* **115,** 873–879 (2002).

7. Bansal, D. *et al.* Defective membrane repair in dysferlin-deficient muscular dystrophy. *Nature* **423,** 168–172 (2003).

8. Illa, I. *et al.* Distal anterior compartment myopathy: A dysferlin mutation causing a new muscular dystrophy phenotype. *Ann. Neurol.* **49,** 130–134 (2001).

9. Selcen, D., Stilling, G. & Engel, A. G. The earliest pathologic alterations in dysferlinopathy. *Neurology* **56,** 1472–1481 (2001).

10. Evesson, F. J. *et al.* Reduced plasma membrane expression of dysferlin mutants is attributed to accelerated endocytosis via a syntaxin-4-associated pathway. *J. Biol. Chem.* **285,** 28529–39 (2010).

11. Miyake, K. Vesicle accumulation and exocytosis at sites of plasma membrane disruption. *J. Cell Biol.* **131,** 1737–1745 (1995).

12. Cai, C. *et al.* MG53 nucleates assembly of cell membrane repair machinery. *Nat. Cell Biol.* **11,** 56–64 (2009).

13. Cai, C. *et al.* Membrane repair defects in muscular dystrophy are linked to altered interaction between MG53, caveolin-3, and dysferlin. *J. Biol. Chem.* **284,** 15894–902 (2009).

14. Matsuda, C. *et al.* The C2A domain in dysferlin is important for association with MG53 (TRIM72). *PLoS Curr.* **4,** e5035add8caff4 (2012).

15. McCann, J. J. *et al.* Supertertiary structure of the synaptic MAGuK scaffold proteins is conserved. *Proc. Natl. Acad. Sci. U. S. A.* **109,** 15775–80 (2012).

16. Ampong, B. N., Imamura, M., Matsumiya, T., Yoshida, M. & Takeda, S. Intracellular localization of dysferlin and its association with the dihydropyridine receptor. *Acta Myol.* **24,** 134–44 (2005).

17. Klinge, L. *et al.* Dysferlin associates with the developing T-tubule system in rodent and human skeletal muscle. *Muscle Nerve* **41,** 166–73 (2010).

18. Azakir, B. A., Di Fulvio, S., Therrien, C. & Sinnreich, M. Dysferlin interacts with tubulin and microtubules in mouse skeletal muscle. *PLoS One* **5,** e10122 (2010).

19. Covian-Nares, J. F., Koushik, S. V, Puhl, H. L. & Vogel, S. S. Membrane wounding triggers ATP release and dysferlin-mediated intercellular calcium signaling. *J. Cell Sci.* **123,** 1884–93 (2010).

20. McNeil, P., Vogel, S., Miyake, K. & Terasaki, M. Patching plasma membrane disruptions with cytoplasmic membrane. *J. Cell Sci.* **113,** 1891–1902 (2000).

21. Pramono, Z. A. D. *et al.* Identification and characterisation of human dysferlin transcript variants: implications for dysferlin mutational screening and isoforms. *Hum. Genet.* **125,** 413–20 (2009).

22. Pramono, Z. A. D., Lai, P. S., Tan, C. L., Takeda, S. & Yee, W. C. Identification and characterization of a novel human dysferlin transcript: dysferlin_v1. *Hum. Genet.* **120,** 410–9 (2006).

23. Gauer, J. W. *et al.* Mechanism for Calcium Ion Sensing by the C2A Domain of Synaptotagmin I. *Biophys. J.* **103,** 238–246 (2012).

24. Davis, D. B., Doherty, K. R., Delmonte, A. J. & McNally, E. M. Calcium-sensitive phospholipid binding properties of normal and mutant ferlin C2 domains. *J. Biol. Chem.* **277,** 22883–8 (2002).

25. Battye, T. G. G., Kontogiannis, L., Johnson, O., Powell, H. R. & Leslie, A. G. W. iMOSFLM: a new graphical interface for diffraction-image processing with MOSFLM. *Acta Crystallogr.* **67,** 271–81 (2011).

26. Winn, M. D. *et al.* Overview of the CCP4 suite and current developments. *Acta Crystallogr.* **67,** 235–42 (2011).

27. Kingsley, P. B. & Feigenson, G. W. 1H-NMR study of the location and motion of ubiquinones in perdeuterated phosphatidylcholine bilayers. *Biochim. Biophys. Acta* **635,** 602–618 (1981).

28. Yokoyama, S. *et al.* Structural genomics projects in Japan.

29. Helfmann, S. *et al.* The crystal structure of the C_2A domain of otoferlin reveals an unconventional top loop region. *J. Mol. Biol.* **406,** 479–90 (2011).

30. Anandakrishnan, R., Aguilar, B. & Onufriev, A. V. H++ 3.0: automating pK prediction and the preparation of biomolecular structures for atomistic molecular modeling and simulations. *Nucleic Acids Res.* **40,** W537–41 (2012).

31. Cates, M. S., Teodoro, M. L. & Phillips, G. N. Molecular mechanisms of calcium and magnesium binding to parvalbumin. *Biophys. J.* **82,** 1133–46 (2002).

32. Zubriene, A. *et al.* Measurement of nanomolar dissociation constants by titration calorimetry and thermal shift assay - radicicol binding to Hsp90 and ethoxzolamide binding to CAII. *Int. J. Mol. Sci.* **10,** 2662–80 (2009).

33. Leavitt, S. & Freire, E. Direct measurement of protein binding energetics by isothermal titration calorimetry. *Curr. Opin. Struct. Biol.* **11,** 560–566 (2001).

34. Radhakrishnan, A., Stein, A., Jahn, R. & Fasshauer, D. The Ca2+ affinity of synaptotagmin 1 is markedly increased by a specific interaction of its C2B domain with phosphatidylinositol 4,5-bisphosphate. *J. Biol. Chem.* **284,** 25749–60 (2009).

35. Lek, A., Lek, M., North, K. N. & Cooper, S. T. Phylogenetic analysis of ferlin genes reveals ancient eukaryotic origins. *BMC Evol. Biol.* **10,** 231 (2010).

36. Therrien, C., Di Fulvio, S., Pickles, S. & Sinnreich, M. Characterization of lipid binding specificities of dysferlin C2 domains reveals novel interactions with phosphoinositides. *Biochemistry* **48,** 2377–84 (2009).

37. Lostal, W. *et al.* Lack of correlation between outcomes of membrane repair assay and correction of dystrophic changes in experimental therapeutic strategy in dysferlinopathy. *PLoS One* **7,** e38036 (2012).

38. Uversky, V. N. What does it mean to be natively unfolded? *Eur. J. Biochem.* **269,** 2–12 (2002).

39. Murray, D. & Honig, B. Electrostatic Control of the Membrane Targeting of C2 Domains. *Mol. Cell* **9,** 145–154 (2002).

40. Ochoa, W. F. *et al.* Structure of the C2 domain from novel protein kinase Cepsilon. A membrane binding model for Ca(2+)-independent C2 domains. *J. Mol. Biol.* **311,** 837–49 (2001).

41. Fisher, C. K. & Stultz, C. M. Protein structure along the order-disorder continuum. *J. Am. Chem. Soc.* **133,** 10022–5 (2011).

42. Halskau, O., Muga, A. & Martinez, A. Linking New Paradigms in Protein Chemistry to Reversible Membrane-Protein Interactions. *Curr. Protein Pept. Sci.* **10,** 21 (2009).

43. Sigurskjold, B. W. Exact analysis of competition ligand binding by displacement isothermal titration calorimetry. *Anal. Biochem.* **277,** 260–6 (2000).

44. Almeida, P. F. F., Pokorny, A. & Hinderliter, A. Thermodynamics of membrane domains. *Biochim. Biophys. Acta* **1720,** 1–13 (2005).

45. Morowitz, H. J. *Energy Flow in Biology*. (Ox Bow Press, 1968).

46. Hilser, V. J. & Thompson, E. B. Intrinsic disorder as a mechanism to optimize allosteric coupling in proteins. *Proc. Natl. Acad. Sci. U. S. A.* **104,** 8311–5 (2007).

47. Fealey, M. E. *et al.* Negative Coupling as a Mechanism for Signal Propagation between C2 Domains of Synaptotagmin I. *PLoS One* **7,** (2012).

48. Fuson, K. *et al.* Alternate Splicing of Dysferlin C2A Confers Ca(2+)-Dependent and Ca(2+)-Independent Binding for Membrane Repair. *Struct. (London, Engl. 1993)* (2013). doi:10.1016/j.str.2013.10.001

49. Letunic, I., Doerks, T. & Bork, P. SMART 7: recent updates to the protein domain annotation resource. *Nucleic Acids Res.* **40,** D302–D305 (2011).

50. Torrecillas, A., Laynez, J., Menéndez, M., Corbalán-García, S. & Gómez-Fernández, J. C. Calorimetric study of the interaction of the C2 domains of classical protein kinase C isoenzymes with Ca2+ and phospholipids. *Biochemistry* **43,** 11727–39 (2004).

51. Chen, J. W., Romero, P., Uversky, V. N. & Dunker, A. K. Conservation of Intrinsic Disorder in Protein Domains and Families: II. Functions of Conserved Disorder. *J. Proteome Res.* **5,** 888–898 (2006).

52. Gennis, R. B. *Biomembranes: Molecular Structure and Function*. (Springer-Verlag, 1988).

53. Hinderliter, A., Almeida, P. F. F., Creutz, C. E. & Biltonen, R. L. Domain Formation in a Fluid Mixed Lipid Bilayer Modulated through Binding of the C2 Protein Motif. *Biochemistry* **40,** 4181–4191 (2001).

54. Hinderliter, A., Biltonen, R. L. & Almeida, P. F. Lipid modulation of protein-induced membrane domains as a mechanism for controlling signal transduction. *Biochemistry* **43,** 7102–10 (2004).

55. Fridriksson, E. K. *et al.* Quantitative analysis of phospholipids in functionally important membrane domains from RBL-2H3 mast cells using tandem high-resolution mass spectrometry. *Biochemistry* **38,** 8056–63 (1999).

56. Fuson, K. *et al.* Alternate splicing of dysferlin C2A confers Ca2+-dependent and Ca2+-independent binding for membrane repair. *Structure* **22,** 104–115 (2014).

57. Gauer, J. W. *et al.* Membrane modulates affinity for calcium ion to create an apparent cooperative binding response by annexin a5. *Biophys. J.* **104,** 2437–47 (2013).

58. Gauer, J. W. *et al.* Membrane Modulates Affinity for Calcium Ion to Create an Apparent Cooperative Binding Response by Annexin a5. *Biophys. J.* **104,** 2437–2447 (2013).

59. Shannon, C. & Weaver, W. *The Mathematical Theory of Communication*. (University of Illinois Press; First Edition, 1971). at <http://www.amazon.com/Mathematical-Theory-Communication-Claude-Shannon/dp/0252725484>

60. BRETSCHER, M. S. Asymmetrical Lipid Bilayer Structure for Biological Membranes. *Nature* **236,** 11–12 (1972).

61. Op den Kamp, J. A. Lipid asymmetry in membranes. *Annu. Rev. Biochem.* **48,** 47–71 (1979).

62. Cho, W. & Stahelin, R. V. Membrane binding and subcellular targeting of C2 domains. *Biochim. Biophys. Acta* **1761,** 838–49 (2006).

63. Rizo, J. & Sudhof, T. C. C2-domains, Structure and Function of a Universal Ca2+-binding Domain. *J. Biol. Chem.* **273,** 15879–15882 (1998).

64. Berman, H. M. *et al.* The Protein Data Bank. *Nucleic Acids Res.* **28,** 235–242 (2000).

65. Xu, J. *et al.* Structure and Ca^{2+}-binding properties of the tandem C_2 domains of E-Syt2. *Structure* **22,** 269–80 (2014).

66. Bakan, A. & Bahar, I. The intrinsic dynamics of enzymes plays a dominant role in determining the structural changes induced upon inhibitor binding. *Proc. Natl. Acad. Sci.* **106,** 14349–14354 (2009).

67. Liu, Y. & Bahar, I. Sequence evolution correlates with structural dynamics. *Mol. Biol. Evol.* **29,** 2253–2263 (2012).

68. Takamori, S. *et al.* Molecular anatomy of a trafficking organelle. *Cell* **127,** 831–46 (2006).

69. Brumm, T., Jørgensen, K., Mouritsen, O. G. & Bayerl, T. M. The effect of increasing membrane curvature on the phase transition and mixing behavior of a dimyristoyl-sn-glycero-3-phosphatidylcholine/ distearoyl-sn-glycero-3-phosphatidylcholine lipid mixture as studied by Fourier transform infrared spectroscopy and. *Biophys. J.* **70,** 1373–9 (1996).

70. Jensen, M. Ø. & Mouritsen, O. G. Lipids do influence protein function-the hydrophobic matching hypothesis revisited. *Biochim. Biophys. Acta* **1666,** 205–26 (2004).

71. Fealey, M. E. & Hinderliter, A. Allostery and instability in the functional plasticity of synaptotagmin I. *Commun. Integr. Biol.* **6,** e22830 (2013).

72. Frazier, A. A., Roller, C. R., Havelka, J. J., Hinderliter, A. & Cafiso, D. S. Membrane-bound orientation and position of the synaptotagmin I C2A domain by site-directed spin labeling. *Biochemistry* **42,** 96–105 (2003).

73. Rufener, E., Frazier, A. A., Wieser, C. M., Hinderliter, A. & Cafiso, D. S. Membrane-Bound Orientation and Position of the Synaptotagmin C2B Domain Determined by Site-Directed Spin Labeling †. *Biochemistry* **44,** 18–28 (2005).

74. Guillén, J. *et al.* Structural insights into the Ca2+ and PI(4,5)P2 binding modes of the C2 domains of rabphilin 3A and synaptotagmin 1. *Proc. Natl. Acad. Sci. U. S. A.* **110,** 20503–8 (2013).

75. Brown, D. A. Lipid rafts, detergent-resistant membranes, and raft targeting signals. *Physiology (Bethesda).* **21,** 430–9 (2006).

76. Rosengarth, A., Rösgen, J., Hinz, H. J. & Gerke, V. A comparison of the energetics of annexin I and annexin V. *J. Mol. Biol.* **288,** 1013–25 (1999).

77. Dill, K. A. Dominant forces in protein folding. *Biochemistry* **29,** 7133–7155 (1990).

78. Illien, F., Piao, H.-R., Coué, M., di Marco, C. & Ayala-Sanmartin, J. Lipid organization regulates annexin A2 Ca(2+)-sensitivity for membrane bridging and its modulator effects on membrane fluidity. *Biochim. Biophys. Acta* **1818,** 2892–900 (2012).

79. Drücker, P., Pejic, M., Galla, H.-J. & Gerke, V. Lipid segregation and membrane budding induced by the peripheral membrane binding protein annexin A2. *J. Biol. Chem.* **288,** 24764–76 (2013).

80. Fajardo, V. A. *et al.* Isolation of sarcolemmal plasma membranes by mechanically skinning rat skeletal muscle fibers for phospholipid analysis. *Lipids* **48,** 421–30 (2013).